AD-A070 643 PMB SYSTEMS ENGINEERING INC SAN FRANCISCO CA F/G 11/2
FAILURE CRITERIA FOR REINFORCED CONCRETE STRUCTURES. VOLUME I. --ETC(U)
MAY 79 R W LITTON, J M GIDWANI F29601-76-C-0135
AFWL-TR-77-239-VOL-1 NL

UNCLASSIFIED

1 OF 2
AD
A070 643

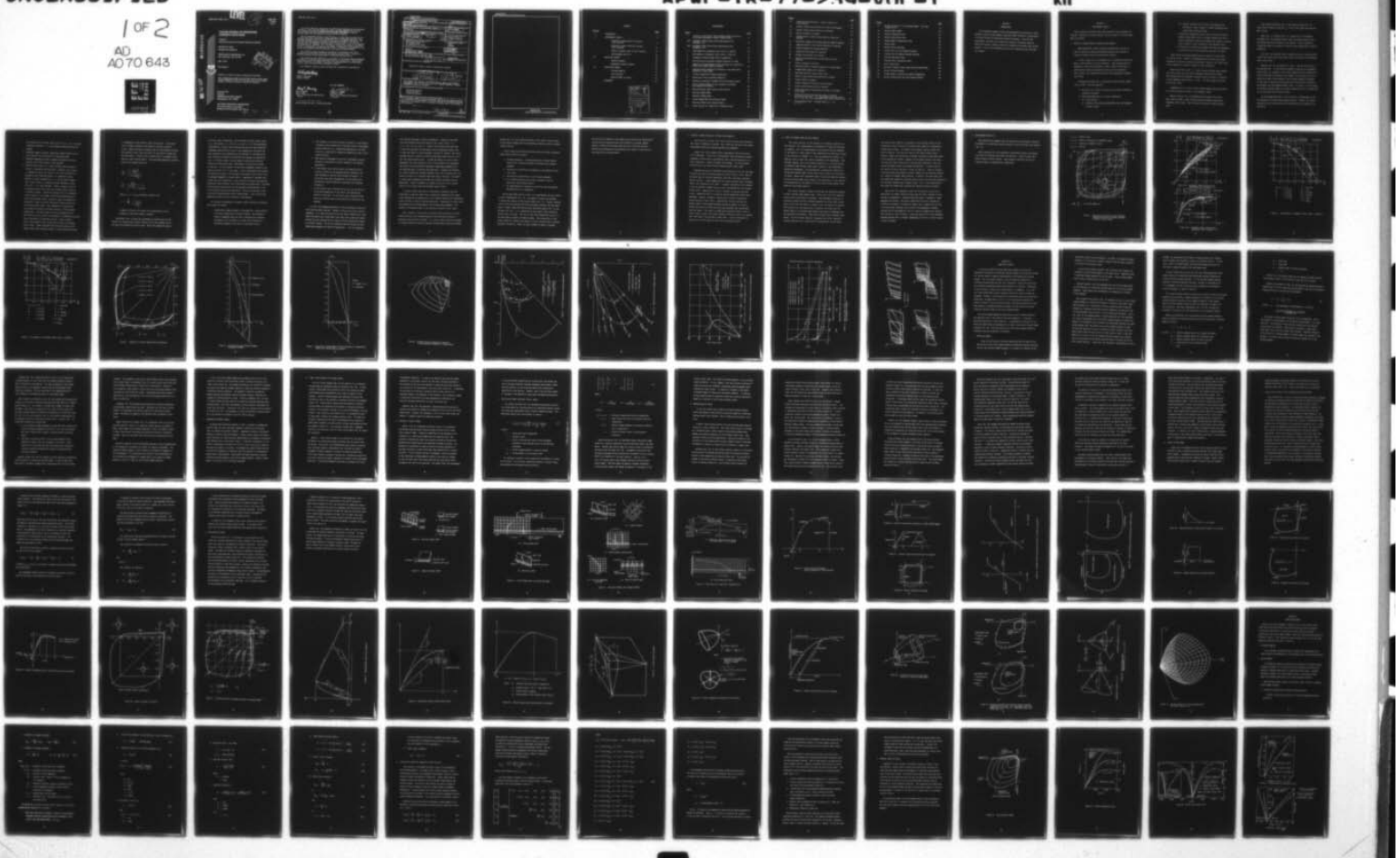

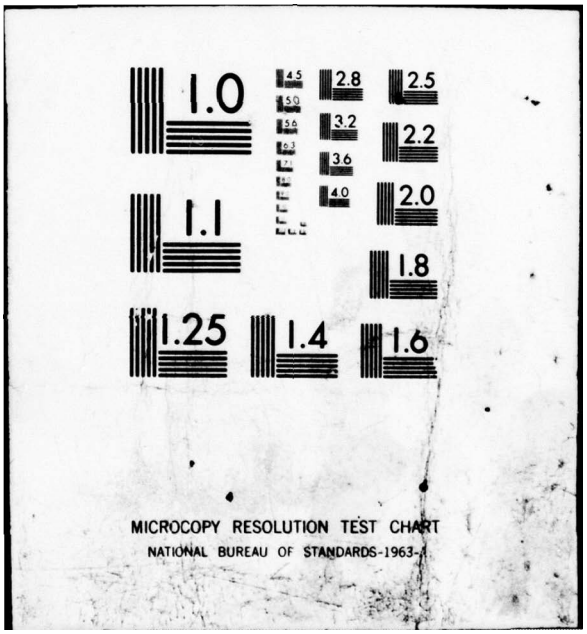
1.0
1.1
1.25
1.4
1.6
1.8
2.0
2.2
2.5
2.8
3.2
3.6
4.0
4.5
5.0
5.6
6.3
MICROCOPY RESOLUTION TEST CHART
NATIONAL BUREAU OF STANDARDS-1963-A

AFWL-TR-77-239, Vol. I

AFWL-TR-
77-239
Vol. I

FAILURE CRITERIA OF REINFORCED CONCRETE STRUCTURES

Volume I
Literature Survey & Proposed Analytical Models

Richard W. Litton
Jawahar M. Gidwani

PMB Systems Engineering, Inc.
San Francisco, CA 94104

May 1979

Final Report

This research was funded by the Defense Nuclear Agency under Subtask Y99QAXSC157, work unit 08, work unit title, "Dynamic Response of Buried Structural Systems and Contents."

Prepared for
Director
DEFENSE NUCLEAR AGENCY
Washington, DC 20305

AIR FORCE WEAPONS LABORATORY
Air Force Systems Command
Kirtland Air Force Base, NM 87117

This final report was prepared by the PMB Systems Engineering, San Francisco, California, under Contract F29601-76-C-0135, Job Order WDNS3428 with the Air Force Weapons Laboratory, Kirtland Air Force Base, New Mexico. Rodney G. Galloway (DES) was the Laboratory Project Officer-in-Charge.

When US Government drawings, specifications, or other data are used for any purpose other than a definitely related Government procurement operation, the Government thereby incurs no responsibility nor any obligation whatsoever, and the fact that the Government may have formulated, furnished, or in any way supplied the said drawings, specifications, or other data, is not to be regarded by implication or otherwise, as in any manner licensing the holder or any other person or corporation, or conveying any rights or permission to manufacture, use, or sell any patented invention that may in any way be related thereto.

This report has been reviewed by the Office of Information (OI) and is releasable to the National Technical Information Service (NTIS). At NTIS, it will be available to the general public, including foreign nations.

This report has been authored by a contractor of the United States Government. Accordingly, the United States Government retains a nonexclusive, royalty-free license to publish or reproduce the material contained herein, or allow others to do so, for the United States Government purposes.

This technical report has been reviewed and is approved for publication.

Rodney G. Galloway

RODNEY G. GALLOWAY
Project Officer

FOR THE COMMANDER

Gary P. Ganong

GARY P. GANONG
Major, USAF
Chief, Technology and Applications Branch

Stewart W. Johnson

STEWART W. JOHNSON
LtColonel, USAF
Chief, Civil Engineering Research Division

DO NOT RETURN THIS COPY. RETAIN OR DESTROY

UNCLASSIFIED

SECURITY CLASSIFICATION OF THIS PAGE (When Data Entered)

REPORT DOCUMENTATION PAGE	READ INSTRUCTIONS BEFORE COMPLETING FORM
1. REPORT NUMBER: AFWL-TR-77-239-Vol-1	2. GOVT ACCESSION NO. / 3. RECIPIENT'S CATALOG NUMBER
4. TITLE (and Subtitle): FAILURE CRITERIA FOR REINFORCED CONCRETE Structures Volume I. Literature Survey & Proposed Analytical Models.	5. TYPE OF REPORT & PERIOD COVERED: Final Report.
	6. PERFORMING ORG. REPORT NUMBER
7. AUTHOR(s): Richard W. Litton and Jawahar M. Gidwani	8. CONTRACT OR GRANT NUMBER(s): F29601-76-C-0135
9. PERFORMING ORGANIZATION NAME AND ADDRESS: PMB Systems Engineering Inc, 500 Sansome Street, San Francisco, CA 94104	10. PROGRAM ELEMENT, PROJECT, TASK AREA & WORK UNIT NUMBERS: 62704H, WDNS3428
11. CONTROLLING OFFICE NAME AND ADDRESS: Director, Defense Nuclear Agency, Washington, DC 20305	12. REPORT DATE: May 1979; NUMBER OF PAGES: 122
14. MONITORING AGENCY NAME & ADDRESS (if different from Controlling Office): Air Force Weapons Laboratory (DES), Kirtland Air Force Base, NM 87117	15. SECURITY CLASS. (of this report): UNCLASSIFIED; 15a. DECLASSIFICATION/DOWNGRADING SCHEDULE

16. DISTRIBUTION STATEMENT (of this Report)

Approved for public release; distribution unlimited

17. DISTRIBUTION STATEMENT (of the abstract entered in Block 20, if different from Report)

18. SUPPLEMENTARY NOTES

This research was funded by the Defense Nuclear Agency under Subtask Y99QAXSC157, work unit 08, work unit title "Dynamic Response of Buried Structural Systems and Contents."

19. KEY WORDS (Continue on reverse side if necessary and identify by block number)

Reinforced Concrete
Failure Criteria
Structural Analysis

20. ABSTRACT (Continue on reverse side if necessary and identify by block number)

This literature summary reviews experimental and analytical studies relevant to the Theoretical Investigation of Failure Criteria for Reinforced Concrete Structures. An extensive list of relevant references used in this survey is also presented.

392 790

DD FORM 1 JAN 73 1473 EDITION OF 1 NOV 65 IS OBSOLETE

UNCLASSIFIED

SECURITY CLASSIFICATION OF THIS PAGE (When Data Entered)

CONTENTS

ILLUSTRATIONS

SECTION I

INTRODUCTION

This literature summary reviews both experimental and analytical studies relevant to the Air Force Weapons Laboratory (AFWL) Theoretical Investigation of Failure Criteria for Reinforced Concrete Structures. First for the experimental, and then for the analytical studies, the summary generally begins with earlier, simpler studies and proceeds to the recent, more refined studies. A list of the references used in this literature survey concludes this summary.

SECTION II

EXPERIMENTAL STUDIES

Static uniaxial and biaxial tests comprise most of the experiments on concrete. Relatively few tests consider triaxial, dynamic, or reinforcement bond slip effects.

1. STATICALLY LOADED BIAXIALLY STRESSED PLAIN CONCRETE

Many experimental studies have been conducted over the last 70 years to confirm or propose new theories governing the strength of statically loaded biaxially stressed plain concrete.

In 1911, Karman (ref. 1) and Baker (ref. 2) tested the validity of Mohr's failure theory for brittle materials. They concluded that (1) depending on the stress combination, either a tensile splitting or a shearing and sliding action governs failure, and (2) contrary to Mohr's theory, the intermediate principal stress magnitude influenced the failure.

Brandtzaeg and Brown (ref. 3) performed similar but more refined tests in 1929. They concluded that

a. The biaxial is at least as great as the uniaxial compressive strength of concrete.
b. Three load phases occur in uniaxial compression
   (1) Linear elastic,
   (2) Inelastic with increased deformation rate and increased Poisson's ratio,

(3) Internal cracking at 75% to 85% of the maximum load, followed by a great increase in lateral deformation and volume under continued loading.

c. In multiaxial compressive stress states frictional resistance against sliding motion acts on a greater surface area than in uniaxial compression, which could explain the increase in applied stress required to start splitting in the multiaxial case.

d. Sliding may be a bond failure between the cement and aggregate; the bond slip may be partly adhesive and partly frictional.

These conclusions agreed somewhat with the internal friction theory of sliding failure. However, the breakdown process and resulting large deformations could not be reconciled with Mohr's theory or any theory based on the assumption of sliding on planes of least resistance.

Bresler and Pister (refs. 4, 5, and 6) studied concrete shear-compression stress states to verify their octahedral shearing stress theory, which assumed that the octahedral shearing stress at failure is a function of the octahedral normal stress $\tau_o = f(\sigma_o)$. For their range of data the relation was linear.

Freudenthal (ref. 7) used a closely related theory based on the effective stress expressed in terms of the octahedral stress.

McHenry and Karni (ref. 8) performed tensile compressive biaxial tests and also found a linear relation between octahedral shearing and octahedral normal stress. Mohr's theory of failure was found not applicable.

Later studies by Bellamy (ref. 9) and Goode and Helmy (ref. 10) found failure criteria of the form $\tau_o = f(\sigma_o)$ to be no more accurate than Mohr's theory.

Foppl (ref. 11), Wastlund (ref. 12), Glomb (ref. 13) and Weigler and Becher (ref. 14) performed biaxial tests on concrete cubes to study the strength and failure aspects of the material. Again, compressive strength was found to be greater in biaxial stress states than in uniaxial compression.

Vile (ref. 15) performed biaxial compressive tests on concrete plates in which the stress strain curves were found to be similar to the uniaxial stress strain curve.

Robinson (ref. 16) continued Vile's tests. From the test results it was observed that: (1) the ultimate strength of concrete is increased by lateral loads, (2) increase in the lateral compressive load increases the load at which major microcracks occur; however, this increase was not as extensive as that of the increase in the ultimate strength of concrete, (3) the loads at which major microcracks occur decrease with increasing water/cement, and the aggregate/cement ratios, in contrast to the strength of concrete, providing there is a lateral compressive load. The effect was not so noticeable for the cracking loads.

The work summarized above is one of the early investigations on the microcracking of concrete under combined stresses. However, the results obtained from this work and microcrack observations do not appear to be conclusive.

was obtained at a principal stress ratio of $\sigma_2/\sigma_1 = 0.5$. For equal compressive stresses $\sigma_1 = \sigma_2$ the strength increase was about 16 percent.

2. Specimens loaded in uniaxial compression showed numerous microcracks parallel to the direction of the applied load.
3. Specimens subjected to biaxial compression showed microcracks parallel to the free surfaces of the specimens.
4. External major stress σ_1 vs. strain relations were plotted for various σ_2 transverse confining loads. Generally, for a given σ_1 compressive stress, the strains in the first direction are decreasing with increasing values of σ_2 compressive stress. However, for equal compression $\sigma_1 = \sigma_2$, and at about ultimate load, larger strains, as compared to those obtained by stress ratio $\sigma_2/\sigma_1 = 0.5$, were recorded. Figure 1 presents a plot of the general shape of the elastic and ultimate stress levels as as defined by Kupfer. Kupfer more recently (ref. 18) conducted further research in an attempt to describe the deformations of plain concrete under biaxial stresses by means of mathematical expression in order to predict the strains resulting from arbitrary plane stress states. Such information is required for the formation of material stiffness matrices in finite element computations. The effort makes use of the decompositions of the stress and strain states into volumetric, or hydrostatic portion, and a distortional, or deviatory portion. Figure 2 shows a plot of the octahedral shear stress-strain curves for different stress ratios. Kupfer concludes that since the curves for different stress ratios coincide closely, a unique relationship which

is independent of the principal stress ratio exists. This assumption is commonly applied to the theory of inelastic isotropic solids. Kupfer continues to present plots and relationships relating the octahedral shear stress and strain to the material tangent bulk and shear moduli. Figures 3 and 4 present plots of octahedral shear stress to shear and bulk moduli. The associated mathematical relationships for the tangent terms are:

$$\frac{G_T}{G_o} = \frac{\left[1 - a\left(\frac{\tau_o}{f_{cu}}\right)^m\right]}{1 + (m-1)a\left(\frac{\tau_o}{f_{cu}}\right)^m} \tag{1}$$

$$\frac{K_T}{K_o} = \frac{G_T/G_o}{e^{-(c\gamma_o)^p}\left[1 - p(c\gamma_o)^p\right]} \tag{2}$$

where a, m, c, p, f_{cu} are material constants and

$$\gamma_o = \frac{f_o}{2G_o} \quad \frac{1}{1 - a\left(\frac{f_o}{f_{cu}}\right)^m} \tag{3}$$

A summary is given in the report for the application of this procedure to the finite element approach.

Buyukozturk (ref. 19) made some refinement of previous work for the behavior of concrete under uniaxial loading, but his main emphasis was on the short-term compressive biaxial cases. Within the compressive region

of biaxial stress combinations, four different principal stress ratios, σ_2/σ_1, were chosen, i.e., 0.0, 0.2, 0.5, and 1.0. For the experimental investigation, a biaxial load testing device was built which permitted independent application of stress in two perpendicular directions and which permitted x-ray examination of the specimen for cracking during test, without the necessity of disturbing the specimen or removing the load. In loading, special care was taken to minimize the restraint offered by loading plates due to deformation in the direction normal to the load. For this purpose, a brush-like arrangement originally proposed by Hilsdorf (ref. 17) was used. In this investigation the concrete was idealized as square, flat specimens consisting of nine circular discs of aggregate embedded in a mortar matrix. Buyukozturk's specimens were tested, and total deformations in two principal directions were measured. Deformation versus external load relationships were established. The effect of the second principal stress on the strength and deformations in the first principal direction was emphasized. Using X-ray procedure, microcracks were examined during actual loading process. Local strains were measured at certain critical locations in the specimen.

On the basis of Buyukozturk's studies, certain important conclusions can be drawn as follows:

1. Significantly higher strength is attainable for a given material in biaxial loading than in uniaxial loading. The strength increase is dependent upon the ratio of the principal stresses, and appears to be a maximum at a stress ratio of about 0.5, diminishing somewhat as the ratio is increased to unity.

2. The stiffness in the first principal direction is significantly increased by the introduction of principal stress in the perpendicular direction; i.e., compressive deformation in the first direction is substantially reduced by compressive stress in the second direction.
3. When spacing of aggregate of one size is decreased, uniaxial strength is decreased but biaxial strength is not affected appreciably.
4. In the uniaxial case, failure occurs by progressive microcracking, starting at the aggregate-mortar interfaces, and later extending as tensile cracks through the mortar. In the biaxial case cracks perpendicular to the plane of the specimen were neither observed by experiment nor predicted by analysis.
5. In the uniaxial case, ultimate failure occurs by splitting in the planes perpendicular to the face of the specimen and parallel to the load. In the biaxial case, ultimate failure occurs by splitting along a plane parallel to the face of the specimen.

Liu (ref. 20) extended Buyukozturk's work by developing a more complete concrete model specimen. Instead of using nine circular disks of aggregate, Liu's model contained thirty with three different disc sizes. Eight such models were tested under short term static compressive loads, applied from zero through the full range of biaxial compressive loading to ultimate strength. The failure envelopes obtained through the tests showed good agreement with those of Buyukozturk's. Liu also subjected

real concrete specimens to biaxial compression. Eighty-four specimens with five different mixes were tested at four stress ratios, i.e., σ_2/σ_1 = 0.0, 0.2, 0.5, and 1.0. Three of the concrete mixes were used to study the influence of water-cement ratio and aggregate-cement ratio. To study the effect of coarse aggregate (concrete vs. mortar), the fourth specimen type was a mortar mix with the same water-cement ratio as one of the first three concrete mixes. To study the effect of size of coarse aggregates, the fifth concrete mix had 1 inch maximum size of aggregate. The results of testing these 84 speciments showed good agreement with the idealized model of concrete used previously. Studying the different mix results showed that ultimate strength of mix five, the mortar mix, was found to be only 8 to 13 percent lower than that of concrete. The effect of using larger aggregate did decrease the ultimate strengths, but not appreciably. Figure 5 presents an ultimate stress plot of the loading results of Liu's tests with the different types of mixes.

A review of many stress-strain relationships proposed by previous researchers in concrete under biaxial loading was conducted in this paper. A new relationship was proposed by Liu for concrete under biaxial compression, biaxial tension, or biaxial tension-compression. Comparisons of values from the proposed rule with experimental data provided good agreement. This relation is discussed further in the analytical portion of this report.

Until recently, little biaxial testing has been carried out in which tension was one of the loadings because of the difficulty involved in applying a tensile load to conrete. As a result, some of the early attempts at studying compression-tension loading involved dubious testing techniques.

Carino (ref. 21), in his paper published in 1974, gives a brief history of the testing problems and the evolutionary process to arrive at today's state of the art.

Carino states the following conclusions from his review of previous direct tension tests on concrete:

1. Concrete possesses a discontinuity point in direct tension, which occurs at about 70 percent of the short-term ultimate strength.
2. The point of discontinuity corresponds to the formation of the first crack.
3. The stress at discontinuity is the long-term strength.
4. In a controlled tensile strain test, concrete is able to attain very large average strains.
5. The creep behavior of concrete in tension has the same general characteristics as in compression.

The concrete model used by Carino in his experimental work was similar to that of Buyukozturk (ref. 19). The method of loading the specimens in tension was similar to that used by Kupfer (ref. 17). Figure 6 presents a plot of the discontinuity and failure envelopes obtained from the experiments. Figure 7 shows the failure curves defined by Kupfer (ref. 17) and Nelissen (ref. 22). It is interesting to note several items concerning Carino's pair of curves. The first is that the discontinuity curve is of the same shape as Kupfer's ultimate envelope. The second point is that Carino states his ultimate curve may be a little inaccurate due to testing apparatus limitations. Hence, he gives credence to Kupfer's envelope.

The last point to mention is that under biaxial tension the discontinuity stress point and ultimate stress point essentially coincide, whereas Kupfer's criterion follows more along the lines of brittle fracture. Possibly the difference can be accounted for by Kupfer's using real concrete and Carino a concrete model.

2. STATICALLY LOADED TRIAXIALLY STRESSED PLAIN CONCRETE

Until the last 10 years, very little testing had been done concerning the triaxial strengths of concrete. Most likely this was due to the severe requirements placed upon testing equipment and procedures.

Hannant (ref. 23) surveyed triaxial experimental testing quite well in his 1968 paper. From a plot of experimental data collected from several researchers, he was able to qualitatively draw a failure envelope in triaxial compression. Figure 8 presents this envelope. The cross-hatched portion of this plot shows the well defined biaxial stress state.

Endebrock and Traina of New Mexico State University (ref. 24) concluded a biaxial and triaxial testing program for the Air Force in 1972. Most of the effort was for triaxial compression, with only a few tests involving tension stresses. A good condensation of previous triaxial tests up through 1969 is also presented in this paper. A general conclusion of this research is that the biaxial strength curve is quite well-defined for all principal stress ratios. Comparisons of triaxial strengths of concrete were made in pure compression only as no previous tension-compression results were published. Figure 9 presents a typical plot of triaxial strength for varying principal stress ratios. Qualitatively the plot confirms the general shape of the strength envelope proposed by Hannant in Figure 8. Further test results by Terra-Tek using cube specimens were incorporated into this report. The results of these tests provided strength curves of similar shapes; however, the actual strength values were found to be somewhat lower than those of the New Mexico State tests. Figure 10 presents the comparison of the two tests for the triaxial compression tests.

3. EFFECT OF DYNAMIC LOADS ON PLAIN CONCRETE

The correct analysis for the response of a complete structural system requires a full understanding of the material of which the structure is composed. This full understanding of the material implies knowledge of the material's simple behavior when experiencing the same type of loads as the structure of interest; i.e., rate and magnitude of loading. For materials such as steel this type of knowledge is well-documented. Plain concrete, however, due to its variable composition, is not well-defined. Its behavior under triaxial quasi-static stresses is just beginning to become well-documented. Also explanations or quantitative theories for how concrete behaves under triaxial quasi-static stress vary from report to report. Hence, until researchers begin to agree upon behavior patterns of plain concrete under static stresses, any quantitative or even qualitative explanations for the behavior of plain concrete under dynamic loads should be scrutizined carefully.

This section presents a summary of work done for determining behavior of plain concrete under dynamic loads. Brink, et al (ref. 25) conducted uniaxial tests on cylindrical specimens. The experimental study was to statically preload the plain concrete specimens to various stress levels, apply a small half-sine wave as a dynamic pulse, and observe the behavior. The motivation for the research was to determine the extent that the dynamic behavior of concrete under dynamic loads would be dependent upon the magnitude of preloading. Three static preload stress conditions were tested. The first stress, 2000 psi, represents the initial loading of concrete where the local stress-strain are proportional to each other.

The second stress, 4000 psi, corresponds to the nonlinear portion of the stress-strain curve; and the last preload stress, 6000 psi, represented a loading near ultimate. The lengths of the dynamic impulses varied from 25 ms to 2650 ms. The results of tests at the lowest preload stress, 2000 psi, showed that application of dynamic load does not have much effect on the response of concrete. However, at the higher preloads, the deviation from the normal stress-strain curve was more pronounced. Also, the shorter the dynamic pulse, the greater the deviation. A typical plot of the results of one of the tests is given in Figure 11. Figure 12 presents a plot describing the increase in elastic modulus for each preload condition as a function of dynamic pulse duration. In general, the study shows that the further the concrete is along the stress-strain curve the more dramatically the stiffness increases due to dynamic loads. Also, it was observed that the higher the loading rate, the more the concrete stiffness increases.

Sparks (ref. 26) conducted a study into the effects of the rate of application of steadily increasing loads upon the static strength of plain concrete in compression. Concretes made with gravel, limestone, or lytag aggregate were tested. The results showed that the static strength and stiffness of concrete is increased at higher rates of application of load. It was found that limestone, the stiffest of the aggregates, produced concrete with an improvement of only 4% in static strength with a hundredfold increase in rate of loading. Lytag, the least stiff of the aggregates, produced concrete with a strength improvement of 16% for a similar increase in rate of loading.

4. REINFORCEMENT BOND SLIP

Bond deterioration between steel and concrete can significantly influence the behavior of reinforced concrete structures, especially under load reversals (ref. 27).

Moritz and Kaku (ref. 28) conducted an experimental program to evaluate local bond slip deterioration under load reversals. Figure 13 shows some typical results of their studies. They proposed a bond slip law but its complexity makes it computationally undesirable.

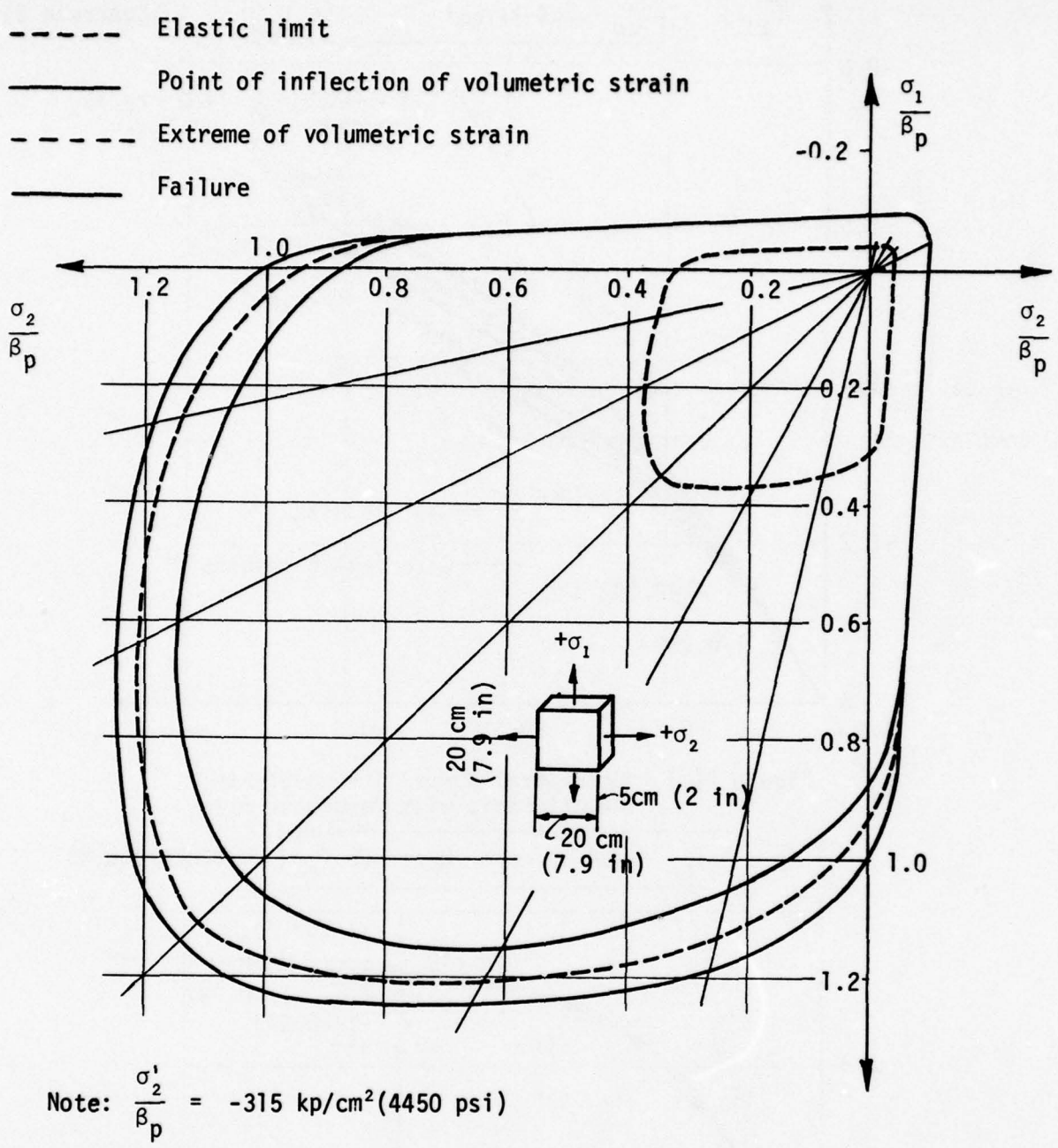

Note: $\frac{\sigma'_2}{\beta_p}$ = -315 kp/cm^2(4450 psi)

Figure 1. Stresses at the Elastic Limit, Minimum Volume and Failure of Concrete Subjected to Biaxial Stress States

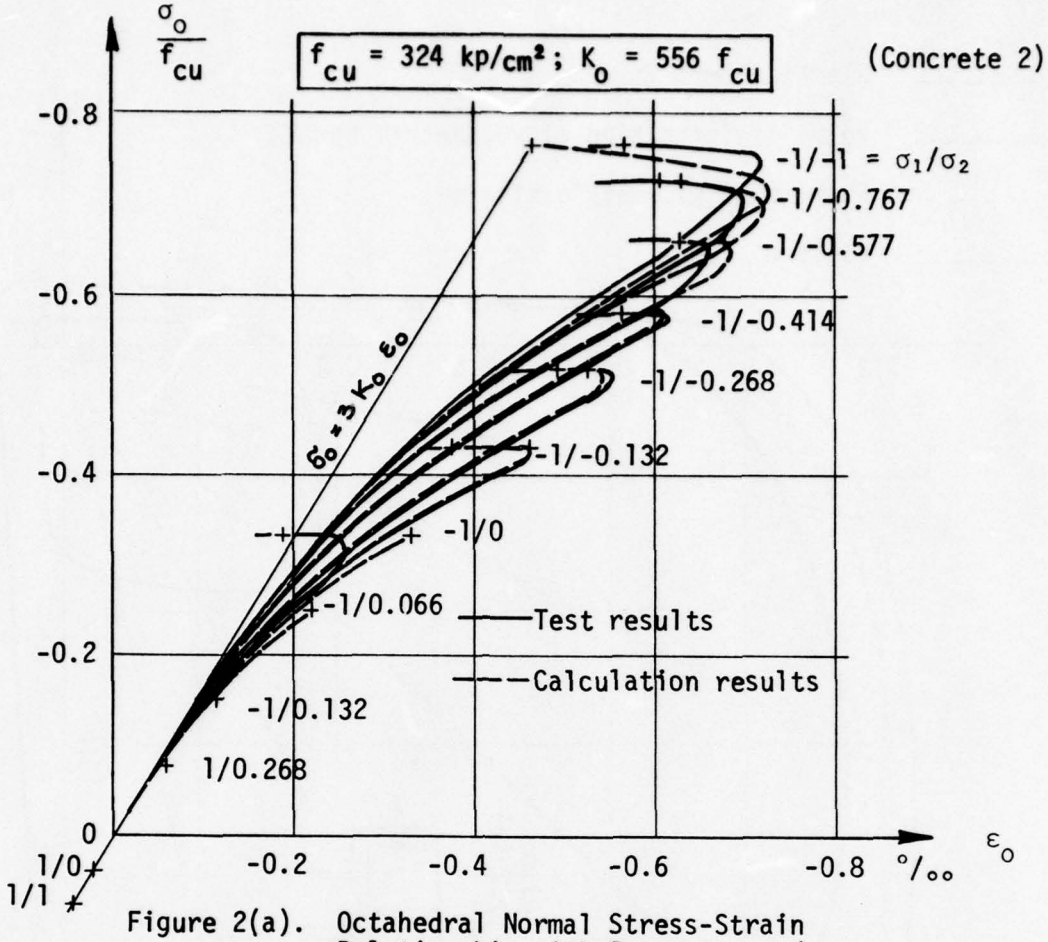

Figure 2(a). Octahedral Normal Stress-Strain Relationship with Parameter σ_1/σ_2

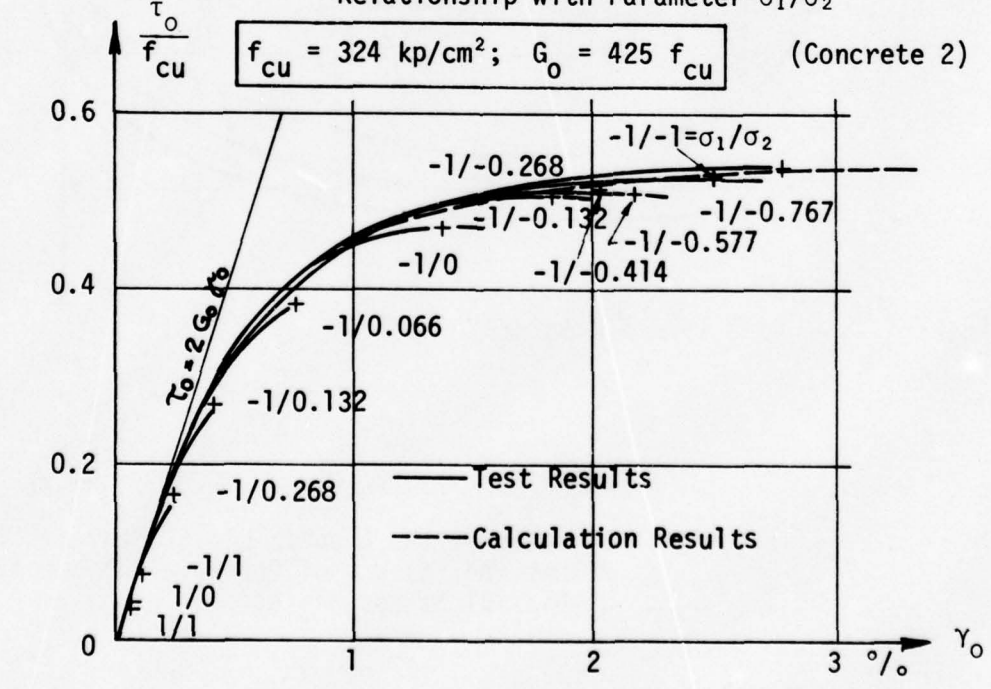

Figure 2(b). Octahedral Shear Stress-Strain Relationship with Parameter σ_1/σ_2

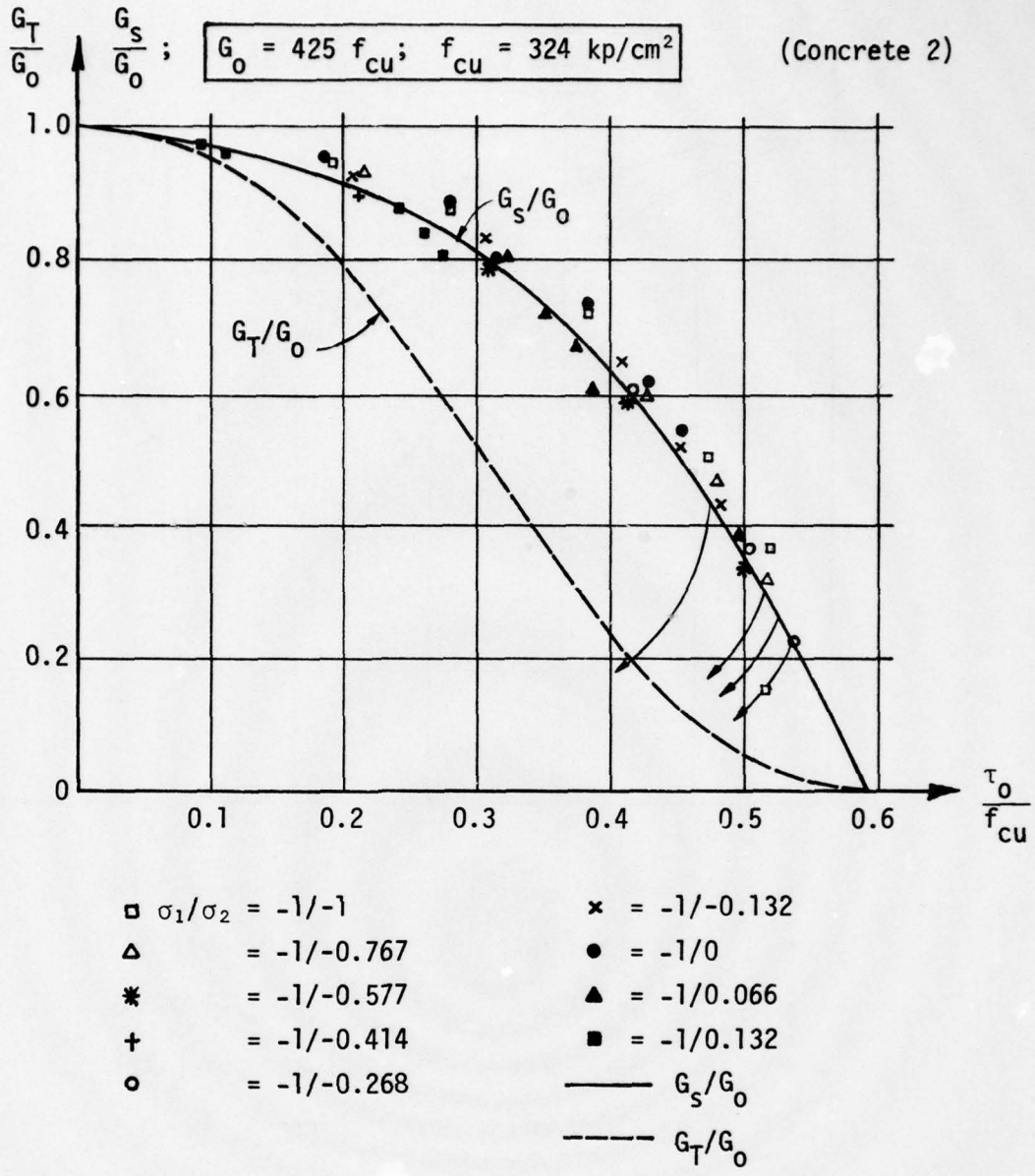

Figure 3. Shear Modulus G--Octahedral Shear Stress τ_o Relation

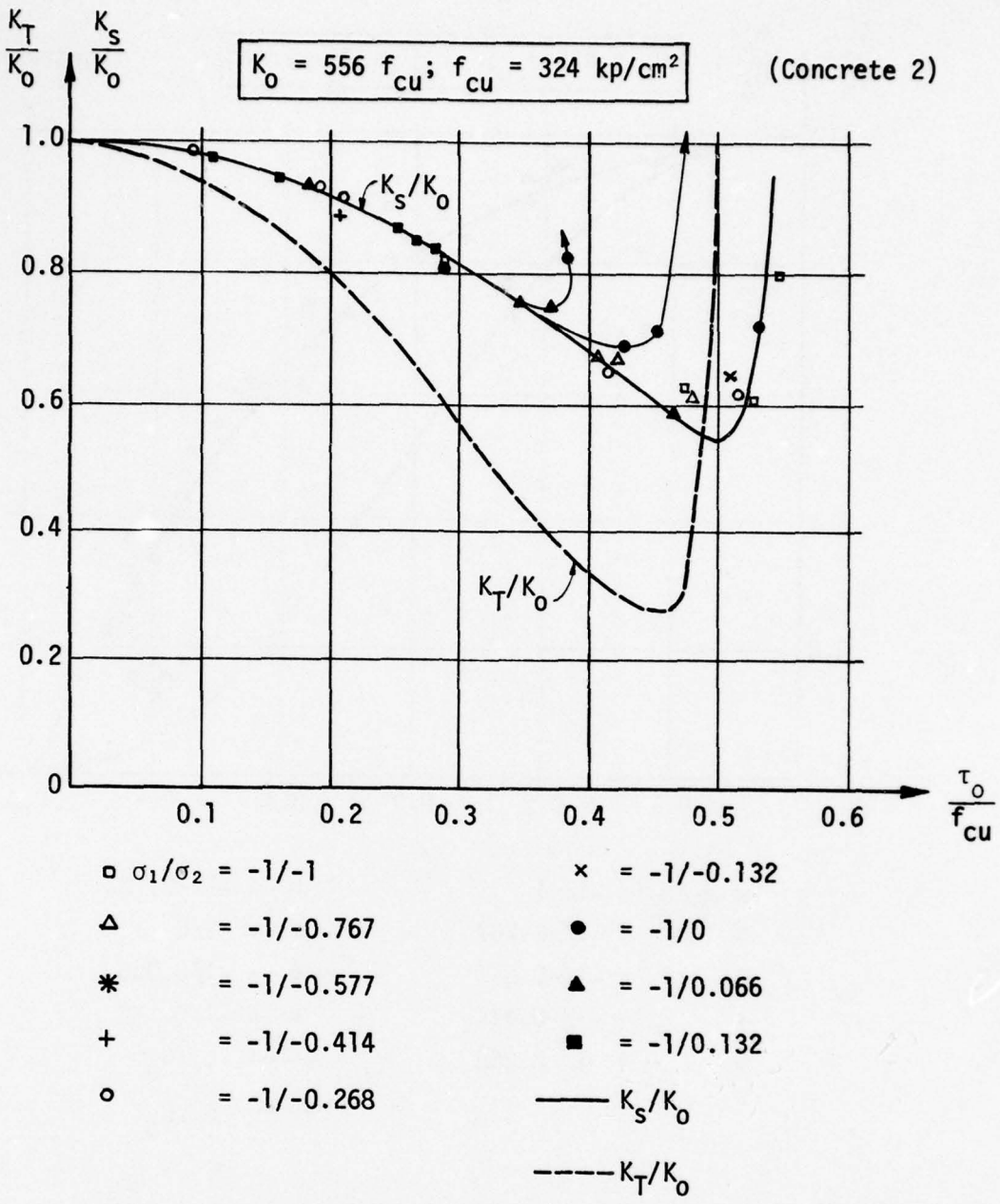

Figure 4. Bulk Modulus K--Octahedral Shear Stress τ_o Relation

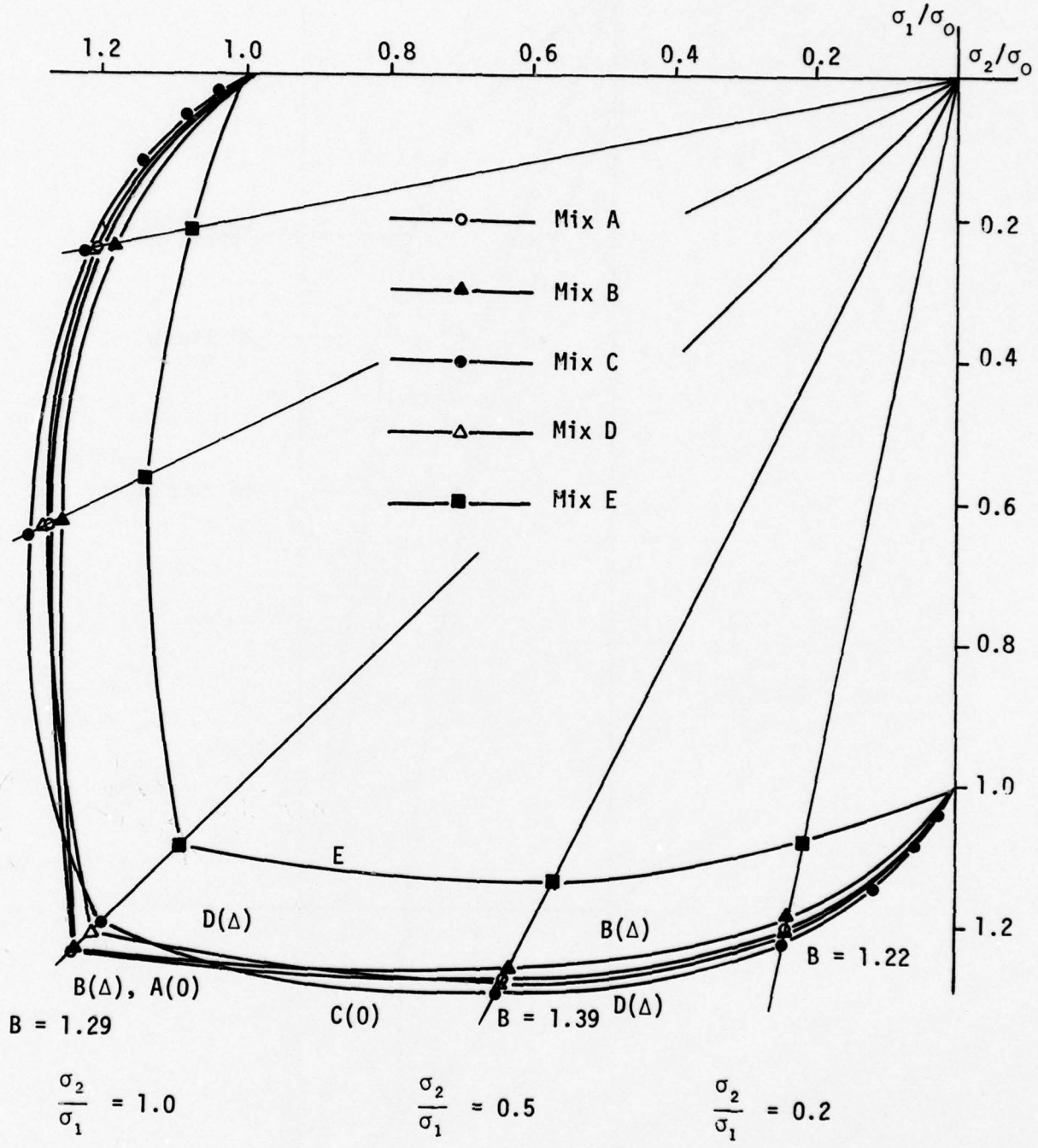

Figure 5. Strength of Concrete under Biaxial Compression

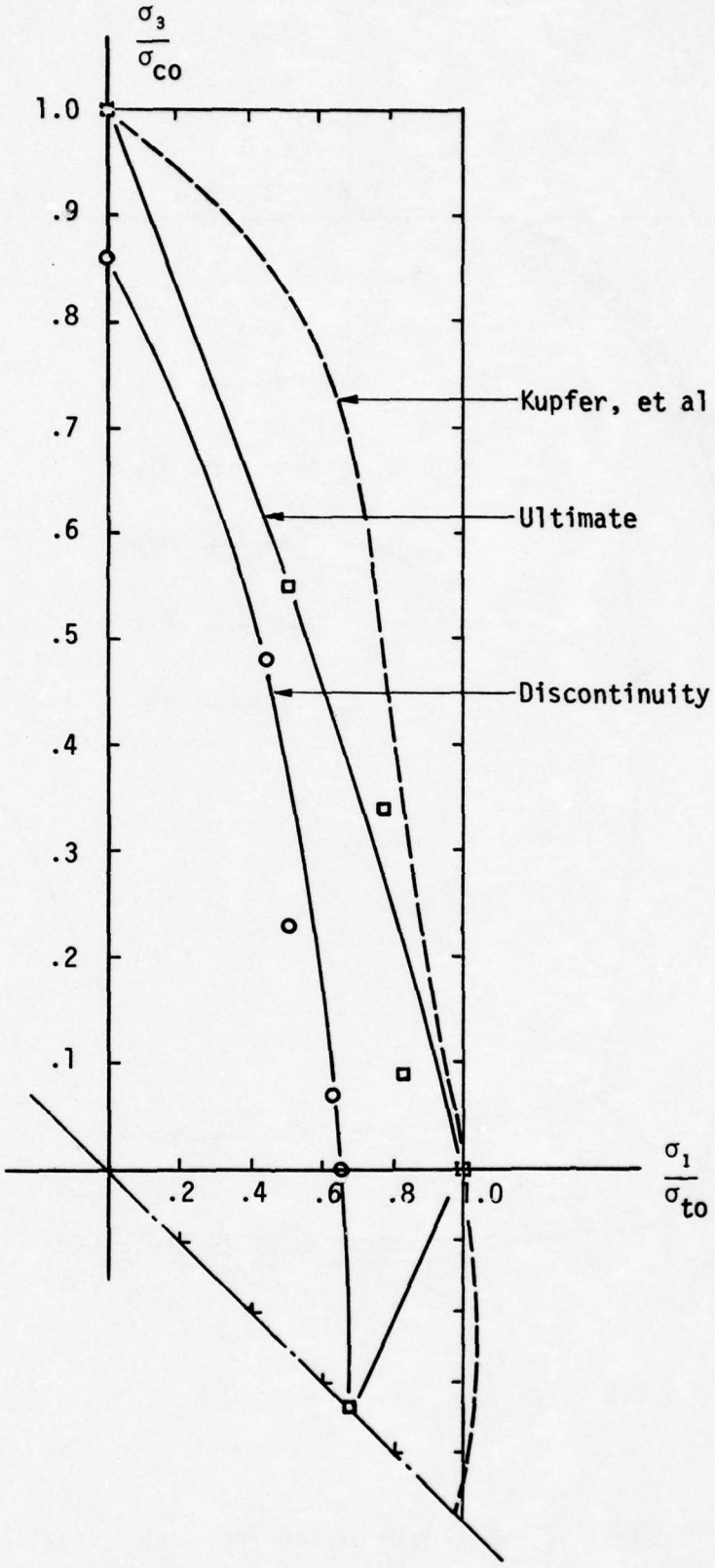

Figure 6. Discontinuity and Ultimate Strength Envelopes for Model

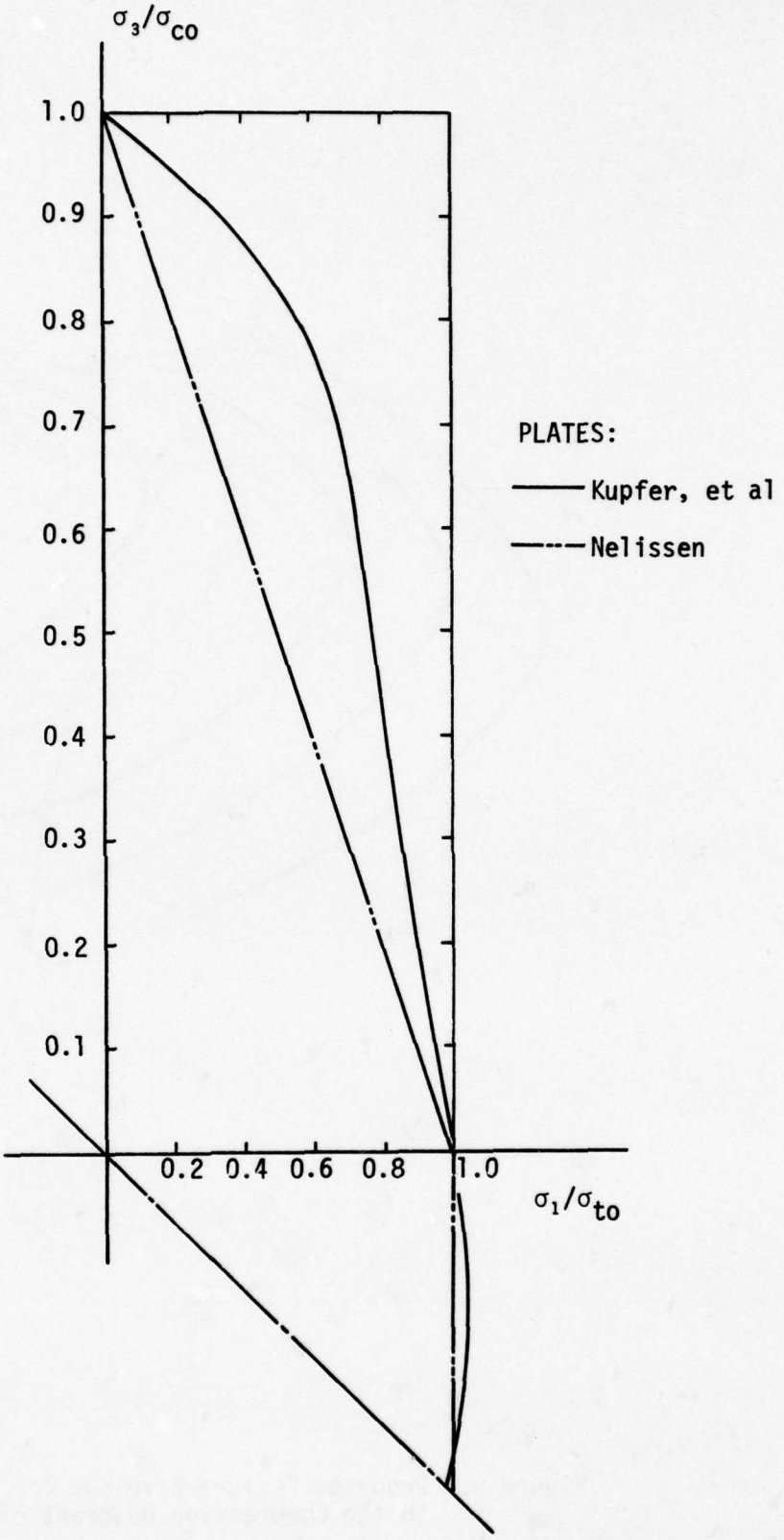

Figure 7. Comparison of Experimental Failure Envelopes for Compression-Tension and Tension-Tension Loadings

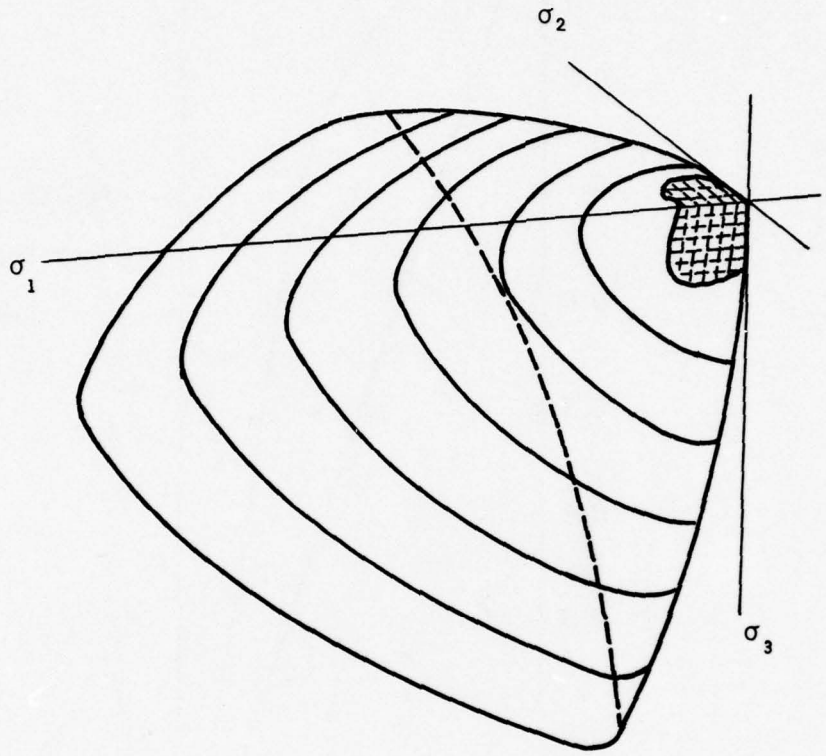

Figure 8. Proposed Failure Envelope for Concrete in the Compression Quadrant of Stress Space

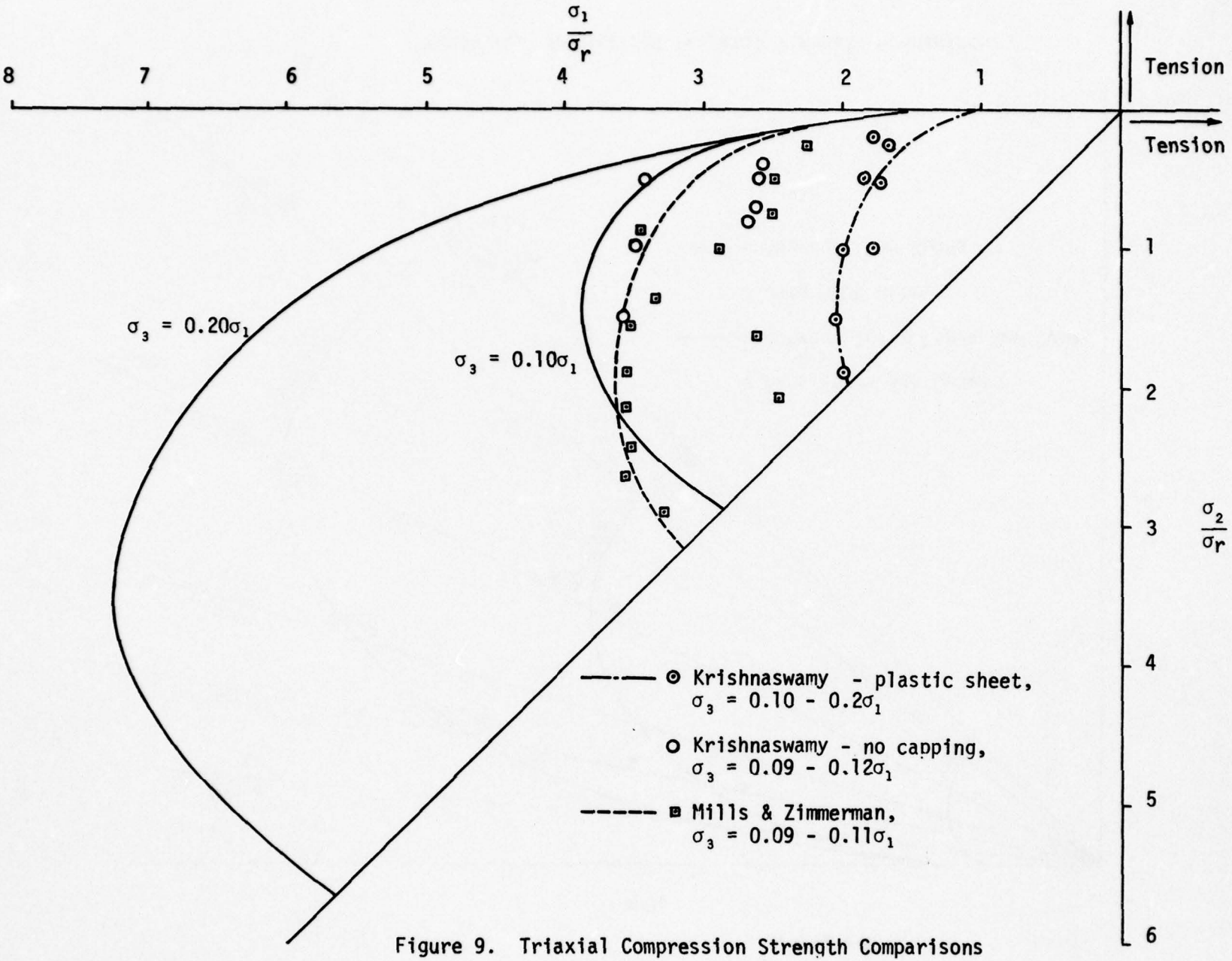

Figure 9. Triaxial Compression Strength Comparisons

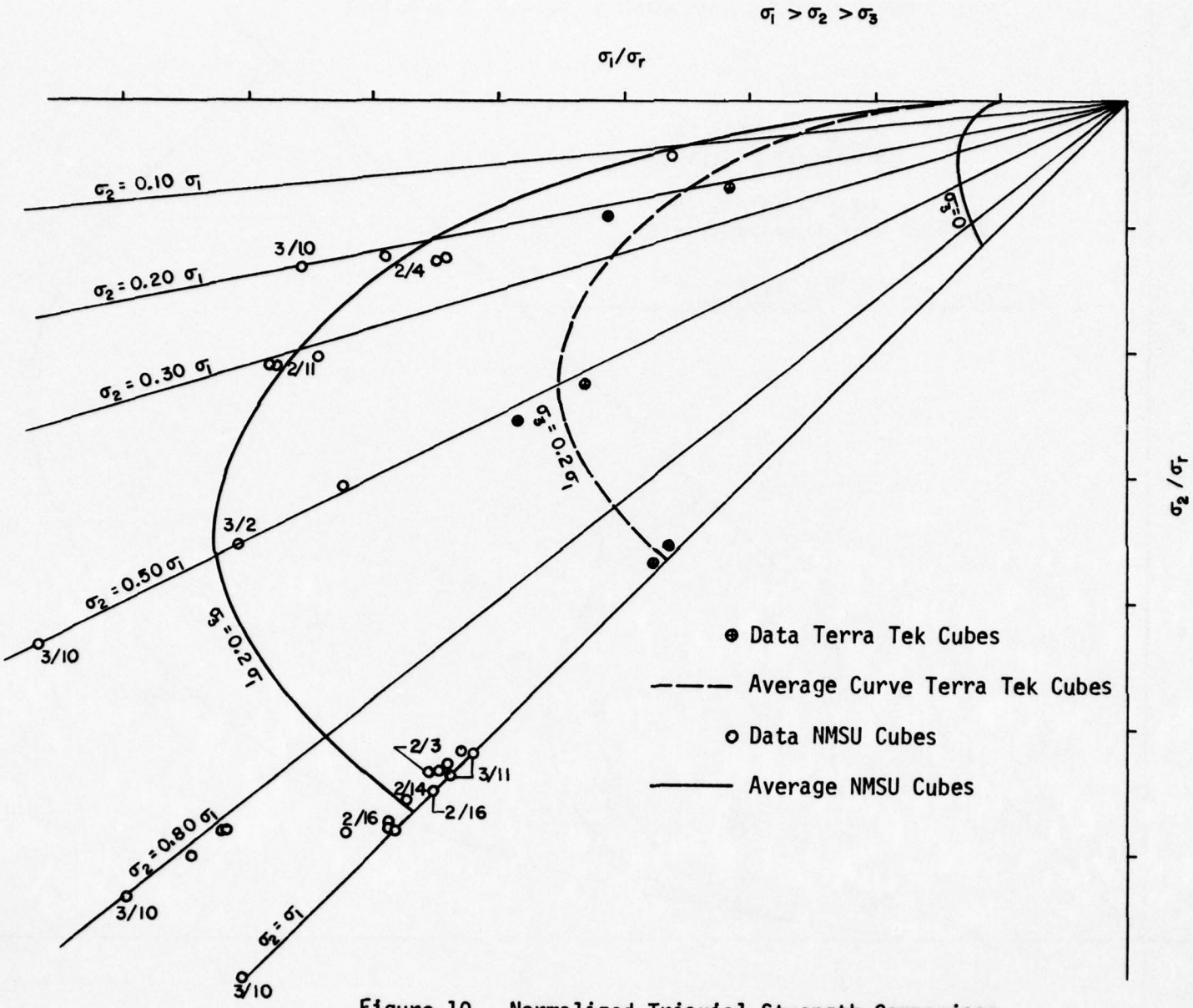

Figure 10. Normalized Triaxial Strength Comparison

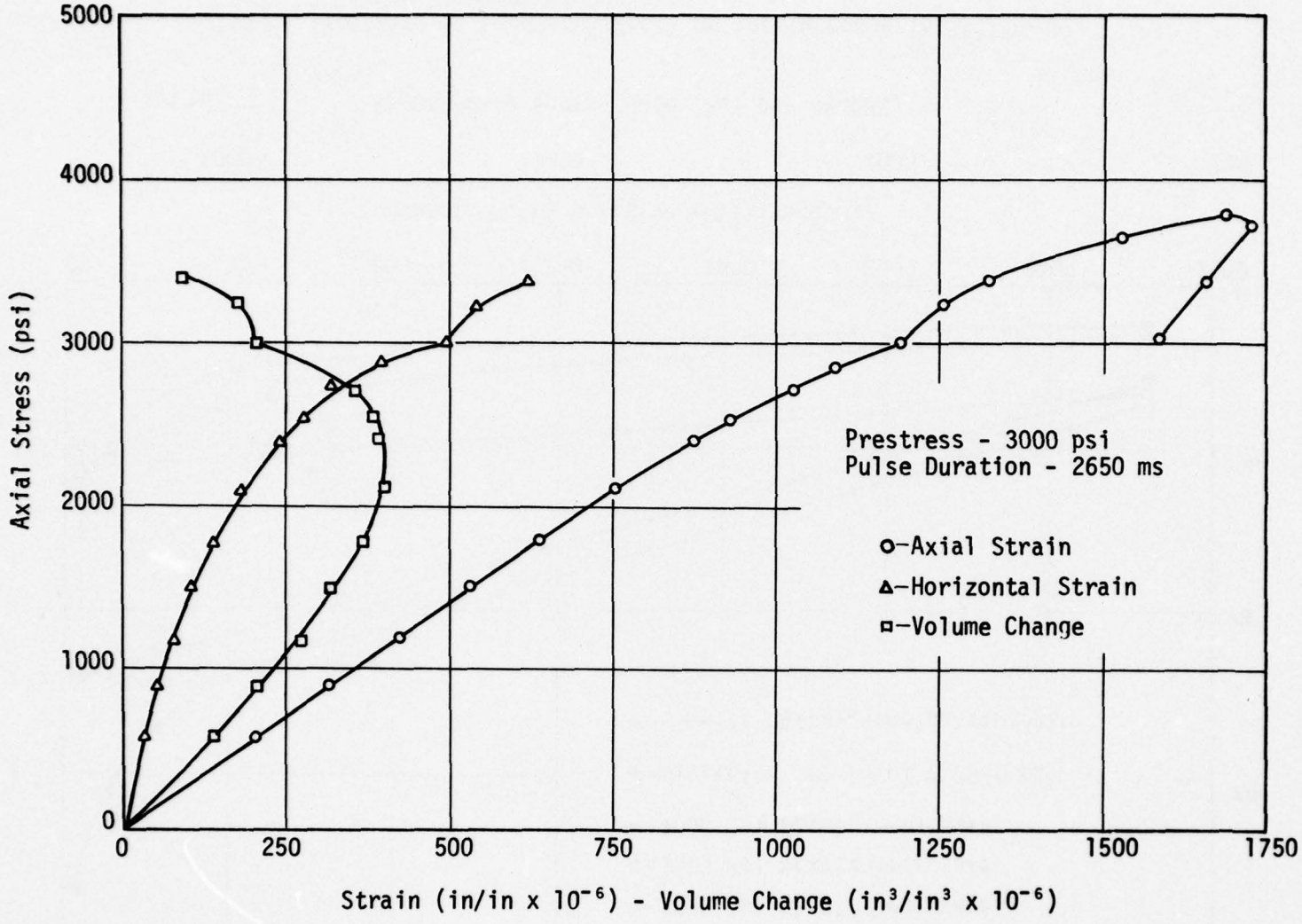

Figure 11. Response of Concrete to Dynamic Pulse with Preload Stress

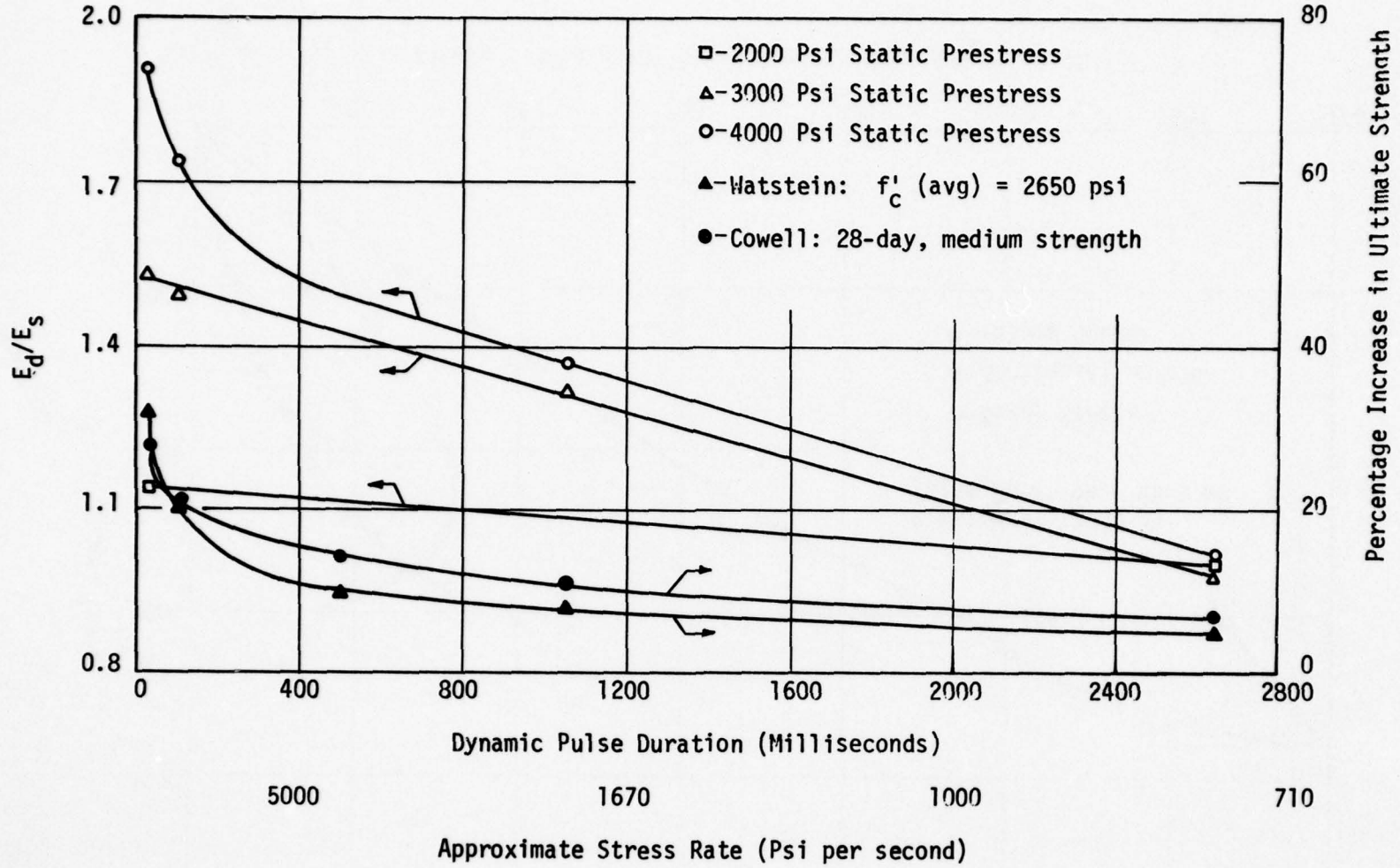

Figure 12. Rate of Loading Effects on the Increase in Stiffness and Strength of Concrete

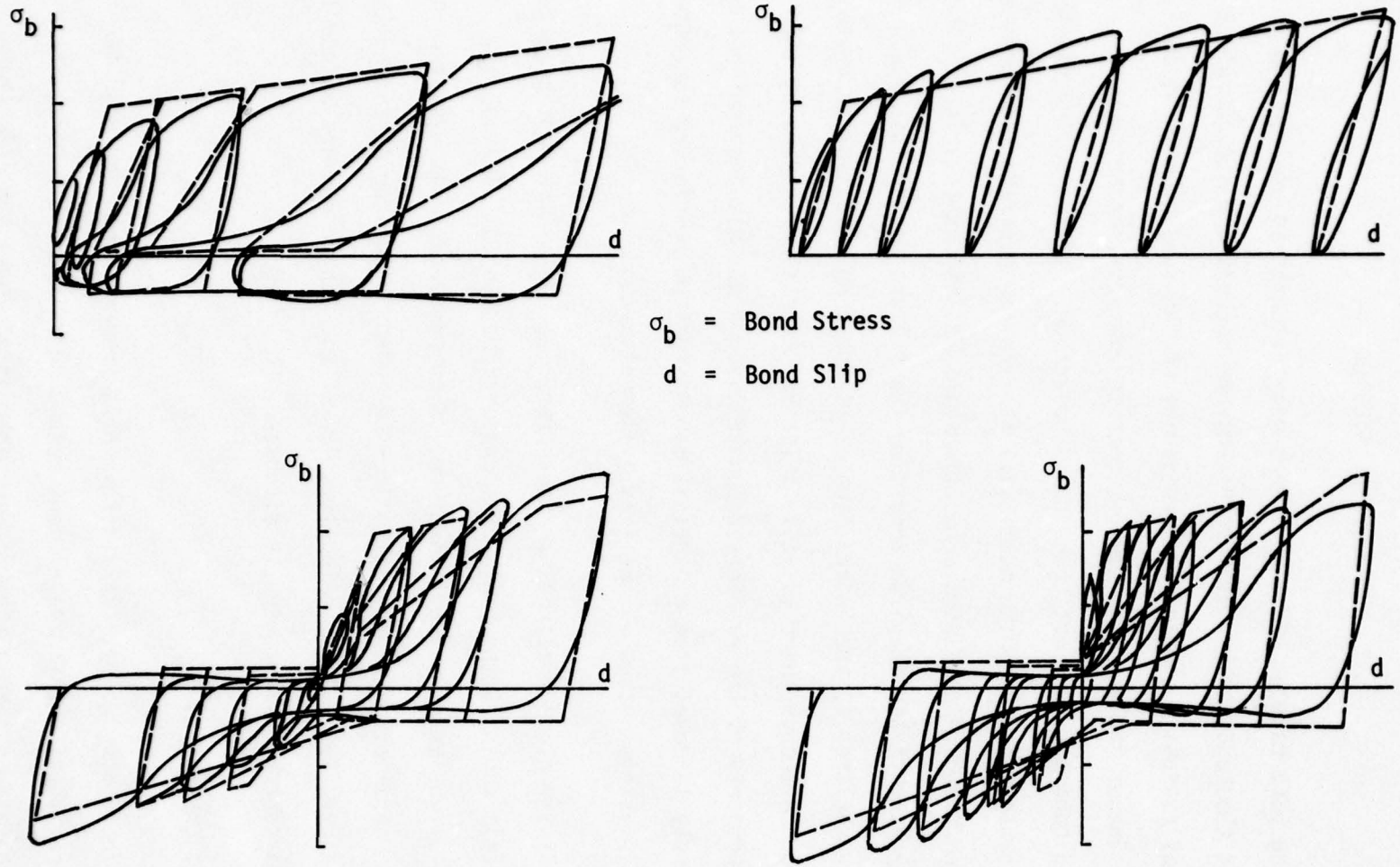

σ_b = Bond Stress

d = Bond Slip

Figure 13. Bond Slip Curves under Various Load Histories

SECTION III

ANALYTICAL STUDIES

In the past decades there have been many attempts to analyze and comprehend the behavior of reinforced concrete members and structural systems. For various reasons a complete understanding of the subject has not been reached. One of the major reasons is that the material properties of reinforced concrete have not been fully understood. There are insufficient data available concerning the multiaxial behavior of concrete. Information on the multiaxial stress-strain relationships is inadequate. It is also not firmly established in which condition the failure cracks initiate and propagate. Neither is the interaction of reinforcing steel and concrete well understood. Although there is still a lot of uncertainty regarding the material property of the reinforced concrete, considerable progress has been made recently in developing analytical models for the reinforced concrete structural systems, based on the finite element method.

The finite element method has been proven as one of the most powerful and versatile tools in the field of structural mechanics. It has been described extensively in the literature. A comprehensive discussion of the theory and application of the method can be found in any one of the well-known textbooks (ref. 29). Only the application of the finite element method to reinforced concrete structures is discussed.

1. ANALYTICAL MODELS

There are two basically different approaches that are used for the application of the finite element method to reinforced concrete structures. The one, the discrete element approach, is to model the concrete and the

reinforcing steel as discrete elements. The other, the composite element approach, is to construct a composite modulus from individual properties of concrete and reinforcing steel.

In the discrete element approach, the reinforced steel elements are connected to the concrete elements at the nodal points. Composite action is enforced through compatibility at the nodes. A bond linkage element may be used to simulate bond slip behavior.

Ngo and Scordelis (ref. 30) presented the first finite element model for the analysis of a reinforced concrete beam with the discrete element approach. Simple beams were represented by two-dimensional triangular finite elements.

Ngo, Scordelis and Franklin (ref. 31) extended the work by using refined linkage elements to include the influence of stirrups, dowel shear, aggregate interlock, etc. Nilson (ref. 32) also refined the work of Ngo and Scordelis by introducing nonlinear material properties and nonlinear bond-slip relationships into the model to analyze beam-type structures. Taylor, etc. (ref. 33, 34) adopted Kupfer, Hilsdorf and Rusch (ref. 35) experimental results incorporated into the discrete element approach to predict the behavior of axisymmetric-type reinforced and prestressed concrete structures. Salam & Mohraz (ref. 36) applied the discrete element approach to study the nonlinear behavior of planar reinforced concrete structures with octahedral shear stress failure criteria to check crack or yield. Since 1973, Argyris et al (refs. 37, 38, 39) studied nonlinear behavior and ultimate load for prestressed and reinforced concrete reactor structures by the discrete element approach. Litton (ref. 27) developed a two-dimensional finite

element for predicting brittle material response under cyclic loading, which included crack formation, closure, and reopening effects. In addition, a bond link element models concrete-reinforcement bond and slip. The results compared favorably with experimental data.

The more recent work by Sarne (ref. 40) uses three-dimensional finite element analysis for reinforced and prestressed concrete structures by using the discrete element approach. For the discrete element approach applied to reinforced concrete structures, concrete is idealized as 2-D or 3-D elements, and the reinforcing steel is modeled by 2-D elements or truss-bar elements, as shown in Figure 14.

The composite element approach combines the variation in steel and concrete properties and constructs a composite modulus or stiffness for a reinforced concrete element to account for the composite behavior of the element. Usually the bond between reinforcing steel and concrete is assumed to be fully effective. But some investigators (ref. 41) still included the influence of the bond slip in the construction of the composite modulus.

Mikkola and Schnobrich (ref. 42) applied the finite element method to study the response of reinforced concrete shells by constructing a composite modulus as follows:

$$\underline{C} = \alpha_c \cdot \underline{C}_c + \alpha_s \cdot \underline{C}_s \qquad (4)$$

in which $\underline{C}$ = material property matrix for a composite element

$\underline{C}_s$ = material property matrix for reinforced steel

$\underline{C}_c$ = material property matrix for plain concrete

α_s = relative area of the reinforcing steel

= A_s/A

A_s = steel area

A = total area

α_c = relative area of the plain concrete

= $1 - \alpha_s$

Scanlon (ref. 43) analyzed slabs with the composite element approach. Time dependent effects of shrinkage and creep were also included.

Yuzugullu and Schnobrich (refs. 44, 45) obtained the composite material property matrix for the reinforced concrete model as the sum of the material property matrices of concrete and reinforcement:

$$\underline{C} = \underline{C}_c + \sum_{i=1}^{n} \alpha_i \underline{C}_s^i \qquad (5)$$

in which α_i = the percentage of reinforcement in i-direction

$$= \frac{\text{area of reinforcement in i-direction}}{\text{concrete area}}$$

Any number of reinforcement directions can be accommodated. Due to the presence of reinforcement, the reinforced concrete model is no longer isotropic. The directions of the principal stresses and the principal strains would be different. Three types of structures, a deep beam, a shear panel, and a shear wall-frame, were analyzed. Aggregate interlock, or the ability of a cracked element to transfer shear, was included in the analysis. A constant value of shear stiffness was assumed for all the cracked elements.

Cervenka (ref. 46), Cervenka and Gerstle (refs. 47, 48) studied the in-plane response of a wall panel with the composite material property matrix calculated in the same way. The shear resistance of the cracked concrete owing to the aggregate interlocking and reinforcement dowel effect was neglected. This may contribute to the underestimation of the stiffness of the theoretical model in the cracked stage.

Hand, Pecknold and Schnobrich (refs. 49, 50) studied the load-deflection history up to failure of reinforced concrete slabs and shells by a layered system (Figure 15). The element is divided into a number of layers over the depth. Each layer is assumed to be in a state of plane stress and may have different material properties corresponding to its material state. Lin (ref. 51), Lin and Scordelis (refs. 52, 53) used the same approach to do nonlinear analysis of reinforced concrete shells of general form. The differences between the two works were

1. A flat triangular element adaptable to free-form shell surfaces and arbitrary boundary geometries was used in Lin's work, while Hand's work used a shallow shell element to analyze plates and shallow shells.
2. The tension stiffening effect of the concrete between cracks, neglected in Hand's work, was included in Lin's work. It was found in Lin's work that the effect had significant influence on the post-cracking load-deflection response of underreinforced concrete structures.

Wanchoo and May (ref. 54) also adopted a similar approach to performing cracking analysis of reinforced concrete plates. It may be noted that the classical Kirchhoff assumption was incorporated into the layer system

approach. The assumption states that a normal remains normal during deformation, so each layer is considered to be in a state of plane stress with properties defined through biaxial stress-strain relationships. Because of this assumption, shear modes of failure with their associated diagonal cracking cannot be solved with this scheme. Three-dimensional models become a necessity for the investigation of any failure development where shear is a major consideration.

Rajagopal (ref. 55) adopted the same approach to study the reinforced concrete beams, beam columns and slabs. Adlstedt (ref. 56) used a similar approach to investigate the nonlinear behavior of reinforced concrete frames. The effects of geometric nonlinearities were considered in both works.

Adham, Braunick and Isenberg (ref. 41) developed for AFWL an equivalent continuum approach, similar to a composite element approach applicable to beams, beam columns and ring beams subjected to static and dynamic loading. A single stress-strain relationship was derived directly for reinforced concrete. Bond slip and dowel shear relations were incorporated into the model.

Basically speaking, the discrete element approach is more straightforward in the mathematical procedures and simpler for computer programming. The composite element approach is more flexible for different arrangements of the reinforcement. The orientation and location of the reinforcement do not influence the arrangement of element mesh for the composite element approach so much as it does for the discrete element approach.

So far, the finite element method has provided the basis for all the analytical solutions, and the nonlinear effect is based on the basic nonlinear stress-strain law. An alternative approach, the modified EI approach, may replace the composite element approach to study the nonlinear response of reinforced concrete structures. The approach is based on an empirical moment-curvature relationship, wherein different flexural rigidities are assumed for different material states. Jofriet and McNiece (ref. 57) used a bilinear moment-curvature relation to study the reinforced concrete plate bending problem. Bell (ref. 58) adopted a similar material idealization to study slabs and shells. Cracking of flat slabs was studied with this approach by Jofriet (ref. 59). The advantage in using the modified EI approach would be in the reduction of computer costs for similar analyses.

2. MATHEMATICAL MATERIAL MODELS

No matter what analytical approach is used, it requires a mathematical material model for each individual component, concrete and reinforcing steel to simulate the material behavior. Compared to concrete, the material property of steel is very well-defined. Current yield criterion and stress-strain relations for steel have been demonstrated to be adequate in predicting steel behavior even in the plastic range. In contrast, the behavior of concrete is complicated, and there still exists a lot of uncertainty regarding the material property of concrete. Any mathematical material model applied in analytical approaches to simulate a realistic behavior of concrete must employ drastic idealizations. Many models have been proposed to simulate reinforced concrete behavior using finite element methods. Review of these models is discussed in the following paragraphs.

a. Linear Elastic Model with Linkage Element

The first finite element model for the analysis of a reinforced concrete beam was developed by Ngo and Scordelis (ref. 30). In their studies, simple beams were analyzed in which the concrete and steel reinforcement were represented by plane stress triangular finite elements. Special linkage elements were developed to connect the reinforcing steel to the concrete to represent the bond-slip phenomena (Figure 16). Linear elastic analyses were performed on reinforced concrete beams with predicted crack patterns to determine principal stresses in the concrete, stresses in the steel reinforcement, and bond stresses. Ngo, Scordelis, and Franklin (ref. 31) extended this work to study shear in beams with diagonal tension cracks. The model was refined by representing the steel reinforcement and the concrete by quadrilateral elements, and the vertical stirrups were modeled by truss bar elements (Figure 17). The influence of dowel shear, aggregate interlock, and horizontal splitting along reinforcement near the support was considered.

However, a linear elastic model is not suitable for the study of the behavior of reinforced concrete structures over the entire range of loading. Nilson (ref. 32) introduced nonlinear material properties and a nonlinear bond-slip relationship into the model and used an incremental loading technique to account for these nonlinearities. In all these studies, cracking of concrete was introduced by physically splitting a node and allowing a separation to develop along interelement boundaries. Cracks were therefore restricted to propagate only along

interelement boundaries. In order to be effective and have the element boundaries in the proper location for the crack, previous knowledge of the location of the crack was required, or undue constraint was placed on the direction of the development of the crack path (Figure 18). Furthermore, the disruption of structural continuity due to cracks results in a continual change in the topology of the structure. This presents a number of analytical difficulties and some computational inefficiency and restricts the model application to static load cases only.

Recently, Ngo (ref. 60) developed a network-topological approach to simulate crack growth by automatically generating crack line in the finite element model. However, this approach is still in the infant stage, and research is needed to make this model more workable.

b. Orthotropic Material Model

Rashid (ref. 61) performed a nonlinear analysis of axisymmetric prestressed concrete nuclear reactor pressure vessels with an orthotropic material model. Instead of redefining the new topology of the structure (i.e., new finite element mesh and connectivities), the cracking of concrete was taken into account by modifying the material properties and redistributing the unbalanced (residual) stresses. The mechanics of accounting for tension cracking involved computation of principal stresses or strains which were then compared with a cracking criterion. If the criterion was met or exceeded, a crack was assumed to have developed, stiffness/modulus normal to the crack was reduced to zero, and the stress field associated with the cracking was redistributed to the rest of the structure. This model allows free development

of cracking without predefining the cracking path, and permits the use of the same structural topology throughout the solution, rather than the necessity for splitting the nodes after cracking and establishing a new topology. However, none of the nonlinear effects of concrete in the compression region were considered realistically.

c. Hypo-Elastic Model (Nonlinear Elastic Model)

Liu, Nilson and Slate (ref. 62) developed an equivalent constitutive relationship for concrete based on an orthotropic material assumption using some experimental data of biaxial compression tests. The equivalent stress-strain relationship is given as

$$\sigma = \frac{\varepsilon E}{(1-\nu\alpha)\left[1 + \left(\frac{1}{1-\nu\alpha}\,\frac{E}{E_s} - 2\right)\left(\frac{\varepsilon}{\varepsilon_p}\right) + \left(\frac{\varepsilon}{\varepsilon_p}\right)^2\right]} \qquad (6)$$

in which

σ, ε = stress and strain respectively

ν = Poisson's ratio

α = ratio of the principal stress in the orthogonal direction to the principal stress in the direction considered.

E = initial tangent modulus in uniaxial loading

E_s = current modulus at the ultimate load

For concrete in tension, it was assumed that the behavior is linear up to failure. For an elastic orthotropic material in biaxial stress, the constitutive relationship may be written as

$$\begin{Bmatrix} \sigma_1 \\ \sigma_2 \\ \tau_{12} \end{Bmatrix} = \begin{bmatrix} E_1^* & \nu^* & \\ \nu^* & {}_2^* & \\ & & G_{12}^* \end{bmatrix} \begin{Bmatrix} \varepsilon_1 \\ \varepsilon_2 \\ \gamma_{12} \end{Bmatrix} \tag{7}$$

where

$$E_1^* = \frac{E_1}{1-\nu_1^2 E_2/E_1} \qquad E_2^* = \frac{E_2}{1-\nu_1^2 E_1/E_2} \qquad G_{12}^* = \frac{E_1 E_2}{E_1+E_2+2\nu_1 E_2}$$

in which

$\sigma_1, \sigma_2, \varepsilon_1, \varepsilon_2$ = principal stresses and strains, respectively.

τ_{12}, γ_{12} = shear stress and strain in principal direction, respectively.

E_1, E_2 = uniaxial tangent modulus in principal direction 1 and 2, respectively.

ν_1 = uniaxial Poisson's ratio in the principal direction 1.

Kupfer and Gerstle (ref. 63) developed another hypo-elastic model based on an isotropic formulation using variable bulk moduli and shear moduli. Another hypo-elastic model for triaxial states of loading was derived by Coon and Evans (ref. 64). Incremental constitutive laws and their associated failure criteria were presented for plain concrete based on an assumption of isotropic material. Argyris, et al. (ref. 37) discuss some of the problems involved in using the hypo-elastic model. With this model the modulus E becomes anisotropic in the nonlinear range, even though the behavior is isotropic in the

initial linear range. This implies different behavior in the principal stress directions. It also suggests that the principal directions of stress and strain are different, introducing coupling between normal stresses and shear strains. It requires an increase in the number of material moduli to define this anisotropic behavior. In addition, failure condition must be supplied to match the realistic deformation behavior of concrete in the ultimate response regime.

d. Combined Behavior Model

In the last several years research has been directed primarily toward development of more realistic analytical models for reinforced concrete and/or plain concrete. Most of them may be included in this group.

A typical stress-strain relation for plain concrete under uniaxial condition is shown in Figure 19. The linear elastic region is followed by a hardening range in which internal microcracking progressively weakens the material property up to the ultimate stress point. Upon continued loading the curve deteriorates, indicating softening in the structure up to the rupture point at which sudden collapse is observed. The behavior in tension is linear elastic followed by a sudden crack.

Cervenka (refs. 46, 47, 48) studied inelastic behavior of reinforced concrete panels by assuming reinforcing steel to be elastic perfectly plastic in both compression and tension (Figure 20). The concrete was assumed to be elastic perfectly plastic in compression and elastic brittle in tension (Figure 21). The von Mises yield criterion for

compression plasticity and maximum normal stress theory for tension cracking was adopted to approximate the failure surface of the concrete in biaxial stress state (Figure 22). Yuzugullu and Schnobrich (refs. 44, 45) applied the same material model for the prediction of inelastic behavior of shear wall-frame systems.

Hand, Pecknold and Schnobrich (refs. 49, 50) derived a layered system to analyze reinforced concrete plates and shallow shells. The concrete was considered as bilinear elastic or perfectly plastic material in compression and elastic brittle in tension (Figure 23). A yield criterion in biaxial stress state proposed by Kupfer, Hilsdorf and Rusch (ref. 35) was used. The yield surface was modified to serve as the transition criterion to determine the boundaries of the different material property zones. This was accomplished by simply scaling down the yield surface of Kupfer, Hilsdorf and Rusch. A crush surface, analogous to the yield surface but in terms of strain, was proposed to limit the deformation behavior of the compression concrete (Figure 24).

Lin and Scordelis (refs. 51, 52, 53) proceeded along a similar approach to perform nonlinear anlaysis of reinforced concrete shells of general form. However, the material model and failure conditions were slightly different from Hand's work. The concrete was assumed to be elastic perfectly plastic in compression and elastic brittle in tension (Figure 25). Because of the tension stiffening effect, the concrete was considered to release its stress gradually after it cracked. Therefore, there existed a cracked unloaded portion in the tension region of the stress-strain curve for concrete (Figure 26). The von Mises yield

criterion was used to approximate the failure surface in biaxial compression (Figure 27). The associated flow rule was assumed to govern the post-yielding stress-strain relations for concrete. A crush surface, analogous to the yield surface but in terms of strains, was postulated to define the complete crush for the yielded concrete (Figure 28). The maximum stress failure theory was adopted for biaxial tensile stress state. For the tension-compression stress state, a straight line was used to approximate the true failure surface (Figure 27). The reinforcing steel in both Lin's and Hand's works was considered as an elastic perfectly plastic material. In addition, the reinforcing bars were assumed to carry only axial stress.

Gormack (ref. 65) adopted a material model similar to the one proposed by Lin and Scordelis to analyze shell walls and two-dimensional structures. The only difference was that the stress-strain curve for concrete in compression proposed by Liu, Nilson and Slate (ref. 62) was used instead of the assumption of elastic perfectly plastic behavior.

Salem and Mohraz (ref. 36) analyzed planar reinforced concrete structures with finite elements. The stress strain curve for concrete with an artificial unloading portion in tension and elastic perfectly plastic behavior in compression was assumed (Figure 29). The octahedral shear stress failure criterion was considered to check yielding or cracking (Figure 30). Crushing of concrete took place if the equivalent uniaxial plastic strain exceeded a prescribed value. The reinforcement was treated as an elastic perfectly plastic material with von Mises yielding criterion.

Darwin and Pecknold (ref. 66) introduced an analytical model for cyclic biaxial loading for reinforced concrete. The constitutive model for plain concrete was developed to match experimental data on monotonic biaxial and cyclic uniaxial loading, and extended to cover cyclic biaxial loading and multidirectional cracking. The analytical biaxial strength envelope for the proposed model is shown in Figure 31. The proposed model under cyclic load is given in Figure 32. The stress-strain equation suggested by Saenz (ref. 67, 68) was used for the ascending portion of the stress-strain curve for the proposed model (Figure 33). An envelope curve, a set of common points, and a set of turning points were introduced to define unloading and reloading behaviors of concrete under cyclic loading. These introductions made the proposed model more complicated in analytical procedure.

Sarne (ref. 40) extended the analytical method to perform three-dimensional nonlinear analysis of reinforced and prestressed concrete structures. The uniaxial stress-strain relation for concrete was based on the one proposed by Saenz (Figure 34). Concrete was checked for tensile failure using the stress in the principal direction. The maximum stress failure theory was adopted for triaxial tensile stress state. The tensile strength was assumed to decrease linearly with increasing compressive stress in other principal directions. The tensile failure surface is shown in Figure 35. Compressive failure of concrete was also checked using principal stresses. The ultimate strength of concrete was assumed to be affected by compressive stresses in the other principal directions. The failure surface proposed by Khan and Sangy (ref. 69) was used because of better compatibility with biaxial failure criterion.

The surface was a cone center along the average axis of all three principal compressive stress directions (Figure 36). No flow rate was used for the plasticity of concrete in compression.

The modulus of elasticity of concrete was determined based on the uniaxial stress-strain relationship. Each principal stress was taken independently to determine the reduction in the modulus in that direction due to the effect of the stresses in the other principal directions.

Unloading of concrete in compression was treated differently than that in tension. The initial modulus was used for unloading from a state of compression. During reloading, the initial modulus was used until the state when the compressive stress in the concrete reached its previous value. In tension while unloading, if the total strain across the crack was still positive, the crack was considered to be open and no rigidity was considered for that direction. If the strain now was negative, the crack was closed and the rigidity of concrete in compression was used, but this principal direction was fixed. For reloading when tension strain was developed, the same crack would open again.

The reinforcing steel was modeled as an elasto-plastic material having the yield and ultimate properties controlled by von Mises criterion. The recent work done by Rajagopal (ref. 55) may be included in this combined behavior model.

Uncracked concrete element with this type of modeled behavior was considered as an isotropic material. After cracking, the element was considered as an anisotropic material with nonlinear response properties. Stresses and/or strains in the principal directions were used to

check the nonlinear behavior of concrete in compression. The constitutive matrix was expressed in the local coordinate system of principal stresses and strains. Once the material was considered anisotropic, the directions of the principal stresses and strains were no longer coincident with the coordinate axes. This condition resulted in the coupling effect between normal stresses and shear strains. This coupling effect was always neglected by most investigators using the combined behavior model. Since the principal stresses were used to check the formation of cracks, the directions of cracks were orthogonal to each other. This assumption is valid if cracks occur at the same time. Cracks developing at different loading stages are not necessarily orthogonal because of the change of state of stress in the section. This type of behavior was also not considered by most researchers using the combined behavior model. Few have made some modifications by assuming that a second crack develops in the direction with an oblique angle to the first crack, but it doesn't necessarily match the actual situation. In addition, for cyclic loading cases, it becomes necessary to keep track of the direction and width of each crack in the structure, which is computationally complex and expensive.

e. Elastic Brittle Model

Litton (ref. 27) adopted an elastic brittle material model for plain concrete to study a reinforced concrete beam and a wall panel under cyclic loading. The emphasis was placed on tensile cracking, with no attention paid to the nonlinear compression response. Hence a simplified fracture surface with a constant fracture stress was assumed. A

concise and general constitutive theory was presented which permits continual monitoring of crack behavior, including crack closure and reopening under cyclic load. A bond link element was also developed.

f. Linear Elastic Plastic Strain Hardening and Fracture Model

Chen and Chen (refs. 70 and 71) studied some punch indentation problems of concrete by proposing constitutive relations for behavior of concrete. The concrete was considered to be a linear elastic plastic strain-hardening and fracture material. The nonlinear effects caused by the plasticity of concrete in compression and cracking of the concrete in tension were considered in the formulation of these equations. The constitutive model was based on three fundamental assumptions; the shape of an initial discontinuous surface, the evolution of subsequent loading surfaces, and the formulation of an appropriate hardening rule. In other words, initial discontinuous surface, failure surface, and stress-strain curve (Figure 37) shall be defined before the constitutive model is constructed. The failure surface was defined in the stress space such that once the stress state reached this surface, the material would completely rupture and could not resist any further loading. The initial discontinuous surface was a stress surface that could be reached only by elastic action. If concrete was stressed beyond its initial discontinuous surface, microcracks would propagate in the concrete resulting in irrecoverable deformations upon unloading. If concrete was reloaded after such an unloading had occurred, additional irrecoverable deformations would not occur until this new subsequent discontinuous surface was reached.

Concrete failure criterion depends on deviatoric stresses and hydrostatic pressure. Two different but similar functions were used for the failure surface in the compression region and in the tension-compression region; i.e.,

$$f_u(\sigma_{ij}) = \frac{\kappa^2}{3} J_2 - \frac{\kappa^2}{36} I_1^2 \pm \frac{1}{12} I_1^2 + \frac{1}{3} A_u I_1 = \tau_u^2 \qquad (8)$$

where the positive sign in the third term defines the compression region, and negative sign defines the tension-compression region. The failure criterion is a function of I_1, the first invariant of the stress state tensor. The dependence of failure criterion on J_3, the third invariant of the deviatoric stress tensor, was not considered to ensure the simplicity of the formulation of the constitutive relations. The inclusion of J_3 will definitely improve the correlations between the model and experimental results.

The initial discontinuous surface is assumed to take the same form as that of the failure surface.

$$f_o(\sigma_{ij}) = \frac{\kappa^2}{3} J_2 - \frac{\kappa^2}{36} I_1^2 \pm \frac{1}{12} I_1^2 + \frac{1}{3} A_o I_1 = \tau_o^2 \qquad (9)$$

in which A_o, τ_o, A_u and τ_u are material constants, which can be determined from simple tests.

The subsequent loading surfaces are assumed to be similar in form to those of the initial discontinuous and failure surfaces.

If plotted in principal stress space, the initial discontinuous and failure surfaces are given (Figure 38). Good agreement with experimental results in the biaxial cases [i.e., Kupfer, etc. (ref. 35) and Ville (ref. 72)] are also shown in Figure 39.

The elastic-plastic stress-strain incremental relationships of concrete are derived using the classical theory of plasticity. The general form of the incremental elastic-plastic strain-stress relationship may be obtained in the form

$$d\sigma_{ij} = C_{ijkl} \; d\varepsilon_{kl} \tag{10}$$

The stress-strain relations expressed explicitly in matrix form may be used in finite element analysis.

The criterion for unloading from plastic state is given as

$$df = \frac{\partial f}{\partial \sigma_{ij}} \; d\sigma_{ij} < 0 \tag{11}$$

and

$$f(\sigma_{ij}) = \tau \tag{12}$$

The criterion for loading is

$$df = \frac{\partial f}{\partial \sigma_{ij}} \, d\sigma_{ij} = 0 \tag{13}$$

or

$$df = \frac{\partial f}{\partial \sigma_{ij}} \, d\sigma_{ij} > 0 \tag{14}$$

It may be noted that no consideration would be given by this model to determine the orientation and the propagation of each individual crack. The microcracks were assumed to be randomly oriented. The cracking was considered from a macroscopic point of view which could be simulated by the behavior of an equivalent continuum. The change of the material properties due to cracking could be considered by changing constitutive relations at integral points.

In addition, the incremental stress-strain relations were derived based on the classical elastic-plastic model. It has been in this field that the finite element method has been applied most successfully.

g. Other Material Models

Willam and Warnke (ref. 73) developed a three-parameter failure surface for concrete subjected to triaxial loading in the tensile region and in the region of low compressive stresses (Figure 40). The failure surface was convex, continuous with a tension cut-off in the tension regime. The model was refined by adding two additional parameters for describing curved meridians, thus extending the range of application to the high compression region (Figure 41). The constitutive relations were constructed based on an elastic plastic formulation with a brittle failure condition in the tensile regime. Based on the normality principal, explicit expressions were developed for the inelastic deformation rate and the corresponding incremental stress-strain relation. No consideration was given to the formation of each individual crack. Cracking was considered from a macroscopic point of view which could be simulated by the behavior of an equivalent continuum. It is a concept similar to the one proposed by Chen and Chen.

Green and Swanson (ref. 74) derived a three-dimensional static constitutive relation for concrete based on an initial plasticity model used by Swanson for rock, with the yield cap suggested by Baron, et al. An associated flow law and a segmented yield function have been used with a hardening law which includes the shear and dilatation terms. But it cannot handle unloading, nor does it fit in detail the stress dependence of yield. It also cannot uniquely represent the maximum stress surface. Like other plasticity cap models, it appears too complicated to fit data to it.

Bazant (ref. 75) extended the endochronic theory for metals (ref. 76) to describe the inelastic behavior and failure of concrete. The model allows a far better description of the behavior of concrete than other constitutive models. It gives an apparently complete description of the nonlinear behavior of concrete, including creep. Although the theory suitably fits finite element analysis, incorporation would require considerable modification to current programs available.

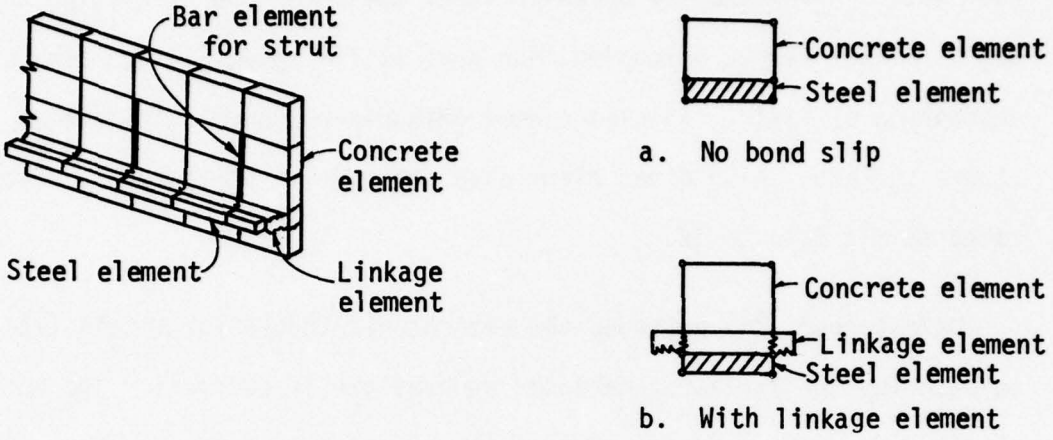

Figure 14. Discrete Element Model

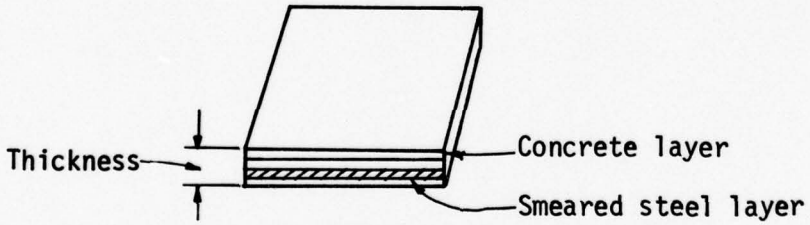

Figure 15. Composite Element Model

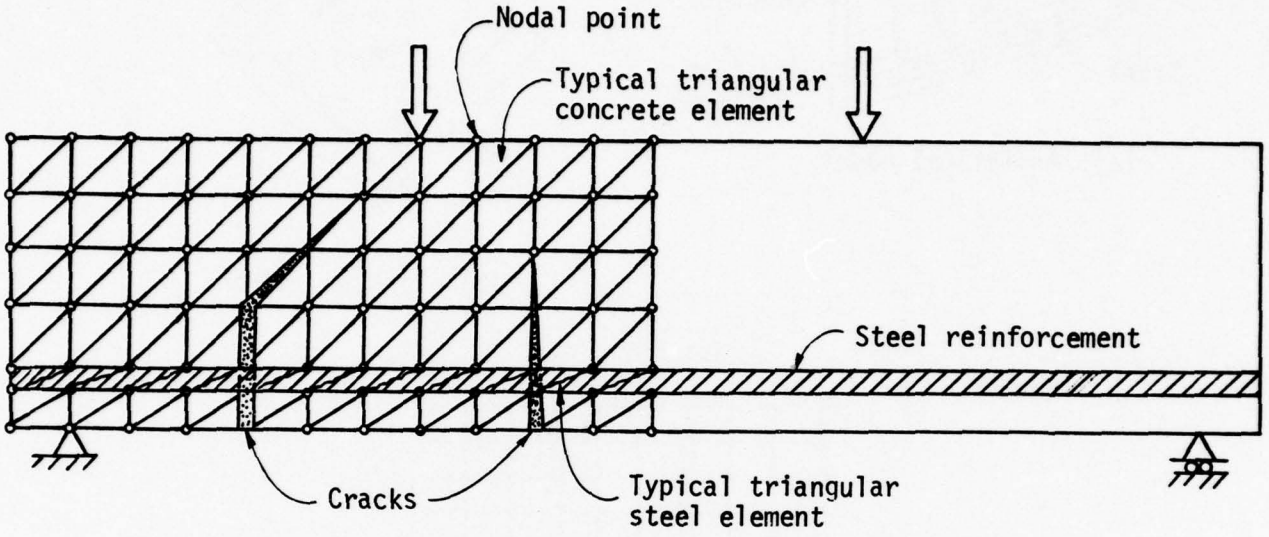

(a) Finite element mesh

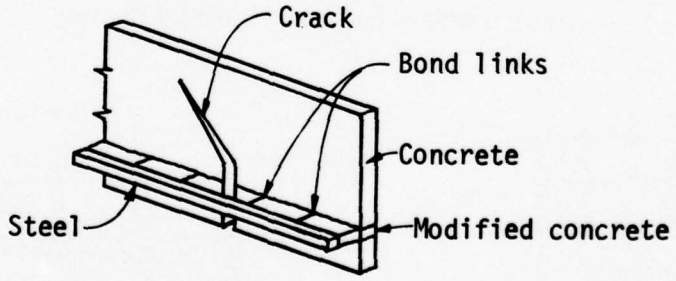

(b) Analytical model

Figure 16. Finite Element Mesh and Analytical Model

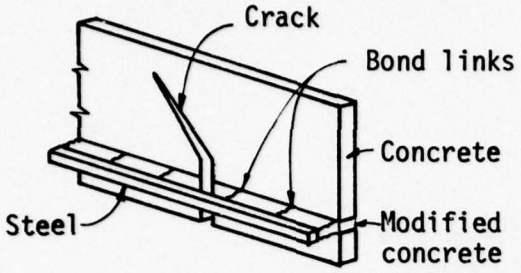

(a) Analytical model

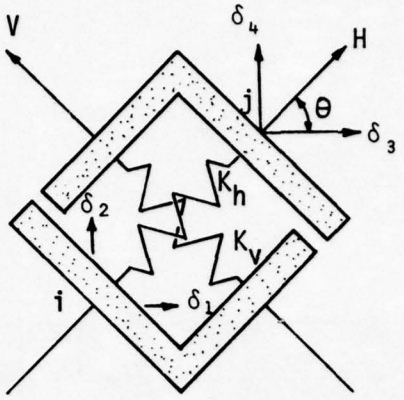

(b) Linkage element

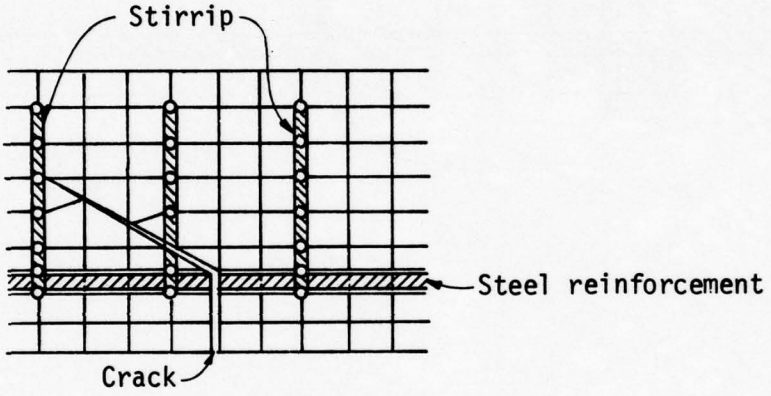

(c) Reinforcement representation

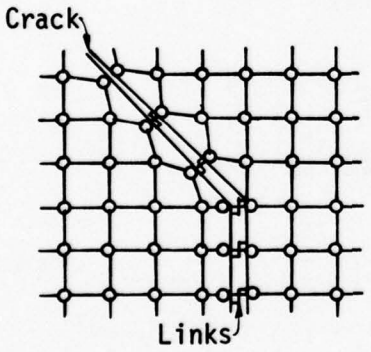

(d) Crack and aggregate interlock

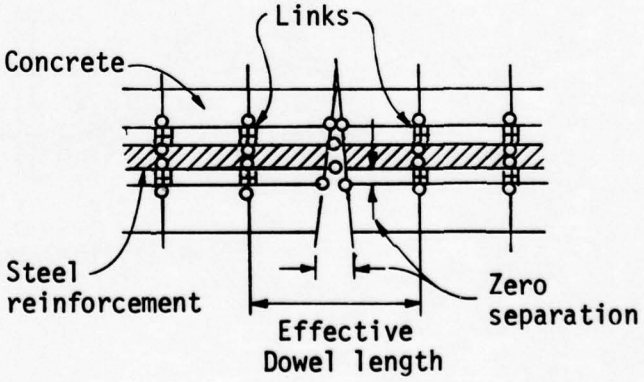

(d) Effective dowel length

Figure 17. Analytical Models and Linkage Elements

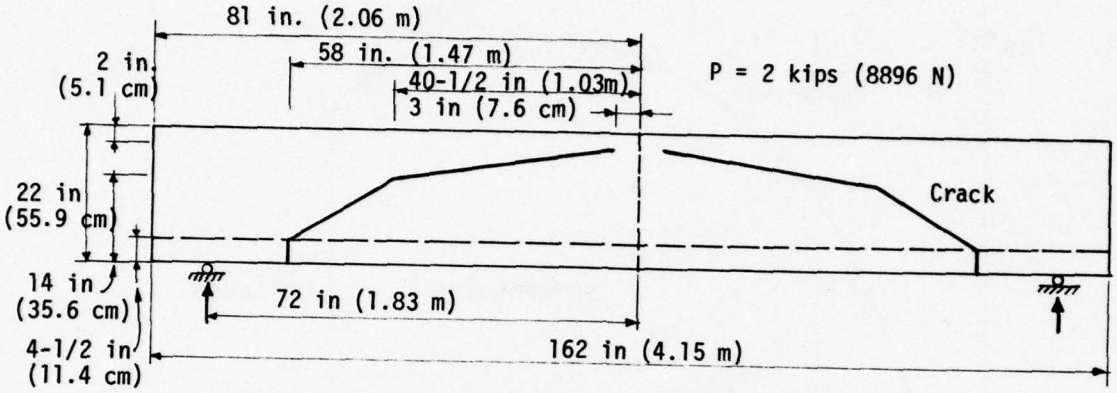

(a) Symmetrical idealized single diagonal crack (beam width = 9 in. [22.86 cm])

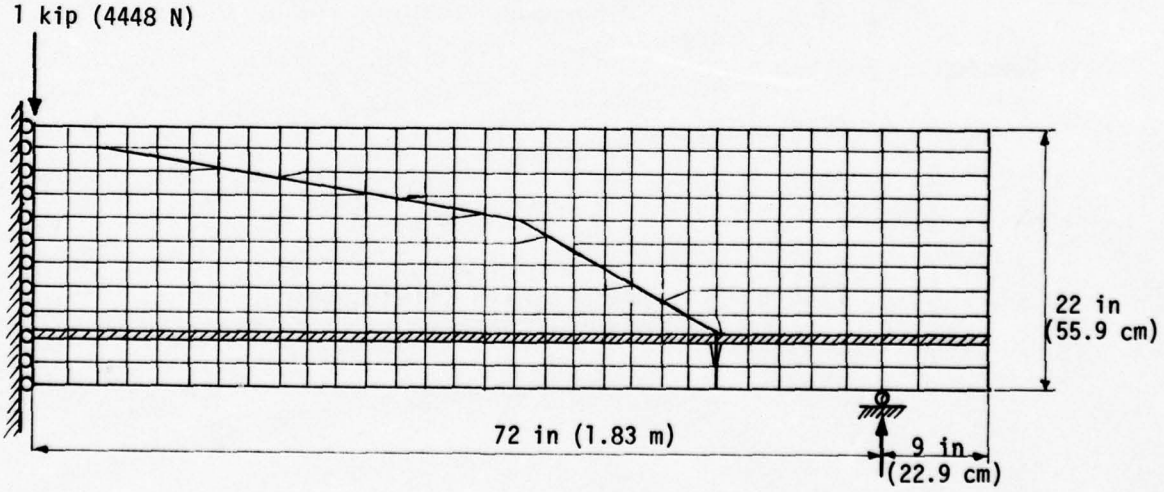

(b) Finite element mesh layout

Figure 18. Linear Analysis of a Beam with a Predefined Crack

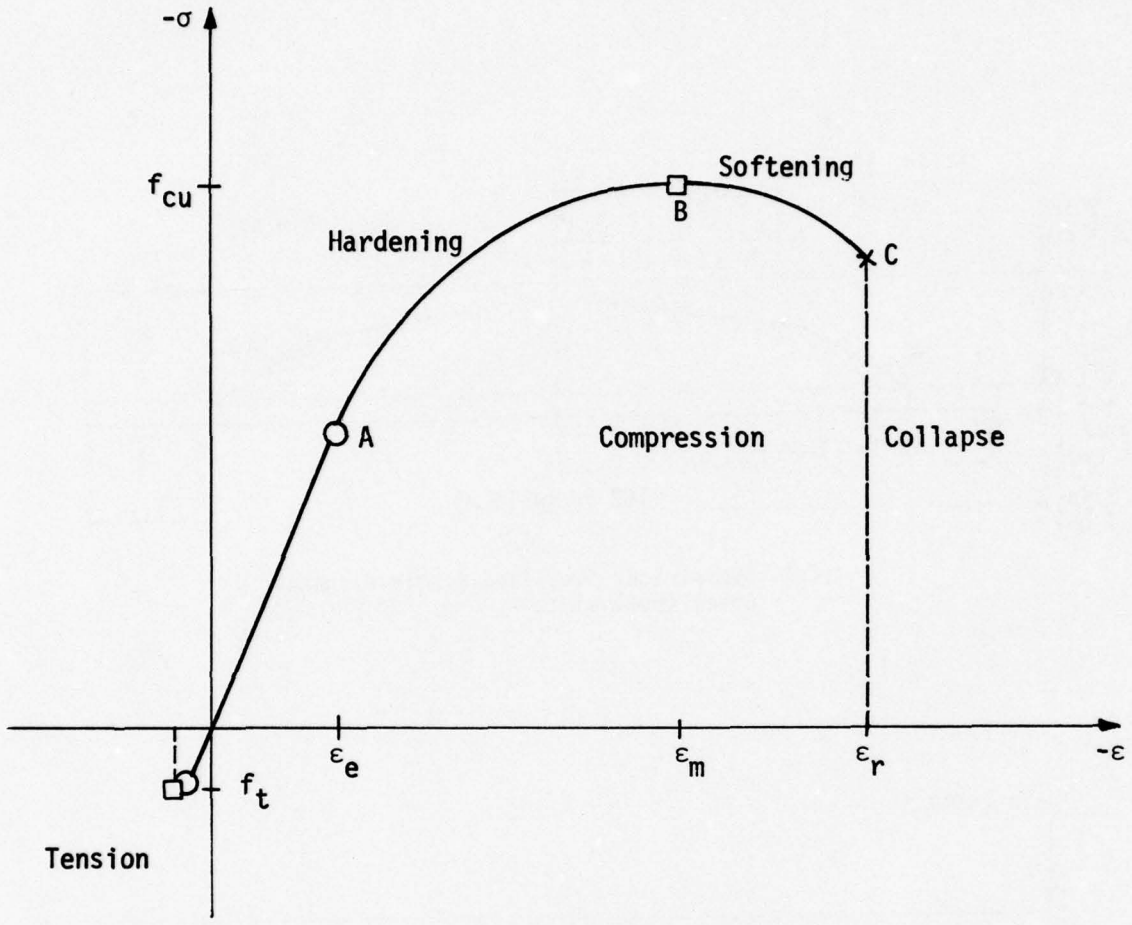

Figure 19. Stress-Strain Relationship.
Uniaxial Behavior of Plain Concrete

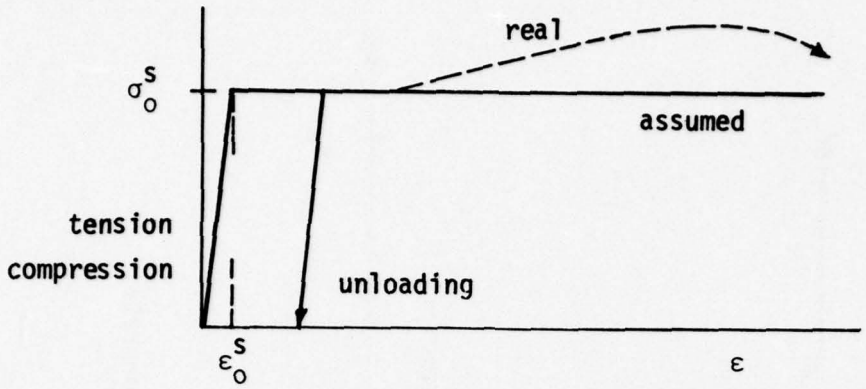

Figure 20. Uniaxial Stress-Strain Relation for Steel Reinforcement

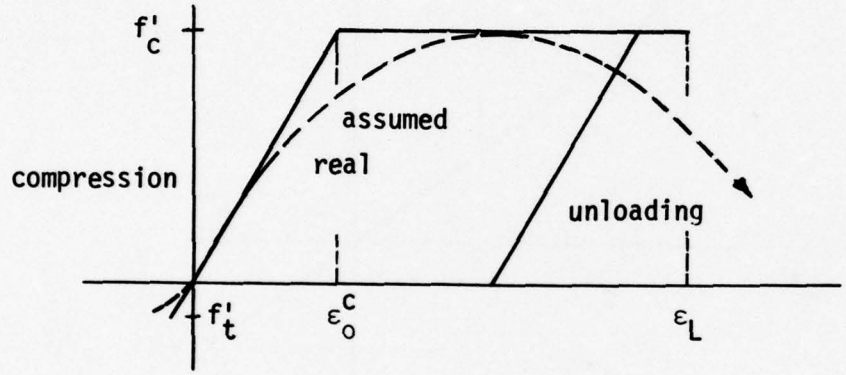

Figure 21. Uniaxial Stress-Strain Relation for Concrete

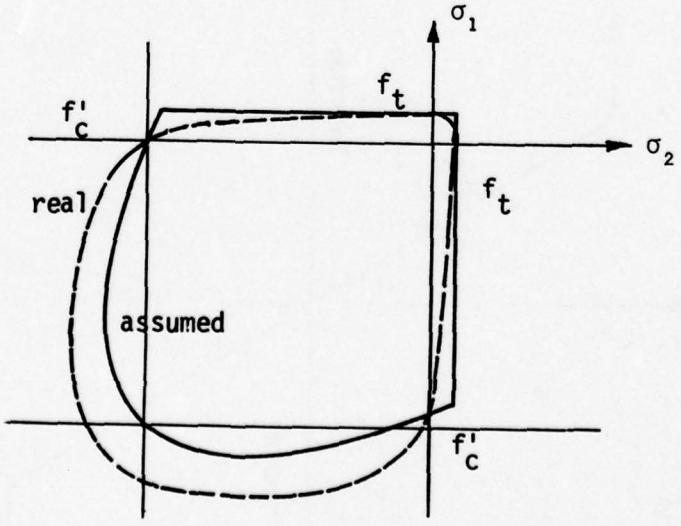

Figure 22. Biaxial Strength of Concrete

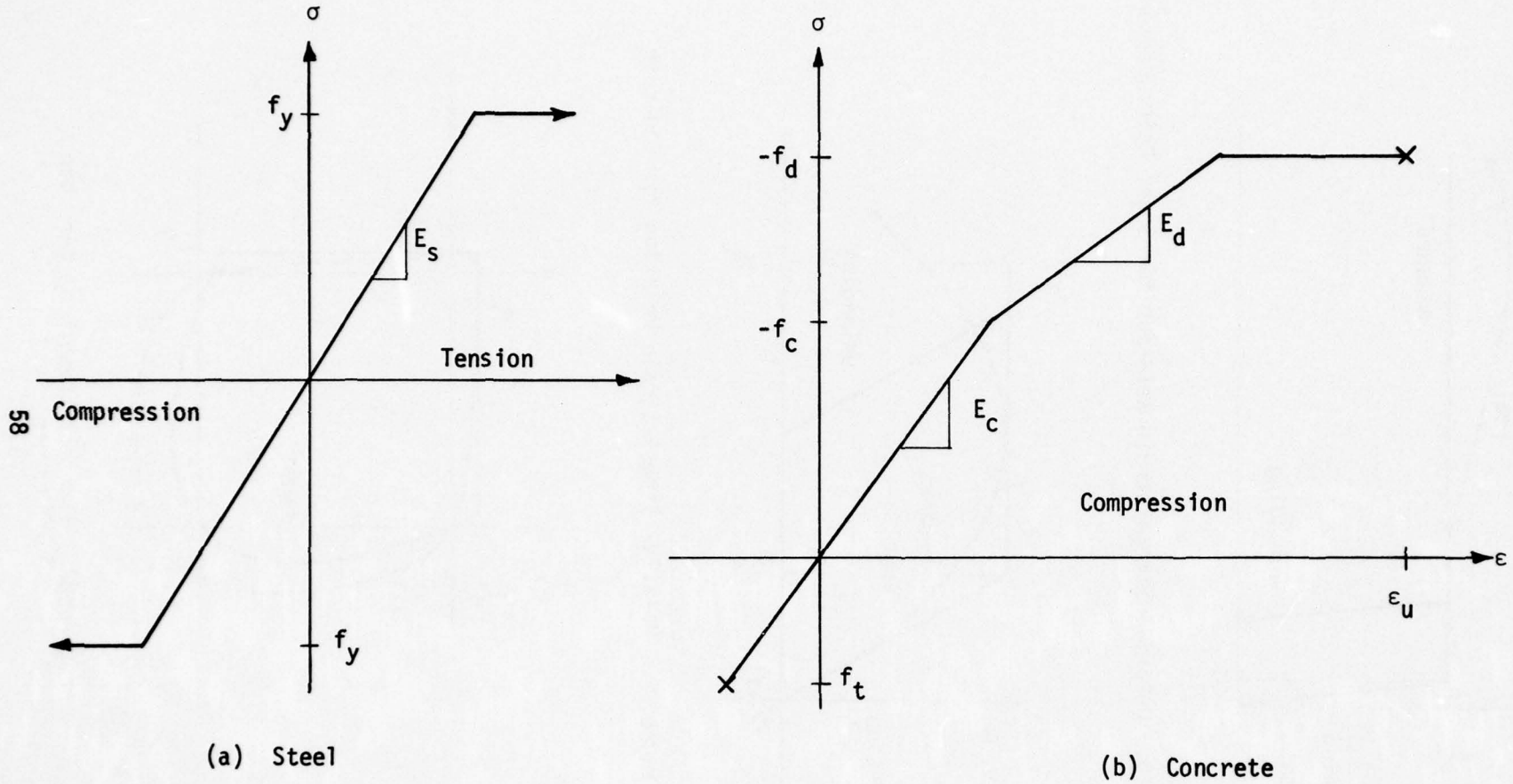

Figure 23. Assumed Uniaxial Stress-Strain Curves for Steel and Concrete

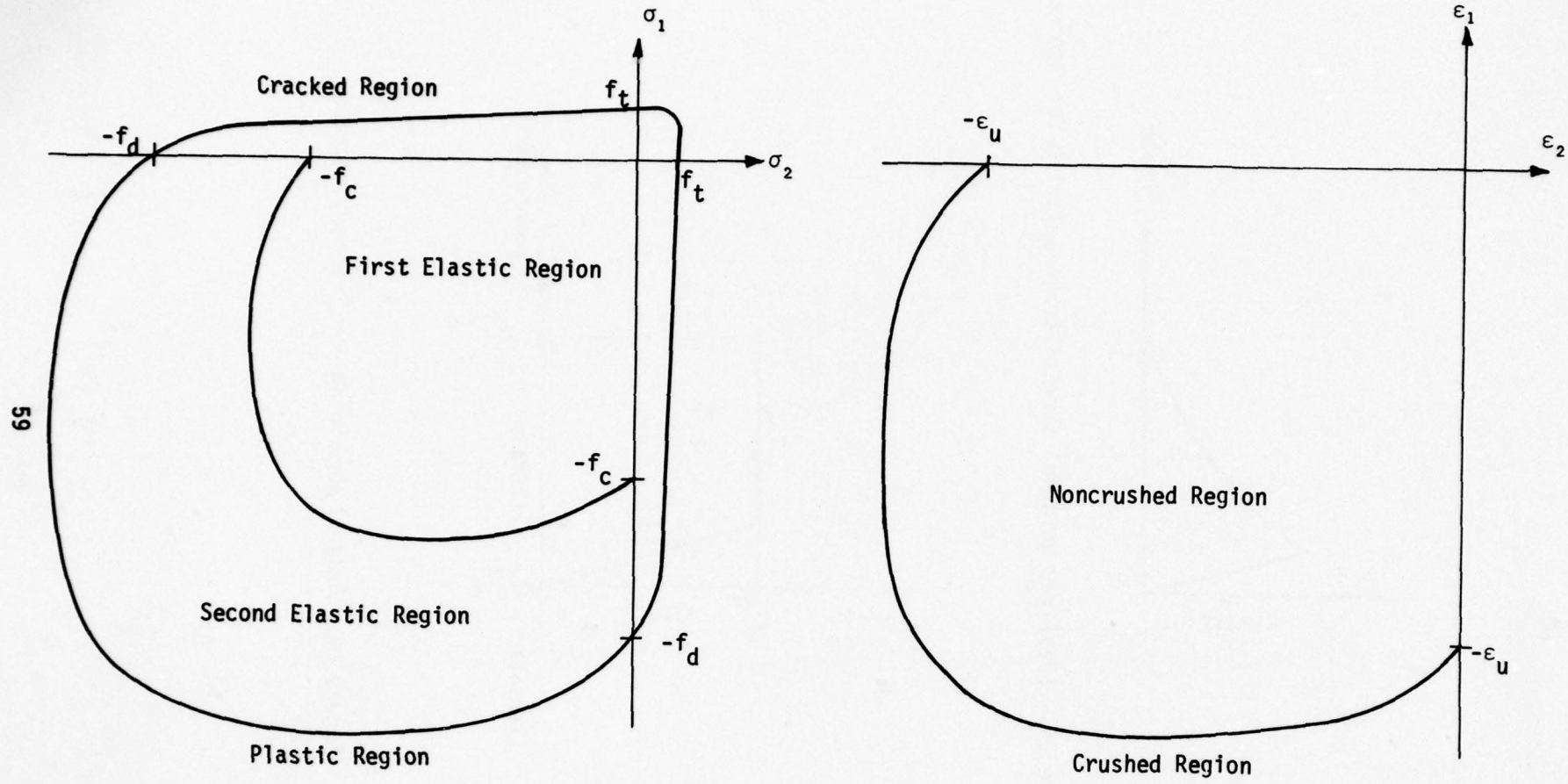

Figure 24. Boundaries between the Different Material Behavior Regions

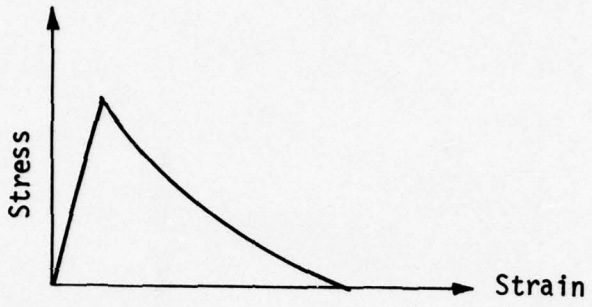

Figure 25. Idealized Uniaxial Stress-Strain Relation for Concrete

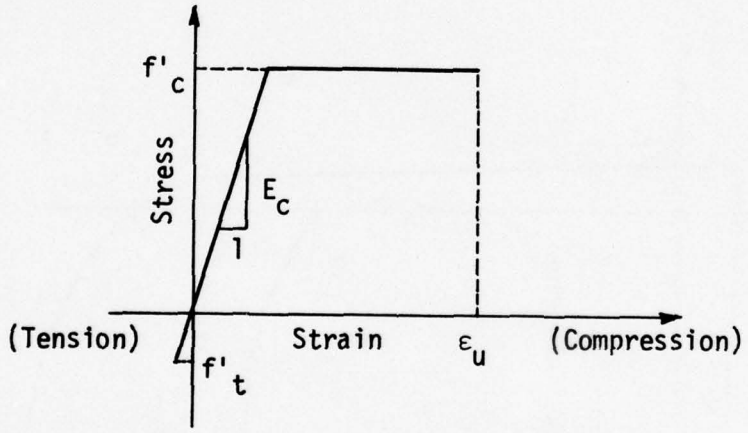

Figure 26. Gradual Unloading for Cracked Concrete

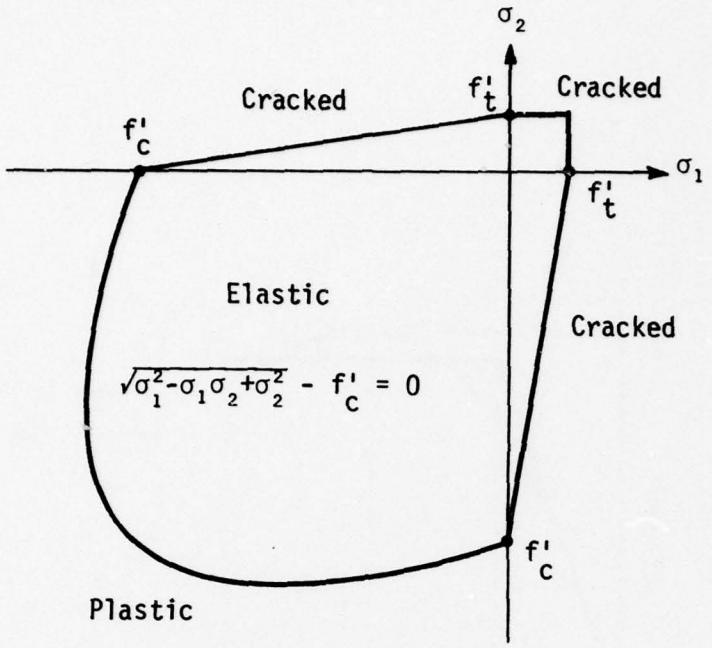

Figure 27. Assumed Failure Surface for Concrete

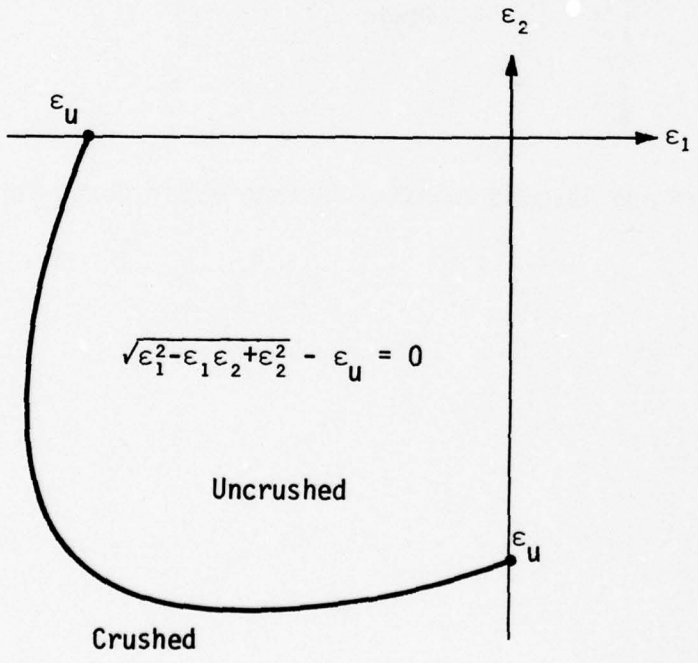

Figure 28. Assumed Crush Surface for Concrete

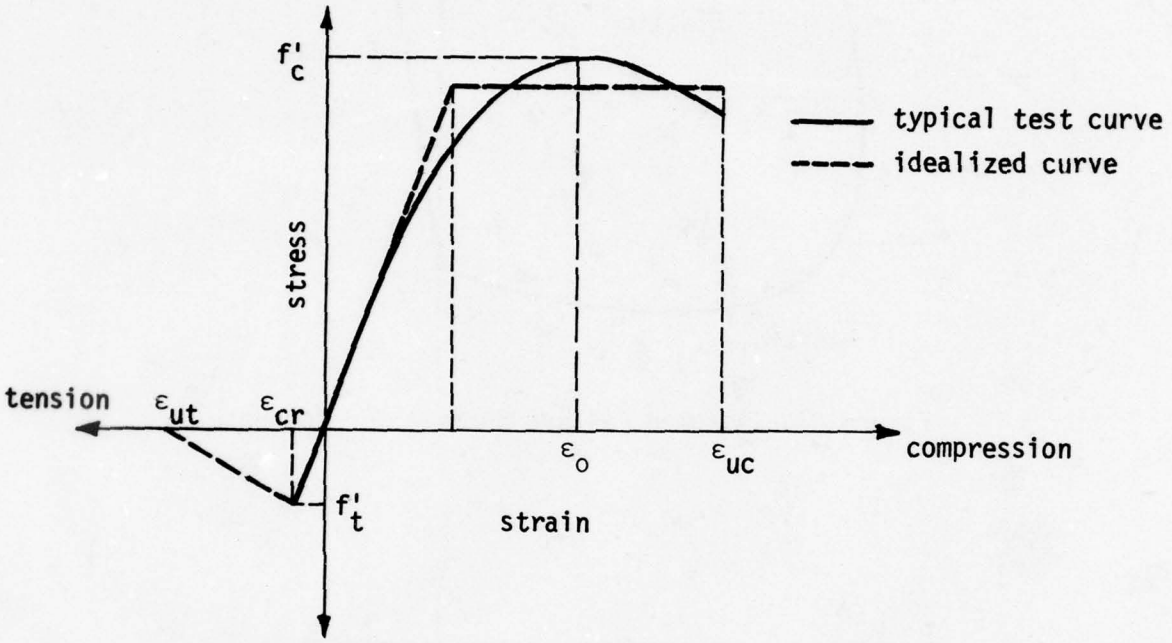

Figure 29. Actual and Assumed Uniaxial Stress-Strain Curve for Concrete

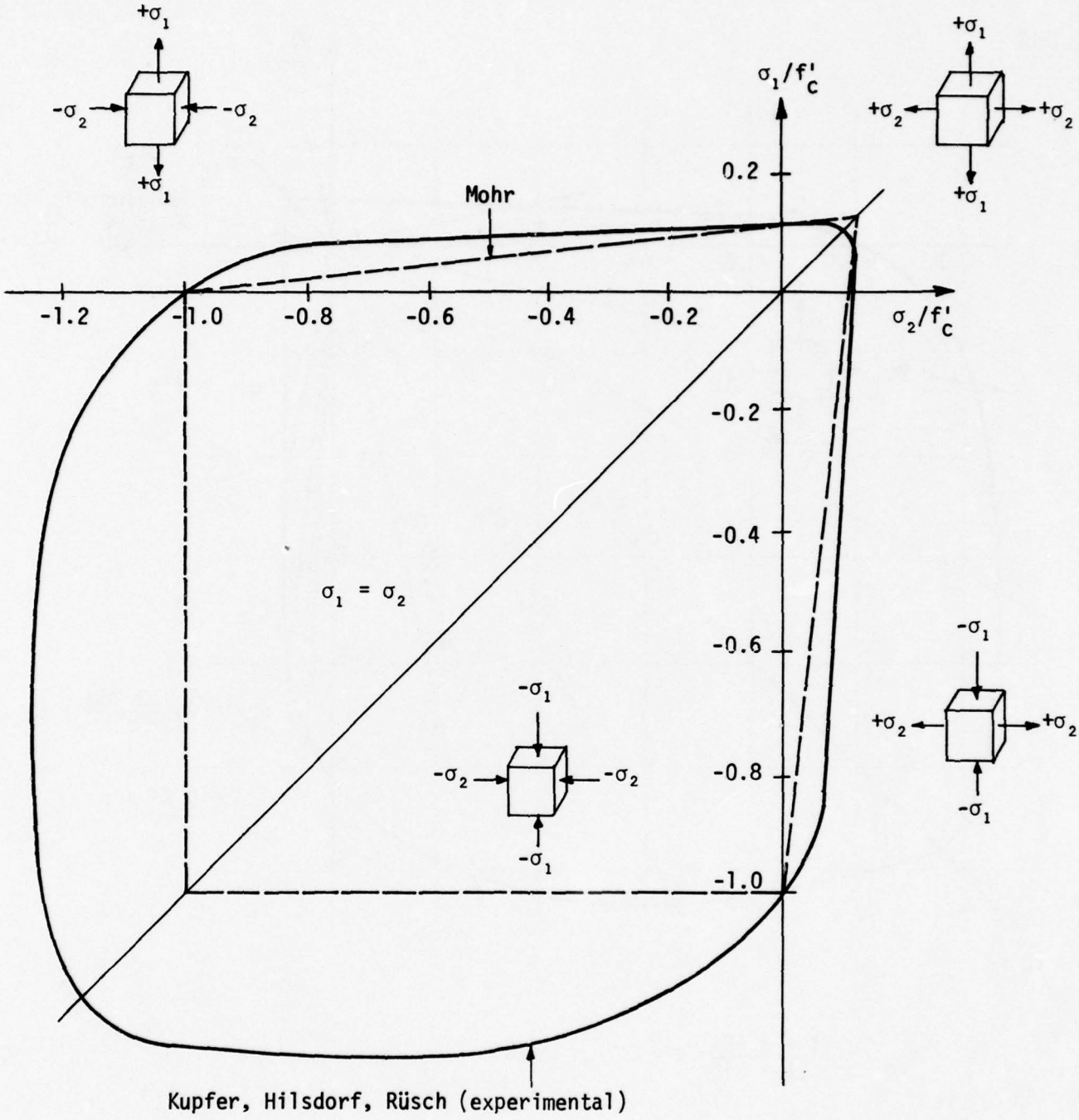

Figure 30. Biaxial Strength of Concrete

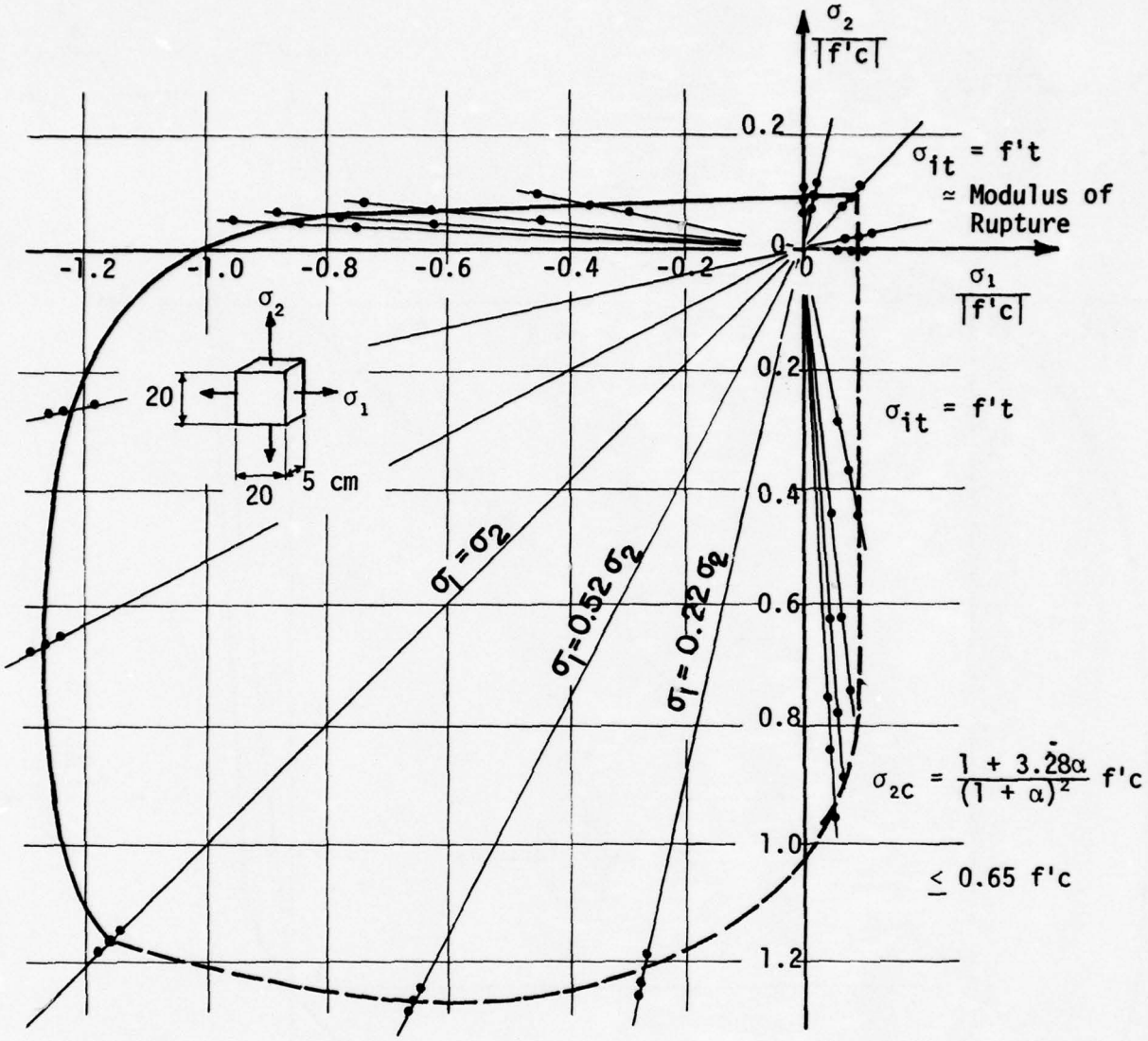

$$\sigma_{2c} = \frac{1 + 3.65\alpha}{(1 + \alpha)^2} \text{ f'c} \qquad = \frac{\sigma_1}{\sigma_2}$$

$$\sigma_{1c} = \alpha\, \sigma_{2c}$$

Figure 31. Analytical Biaxial Strength Envelope for Proposed Model

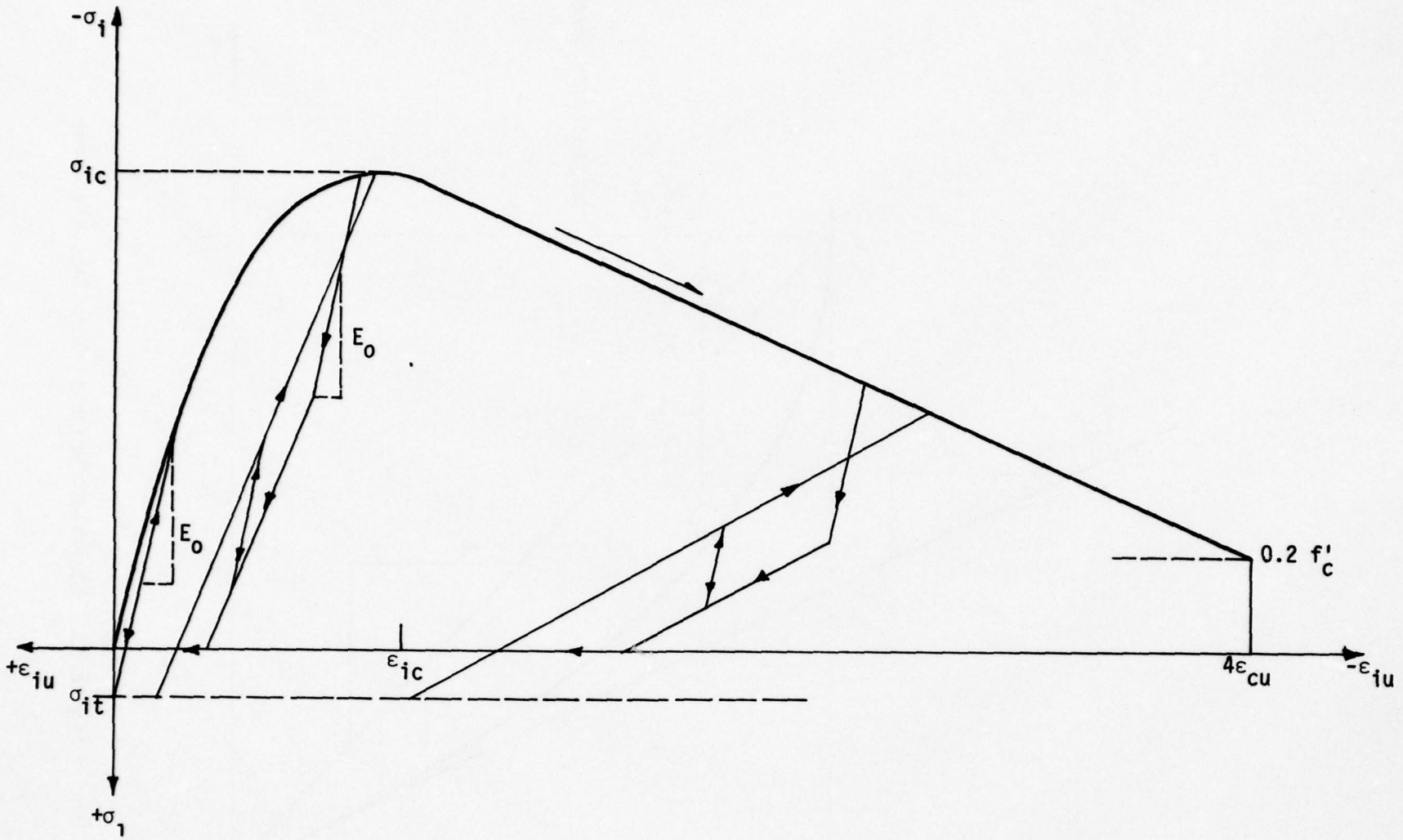

Figure 32. Proposed Model under Cyclic Behavior

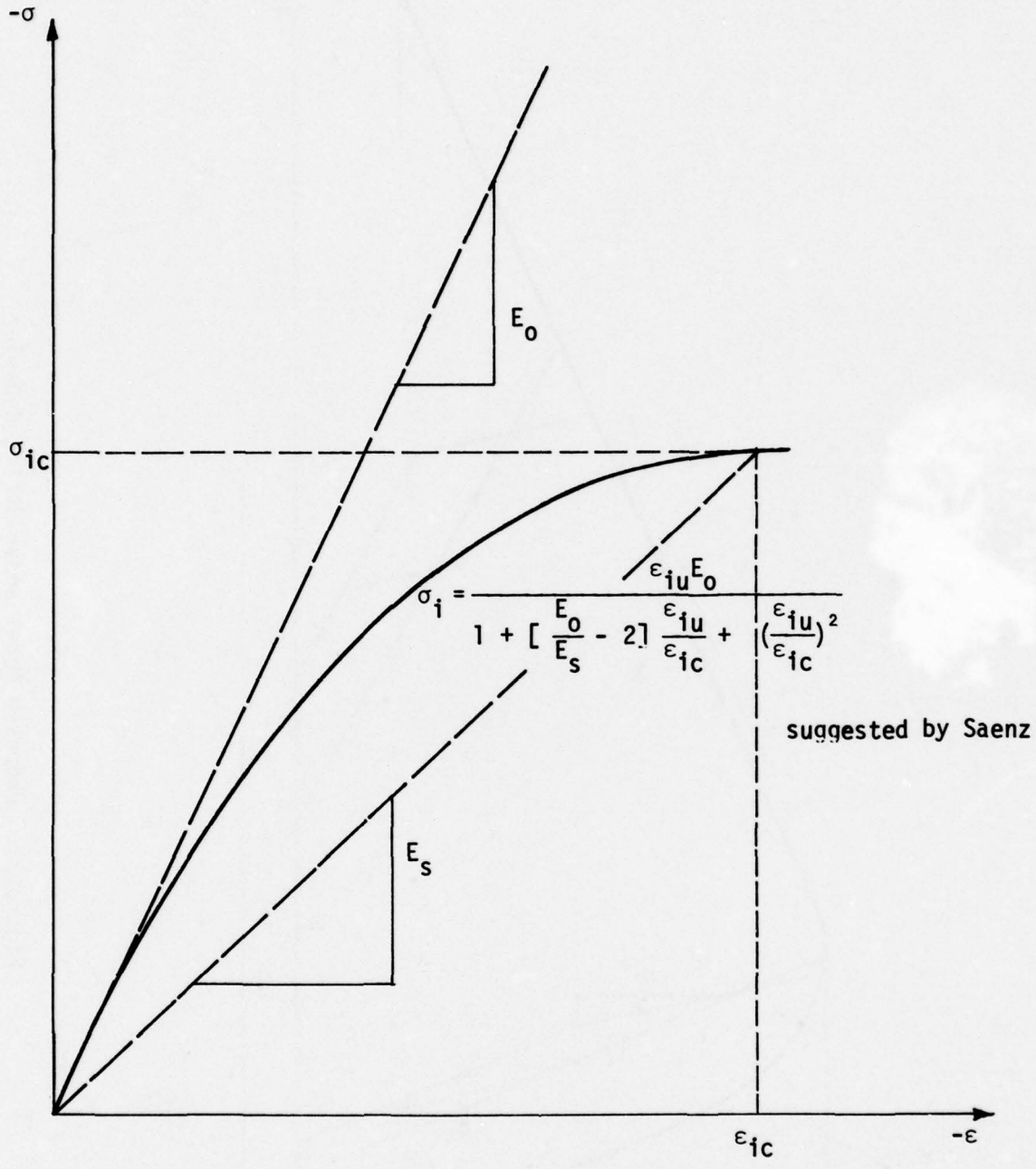

Figure 33. Equivalent Uniaxial Stress-Strain Curve

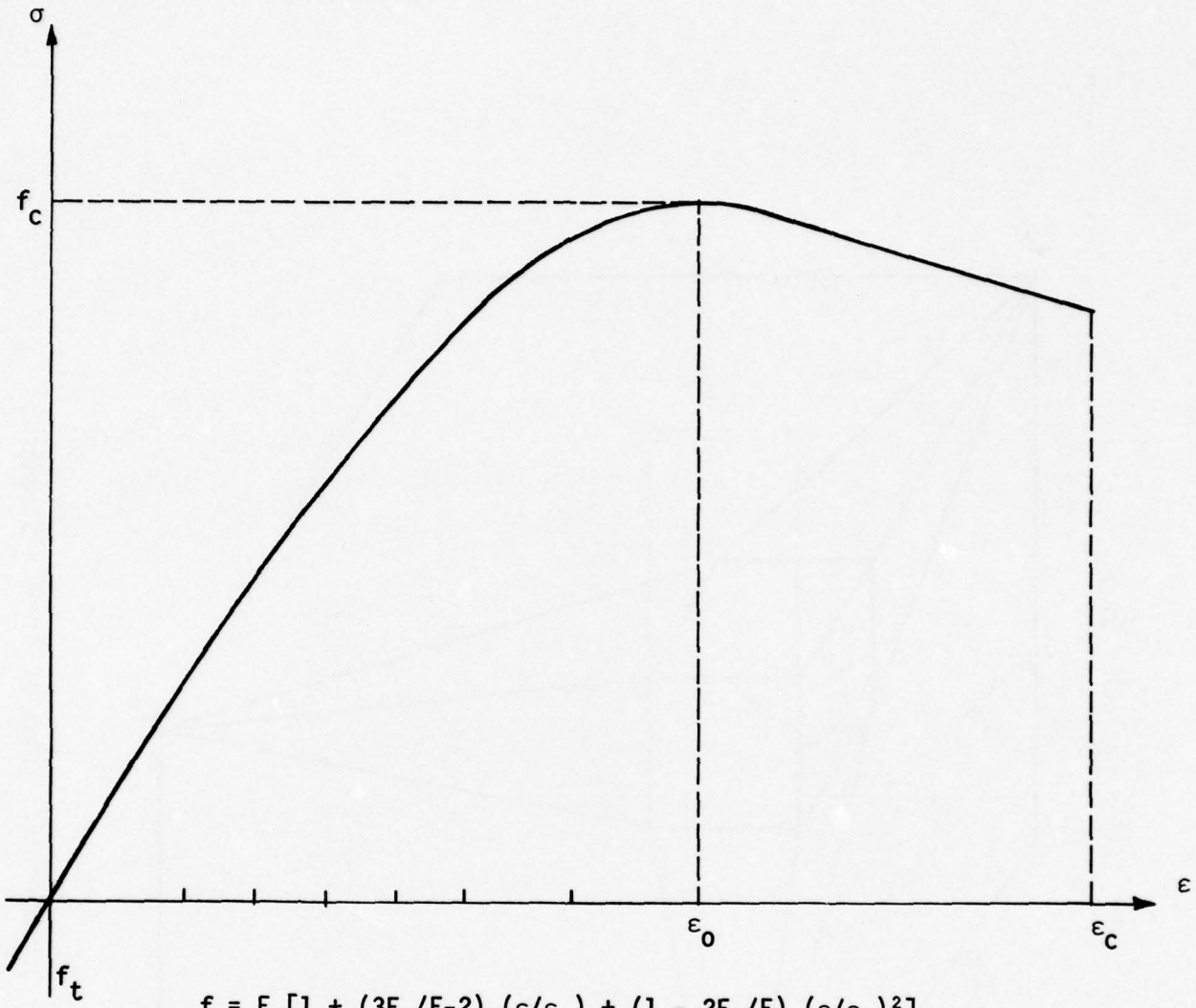

$$f = E_\varepsilon[1 + (3E_o/E-2)\ (\varepsilon/\varepsilon_o) + (1 - 2E_o/E)\ (\varepsilon/\varepsilon_o)^2]$$

Where: f, ε Concrete stress and strain, respectively

ε_o Ultimate strain = $(31.5 - \sqrt[4]{f'_c}) * \sqrt[4]{f'_c} * 10^{-3}$

E Initial Young's modulus

E_o Secant modulus at the ultimate stress (f'_c/ε_o)

Figure 34. Uniaxial Stress-Strain Relationship for Concrete

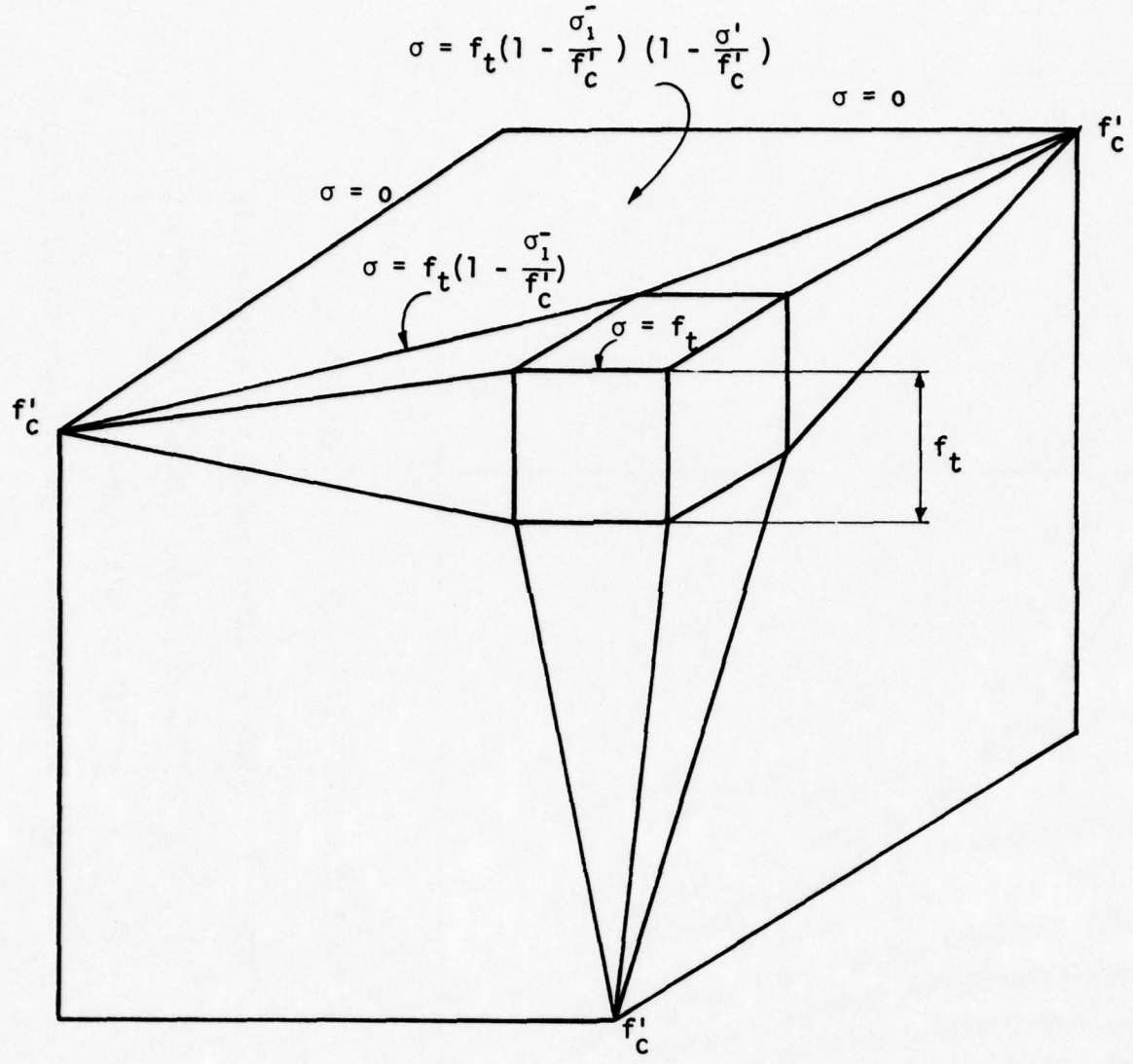

Figure 35. Triaxial Tensile Strength

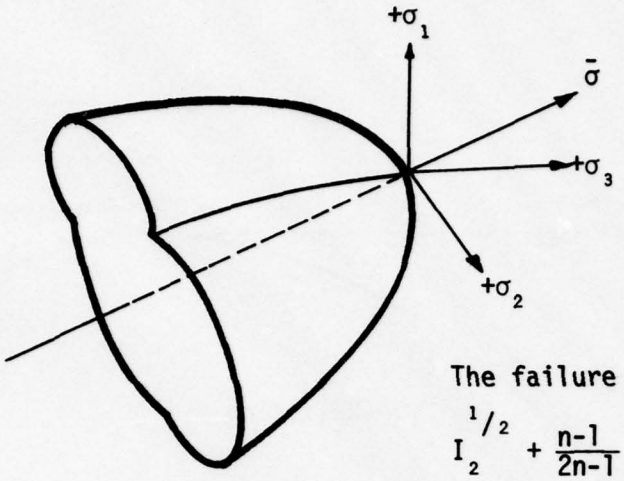

The failure function:

$$I_2^{1/2} + \frac{n-1}{2n-1} I_1 + \frac{n}{2n-1} f'_c = 0$$

where:

n = the ratio of the biaxial compressive strength to the uniaxial strength
= 1.25

$$I_1 = \sigma_1 + \sigma_2 + \sigma_3$$

$$I_2 = \frac{3}{2}\left[(\sigma_1-\bar{\sigma})^2+(\sigma_2-\bar{\sigma})^2+(\sigma_3-\bar{\sigma})^2\right]$$

and $\bar{\sigma} = \dfrac{\sigma_1+\sigma_2+\sigma_3}{3}$

in which $\sigma_1, \sigma_2, \sigma_3$ are principal stresses.

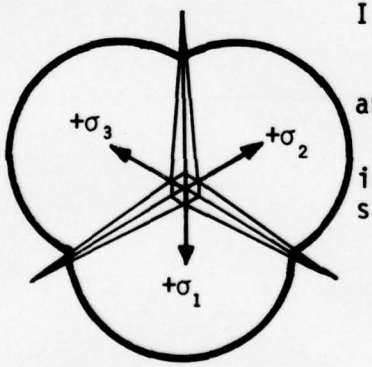

Figure 36. Triaxial Compressive Stresses Failure Surface

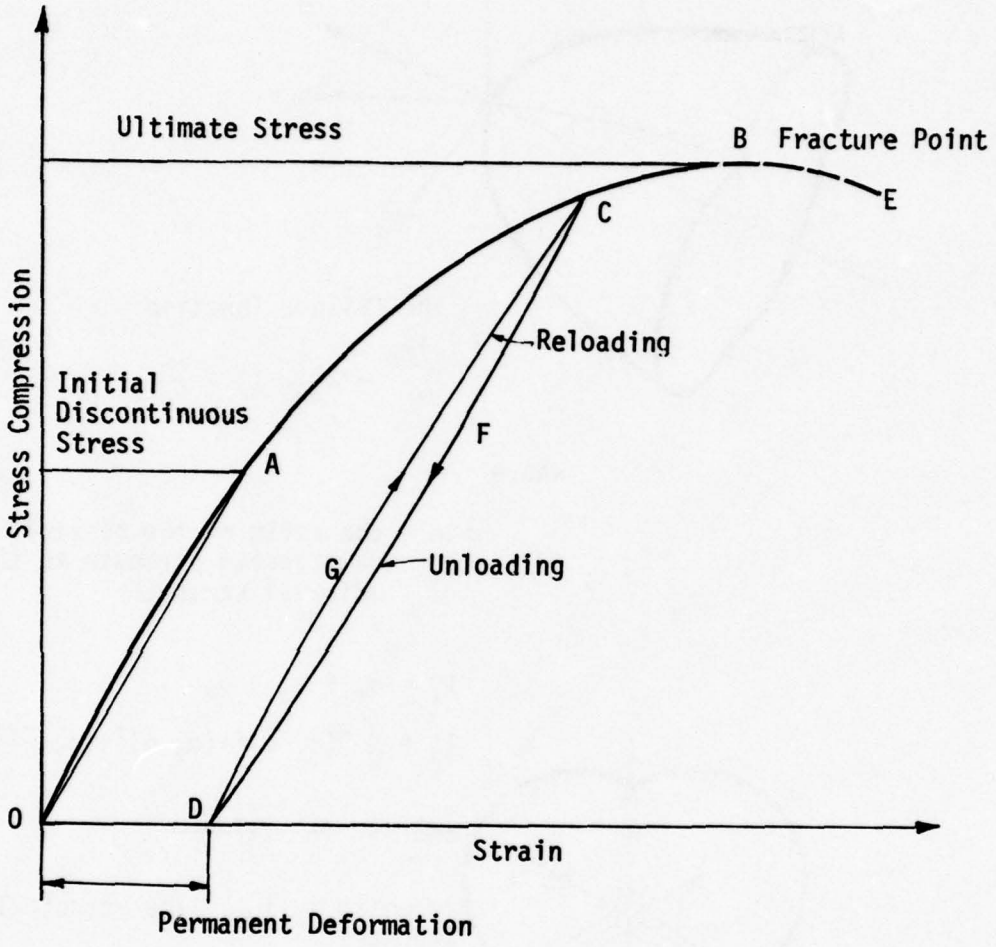

Figure 37. Typical Stress-Strain Curve for Concrete

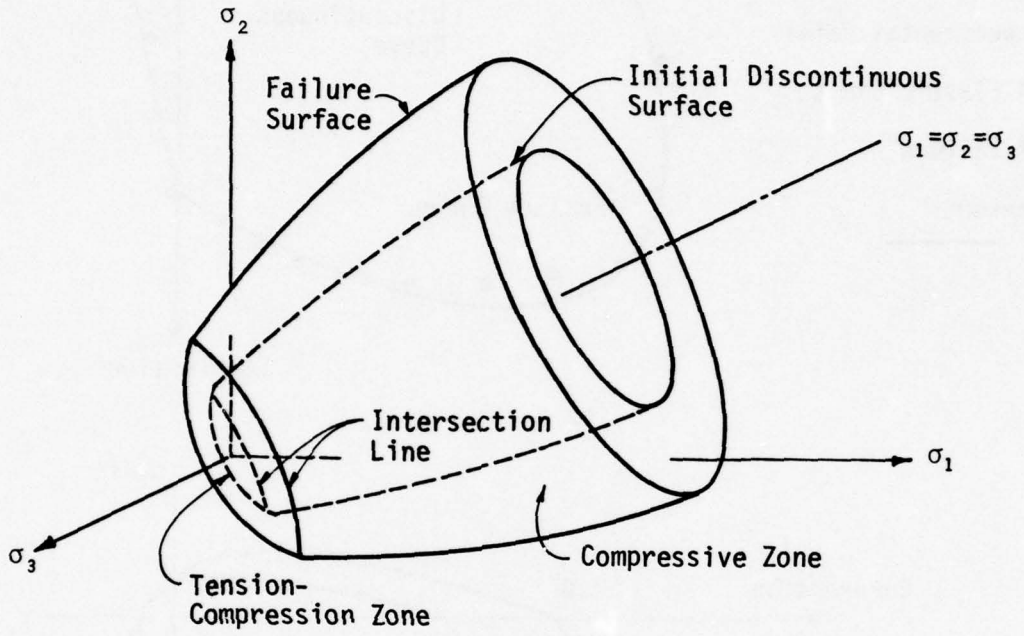

Figure 38. Failure and Initial Discontinuous Surfaces in Principal Stress Space

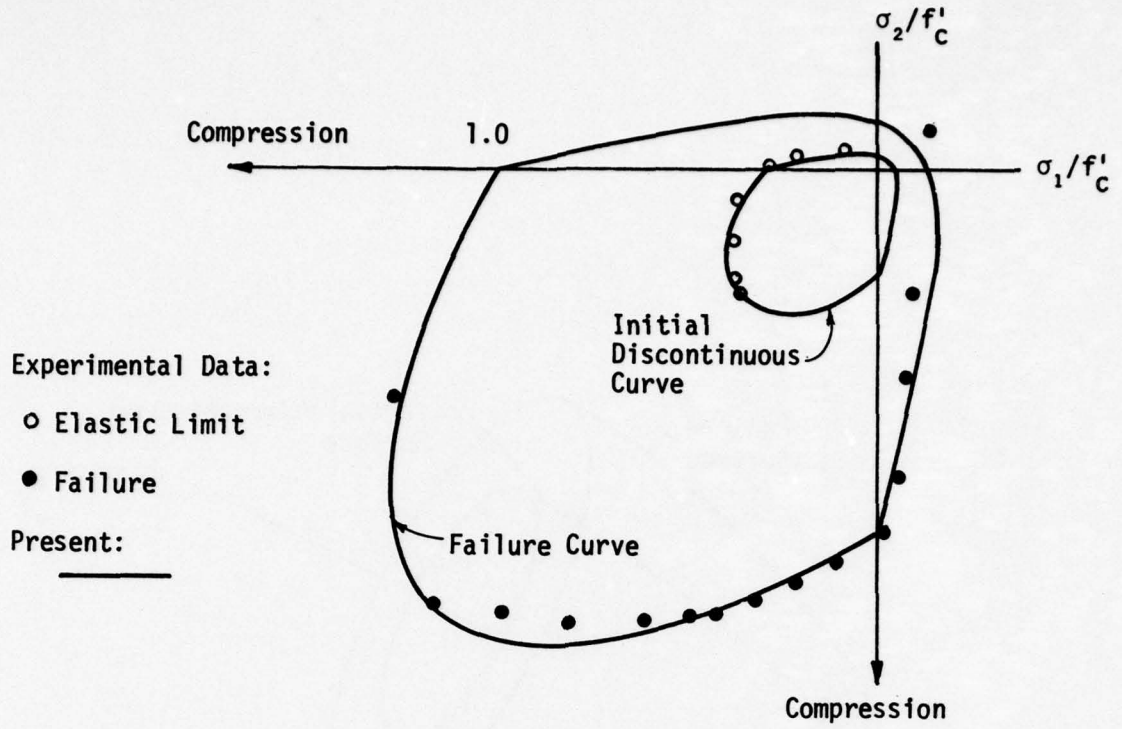

(a)

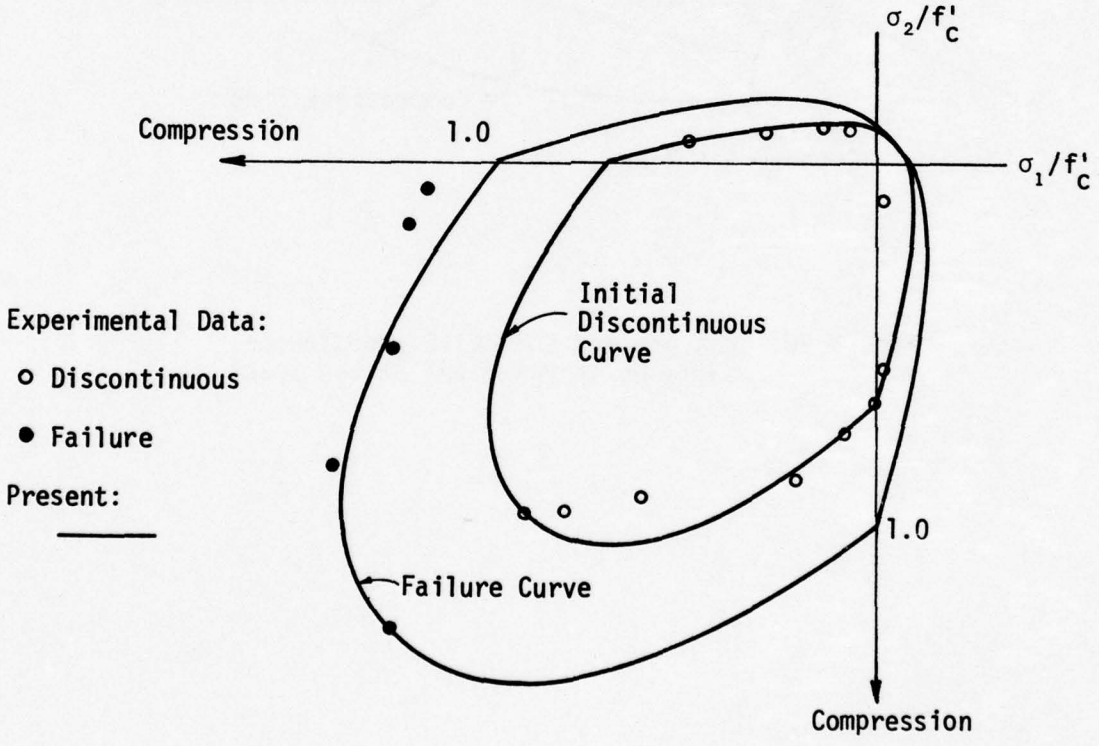

(b)

Figure 39. Failure and Initial Discontinuous Curves in Biaxial Principal Stress Space: (a) Experimental Data from Kupfer et al. (ref. 35); (b) Experimental Data from Ville (ref. 72).

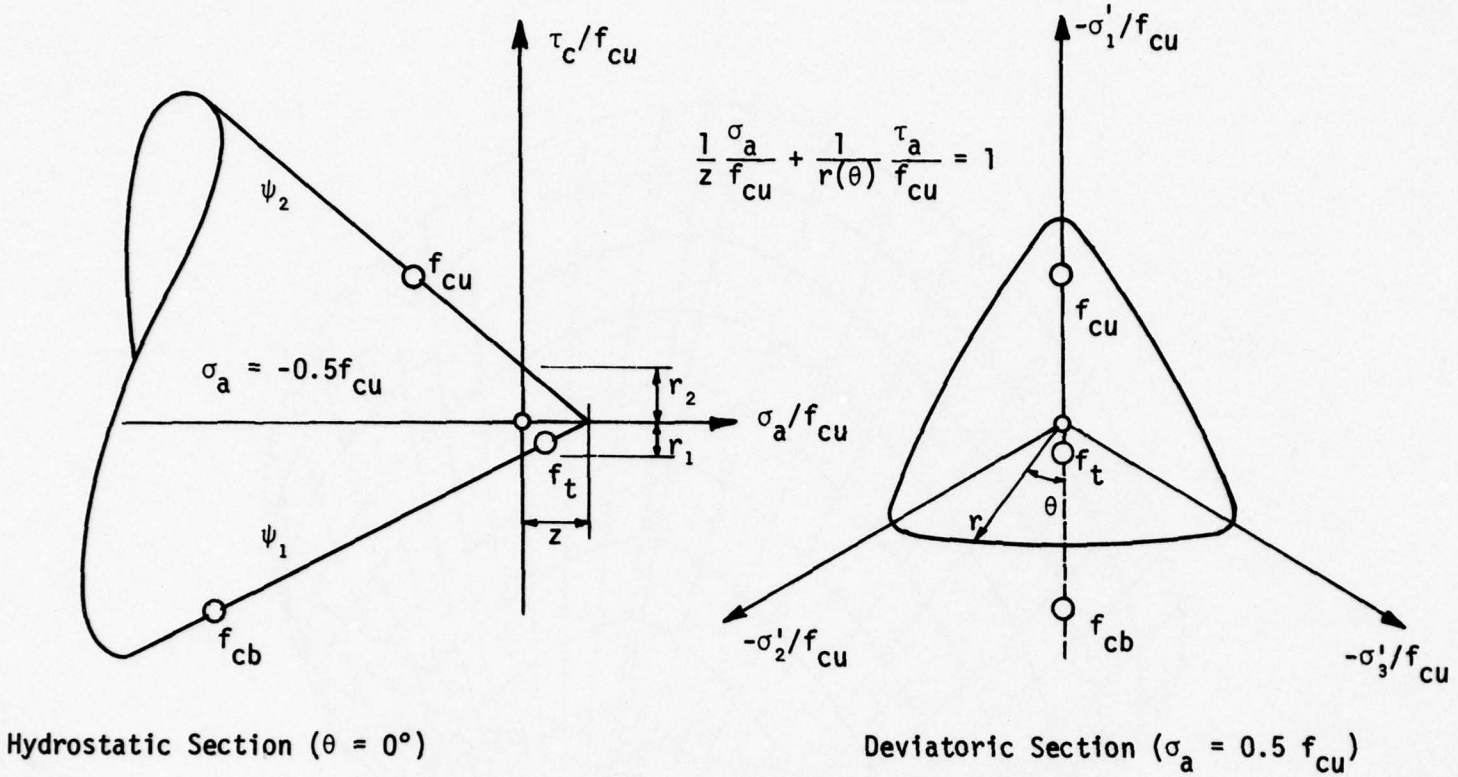

Hydrostatic Section ($\theta = 0°$)

Deviatoric Section ($\sigma_a = 0.5\ f_{cu}$)

Figure 40. Three Parameter Model
Strength Ratios $\alpha_u = 1.3$, $\alpha_z = 0.10$

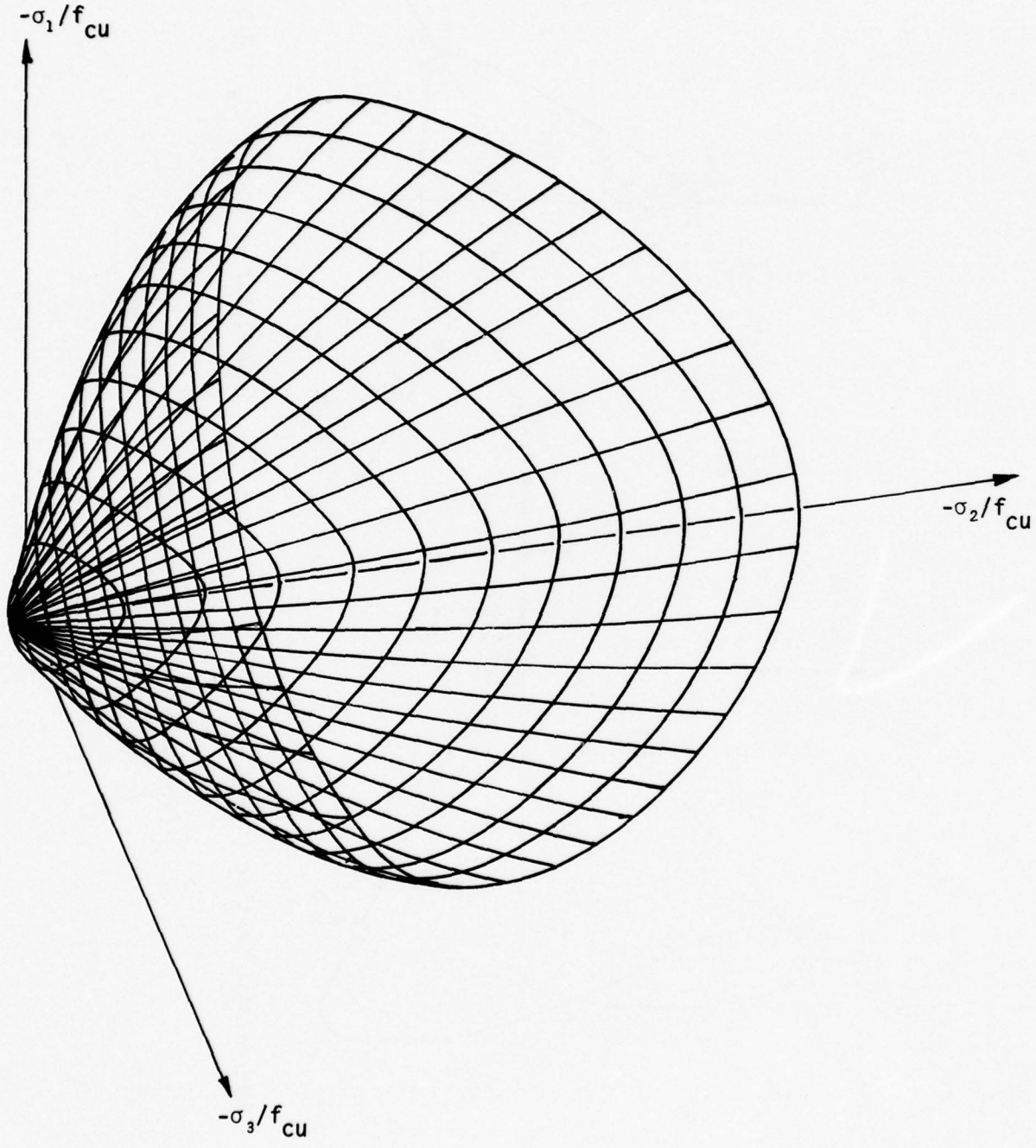

Figure 41. Failure Surface of a Five Parameter Model. Test Data "Launay, et al."

SECTION IV

CONSTITUTIVE MODELS

Based on the study presented in Sections 2 and 3, this section recommends some constitutive models and associated failure criteria available for practical application in reinforced concrete structural response prediction by the finite element method. Basically, two constitutive models are discussed in detail: One, proposed by Bazant and Bhat (ref. 75) and the other proposed by Chen and Chen (refs. 70 and 71).

1. DISCRETE MODELING

Plain concrete, reinforcing steel, and bond link relationships will enable detailed representation of the component parts of reinforced concrete.

2. PLAIN CONCRETE

The Endochronic Theory of Inelasticity and Failure of Concrete proposed by Bazant and Bhat (ref. 75) provides the most complete constitutive law capable of response prediction for varied multistress states. Although the theory suitably fits finite element analysis, incorporation would require considerable modification to current programs available.

Chen and Chen's model, though less accurate, would fit well in standard finite element programs.

a. Constitutive Relationship Proposed by Bazant and Bhat:

The basic stress-strain relation for concrete suggested by Bazant and Bhat is

1. Deviatoric increment component

$$de_{ij} = \frac{dS_{ij}}{2G} + de_{ij}'' \qquad de_{ij}'' = \frac{S_{ij}}{2G}\, dz \tag{15}$$

2. Volumetric increment component:

$$d\varepsilon = \frac{d\sigma}{3K} + d\varepsilon'' \qquad d\varepsilon'' = d\lambda + \frac{\sigma}{3K} \cdot \frac{dt}{\tau_1} + d\varepsilon^{\circ} \tag{16}$$

where

de_{ij}, dS_{ij} = deviatoric strain and stress increments

$d\varepsilon$, $d\sigma$ = volumetric strain and stress increments

S_{ij} = deviatoric stress components

dz = intrinsic time. Details of this parameter are in paragraph 6.

$d\lambda$ = inelastic dilatancy; inelastic volumetric strain.

$d\varepsilon^{\circ}$ = stress-independent inelastic strain (thermal dilatation or shrinkage)

G, K = updated shear and bulk moduli.

τ_1 = relaxation time. The term of (dt/τ_1) relates to the creep effect.

The procedures to apply the stress-strain relation in the finite element method suggested is as follows:

1. After the linearization problem is solved, the displacement increments and the corresponding strain increments in the current time step become known: $\Delta \underline{r}$, $\Delta \underline{\varepsilon}_{ij}$.

2. Evaluate the parameter $\Delta\xi$ from deviatoric strain increment Δe_{ij}

$$\delta\xi = \sqrt{J_2(\Delta\underline{\varepsilon})} = \sqrt{1/2\ \Delta e_{ij}\cdot\Delta e_{ij}} \tag{17}$$

3. Compute the value of $\Delta\eta$ from the parameter $\Delta\xi$ by

$$\Delta\eta = F(\underline{\varepsilon},\underline{\sigma})\Delta\xi \tag{18}$$

in which

$$F(\underline{\varepsilon},\underline{\sigma}) = a_0 + \frac{a_2[J_2(\underline{\varepsilon})]^{1/2} F_3(\max\varepsilon)}{1 - a_1 I_1(\underline{\sigma}) - a_3 I_3(\underline{\sigma})} \tag{19}$$

with

$$a_0 = 0.2$$

$$a_1 = 0.4/f'_c$$

$$a_2 = 2500$$

$$a_3 = 5/f'^3_c$$

$$\eta = \eta + \Delta\eta$$

$$\varepsilon_0 = 0.0001$$

4. Calculate $\Delta\zeta$ from $\Delta\eta$ by

$$\Delta\zeta = \Delta\eta/f(\eta) \tag{20}$$

with

$$f(\eta) = 1 + \beta_1\eta + \beta_2\eta^2 \tag{21}$$

$$\beta_1 = 30$$

$$\beta_2 = 4500$$

5. Relaxation time τ_1 for creep:

$$\tau_1 = \tau_a + \tau_b(t - t_o) \tag{22}$$

τ_a, τ_b = known constants

6. Then the intrinsic time

$$\Delta z = \sqrt{(\frac{\Delta\zeta}{Z_1})^2 + (\frac{\Delta t}{\tau_1})^2} \tag{23}$$

where

Z_1 = Constant

= 0.002

7. Inelastic dilatancy $\Delta\lambda$

$$\Delta\lambda = \frac{1-\lambda/\lambda_0}{1-C_1 I_1(\underline{\sigma})} [(\frac{\lambda}{\lambda_0}) + (\frac{J_2(\underline{\varepsilon})}{C_2^2 + J_2(\underline{\varepsilon})})^3] \Delta\xi \tag{24}$$

with

$C_1 = 1/f'_c$

$C_2 = 0.0005$

$\lambda_0 = 0.0001$

and

$\lambda = \lambda + \Delta\lambda$

8. Shear modulus and bulk modulus

$$G = G_0 \left(1 - 0.25 \frac{\lambda}{\lambda_0}\right) \text{ with } G_0 = \frac{E_0}{2(1+\nu)} \tag{25}$$

$$K = K_0 \left(1 - 0.25 \frac{\lambda}{\lambda_0}\right) \text{ with } K_0 = \frac{E_0}{3(1-2\nu)} \tag{26}$$

9. Elastic strain increment

$$\Delta e''_{ij} = \frac{S_{ij}}{2G} \cdot \Delta z \tag{27}$$

$$\Delta \varepsilon''_0 = \Delta\lambda + \frac{\sigma}{3K} \left(\frac{dt}{\tau_1}\right) + \Delta\varepsilon^0 \tag{28}$$

10. Stress-strain relation:

$$\Delta e_{ij} = \frac{\Delta S_{ij}}{2G} + \Delta e''_{ij} \tag{29}$$

or

$$\Delta S_{ij} = 2G \left(\Delta e_{ij} - \Delta e''_{ij}\right) \tag{30}$$

and

$$\Delta \varepsilon = \frac{\Delta\sigma}{3K} + \Delta\varepsilon'' \tag{31}$$

or

$$\Delta\sigma = 3K(\Delta\varepsilon - \Delta\varepsilon'') \tag{32}$$

It may be noted that the strain increment calculated in each time step shall be decomposed into deviatoric strain components Δe_{ij} and volumetric strain components $\Delta\varepsilon$.

11. Total stress increment:

$$\Delta\sigma_{ij} = \Delta S_{ij} + \Delta\sigma \tag{33}$$

b. Constitutive Equations Suggested by Chen and Chen

The concrete is considered an elastic plastic strain-hardening and fracture material. The theory uses a failure surface, initial discontinuous surface, and subsequent discontinuous surface or loading surface to define the behavior (Figure 42). Stress states causing complete rupture and inability to resist further loading define the failure surface. The initial yield surface can only be reached by elastic action; unloading within this surface causes no permanent deformation. Straining beyond this surface causes permanent deformation and modifies the shape of the surface at which subsequent straining causes permanent deformation. This new surface is the loading surface.

Both the failure and initial discontinuous surface depend on the deviatoric stresses and hydrostatic pressure and are expressed in terms of I_1, and J_2:

$$f_u(\sigma_{ij}) = \frac{\kappa^2}{3} J_2 - \frac{\kappa^2}{36} I_1^2 \pm \frac{1}{3} A_u I_1 = \tau^2_u \tag{34}$$

$$f_o(\sigma_{ij}) = \frac{\kappa^2}{3} J_2 - \frac{\kappa^2}{36} I_2^2 \pm \frac{1}{3} A_o I_1 = \tau^2_o \tag{35}$$

where the sign of the third term is positive in compression regions and negative in tension-compression regions, and A_o, τ_o, A_u, and τ_u are material constants which can be determined from simple tests. The value of κ is set to 3 based on experimental results. The subsequent loading surfaces are bounded by the initial discontinuous and failure surfaces, and assume a similar shape; it translates along the axis and expands isotropically:

$$f(\sigma_{ij}) = \frac{\frac{\kappa^2}{3} J^2 - \frac{\kappa^2}{36} I_1^2 \pm \frac{1}{12} I_1^2 + \frac{\beta}{3} I_1}{1 - \frac{\alpha}{3} I_1} = \tau_2^2$$

where α and β depend on A_u, A_o, τ_u, τ_o.

Using the normality condition, the incremental stress-strain relations are derived directly from the loading surface. In the three-dimensional case, the incremental relation is

$$\begin{Bmatrix} d\sigma_{xx} \\ d\sigma_{yy} \\ d\tau_{zz} \\ d\tau_{xy} \\ d\tau_{yz} \\ d\tau_{zx} \end{Bmatrix} = \frac{E}{(1+\nu)(1-2\nu)} \begin{bmatrix} 1-\nu-\omega\Phi_{11} & \nu-\omega\Phi_{12} & \nu-\omega\Phi_{13} & -\omega\Phi_{14} & -\omega\Phi_{15} & -\omega\Phi_{16} \\ & 1-\nu-\omega\Phi_{22} & \nu-\omega\Phi_{23} & -\omega\Phi_{24} & -\omega\Phi_{25} & -\omega\Phi_{26} \\ & & 1-\nu-\omega\Phi_{33} & -\omega\Phi_{34} & -\omega\Phi_{35} & -\omega\Phi_{36} \\ & & & \frac{1-2\nu}{2} - \omega\Phi_{44} & -\omega\Phi_{46} & -\omega\Phi_{46} \\ & & & & \frac{1-2\nu}{2} - \omega\Phi_{55} & -\omega\Phi_{56} \\ & \text{SYMMETRIC} & & & & \frac{1-2}{2} - \omega\Phi_{66} \end{bmatrix} \begin{Bmatrix} d\varepsilon_{xx} \\ d\varepsilon_{yy} \\ d\varepsilon_{zz} \\ d\gamma_{xy} \\ d\gamma_{yz} \\ d\gamma_{zx} \end{Bmatrix} \quad (36)$$

where

$$\frac{1}{\omega} = \{(1-2\nu)\ (2\eta^2\ J_2+3\rho^2) \ +\ 9\nu\rho^2\} = \frac{mH\ \ (1+\nu)\ (1-2\nu)}{E}\ \sqrt{(2\eta^2\ J_2\ +\ 3\rho^2)}$$

$$\Phi_{11} = \{(1-2\nu)\ (\eta S_{xx} + \rho) + 3\nu\rho\}^2$$

$$\Phi_{12} = \{(1-2\nu)\ (\eta S_{xx} + \rho) + 3\nu\rho\}\ \ \{(1-2\nu)\ (\eta S_{yy} + \rho) + 3\nu\rho\}$$

$$\Phi_{13} = \{(1-2\nu)\ (\eta S_{xx} + \rho) + 3\nu\rho\}\ \ \{(1-2\nu)\ (\eta S_{zz} + \rho) + 3\nu\rho\}$$

$$\Phi_{14} = \{(1-2\nu)\ (\eta S_{xx} + \rho) + 3\nu\rho\}\ \ \{(1-2\nu)\ \ \eta\tau_{xy}\}$$

$$\Phi_{15} = \{(1-2\nu)\ (\eta S_{xx} + \rho) + 3\nu\rho\}\ \ \{(1-2\nu)\ \ \eta\tau_{yz}\}$$

$$\Phi_{16} = \{(1-2\nu)\ (\eta S_{xx} + \rho) + 3\nu\rho\}\ \ \{(1-2\nu)\ \ \eta\tau_{zx}\}$$

$$\Phi_{22} = \{(1-2\nu)\ (\eta S_{yy} + \rho) + 3\nu\rho\}^2$$

$$\Phi_{23} = \{(1-2\nu)\ (\eta S_{yy} + \rho) + 3\nu\rho\}\ \ \{(1-2\nu)\ (\eta S_{zz} + \rho) + 3\nu\rho\} \qquad (37)$$

$$\Phi_{24} = \{(1-2\nu)\ (\eta S_{yy} + \rho) + 3\nu\rho\}\ \ \{(1-2\nu)\ \ \eta\tau_{xy}\}$$

$$\Phi_{25} = \{(1-2\nu)\ (\eta S_{yy} + \rho) + 3\nu\rho\}\ \ \{(1-2\nu)\ \ \eta\tau_{yz}\}$$

$$\Phi_{26} = \{(1-2\nu)\ (\eta S_{yy} + \rho) + 3\nu\rho\}\ \ \{(1-2\nu)\ \ \eta\tau_{zx}\}$$

$$\Phi_{33} = \{(1-2\nu)\ (\eta S_{zz} + \rho) + 3\nu\rho\}^2$$

$$\Phi_{34} = \{(1-2\nu)\ (\eta S_{zz} + \rho) + 3\nu\rho\}\ \ \{(1-2\nu)\ \ \eta\tau_{xy}\}$$

$$\Phi_{35} = \{(1-2\nu)\ (\eta S_{zz} + \rho) + 3\nu\rho\}\ \ \{(1-2\nu)\ \ \eta\tau_{yz}\}$$

$$\Phi_{36} = \{(1-2\nu)\ (\eta S_{zz} + \rho) + 3\nu\rho\}\ \ \{(1-2\nu)\ \ \eta\tau_{zx}\}$$

$$\Phi_{44} = \{(1-2\nu)\ \ \eta\tau_{xy}\}^2$$

$$\Phi_{45} = \{(1-2\nu)\ \eta\tau_{xy}\}\ \{(1-2\nu)\ \eta\tau_{yz}\}$$

$$\Phi_{46} = \{(1-2\nu)\ \eta\tau_{xy}\}\ \{(1-2\nu)\ \eta\tau_{zx}\}$$

$$\Phi_{55} = \{(1-2\nu)\ \eta\tau_{yz}\}^2$$

$$\Phi_{56} = \{(1-2\nu)\ \eta\tau_{yz}\}\ \{(1-2\nu)\ \eta\tau_{zx}\}$$

$$\Phi_{66} = \{(1-2\nu)\ \eta\tau_{zx}\}^2$$

All parameters can be easily calculated, excepting the value of H. The value of H, defined as the strain-hardening rate, can be written in terms of the slope of the equivalent stress-strain curve:

$$H = 2\sigma_e H' \tag{38}$$

where

$$H' = d\sigma_e/d\varepsilon^\rho$$

σ_e = the equivalent stress = $\sqrt{f}$

The $\sigma_e \sim \varepsilon^\rho$ curves in the compression region and the tension-compression region are different. These $\sigma_e \sim \varepsilon^\rho$ curves are assumed to be identical in form and shall be obtained from tests. The curves are nonlinear in nature.

Since the derivation of the incremental stress-strain equation was based on the elastic-plastic model, any finite element program for elastic-plastic analysis may incorporate this material model without much difficulty.

Both the endochronic theory derived by Bazant and the elastic-plastic, strain hardening and fracture material model proposed by Chen and Chen have been presented. Both of them appear to be promising for finite element analysis. However, the Bazant model provides a better degree of fit with experimental data than the Chen and Chen model. The endochronic theory has been compared extensively to different experimental tests, i.e.,

1. Uniaxial compression test by Hognestad et al. (Figure 43).
2. Biaxial stress-strain test by Kupfer et al. (Figures 44, 45, 46), and biaxial failure envelope (Figure 47).
3. Triaxial tests for low and medium strength concrete by Balmer, 1949, and Richart, et al., 1928 (Figures 48 and 49).
4. Torsion-compression tests by Bresler, Pister and Gorde, Helony (Figure 50).
5. Uniaxial cyclic compression tests by Sinha et al., 1964, and Shak et al., 1970 (Figure 51).
6. Creep tests (Figure 52, Figure 53).

Chen and Chen's model has been compared only to the biaxial tests conducted by Kupfer et al. (ref. 35). The figures provided by Bazant and Chen and Chen are given herein (Figures 42, 54, 55, 56). Obviously, Bazant's model is better than Chen and Chen's. However, it shall be noted

that the derivation of Chen and Chen's model was mainly based on the classical elastic-plastic theory. It is in that field that the finite element method has been applied most successfully. Further, the incremental stress-strain relations for both two-dimensional and three-dimensional stress states have been developed in a matrix form that is easily incorporated into any existing programs.

3. MATERIAL MODEL FOR STEEL

Compared to plain concrete, the material property of steel is very well-defined. Current yield criterion and stress-strain relations for steel have been demonstrated to be adequate in predicting steel behavior even in the plastic range. An elastic-plastic model with von Mises yield criterion and the associated flow rule may be assumed for reinforcing steel. The von Mises criterion can be used assuming either perfectly plastic conditions or strain-hardening situations. The procedures and formulations for the finite-element method applied in elastic-plastic analysis have been well-developed. It would not be difficult to handle steel in reinforced concrete analysis.

The reinforcing steel, in finite element analysis, may be treated as individual truss bars, or assumed to be distributed uniformly (smeared) over the entire element region and represented by 2-D or 3-D solid finite elements.

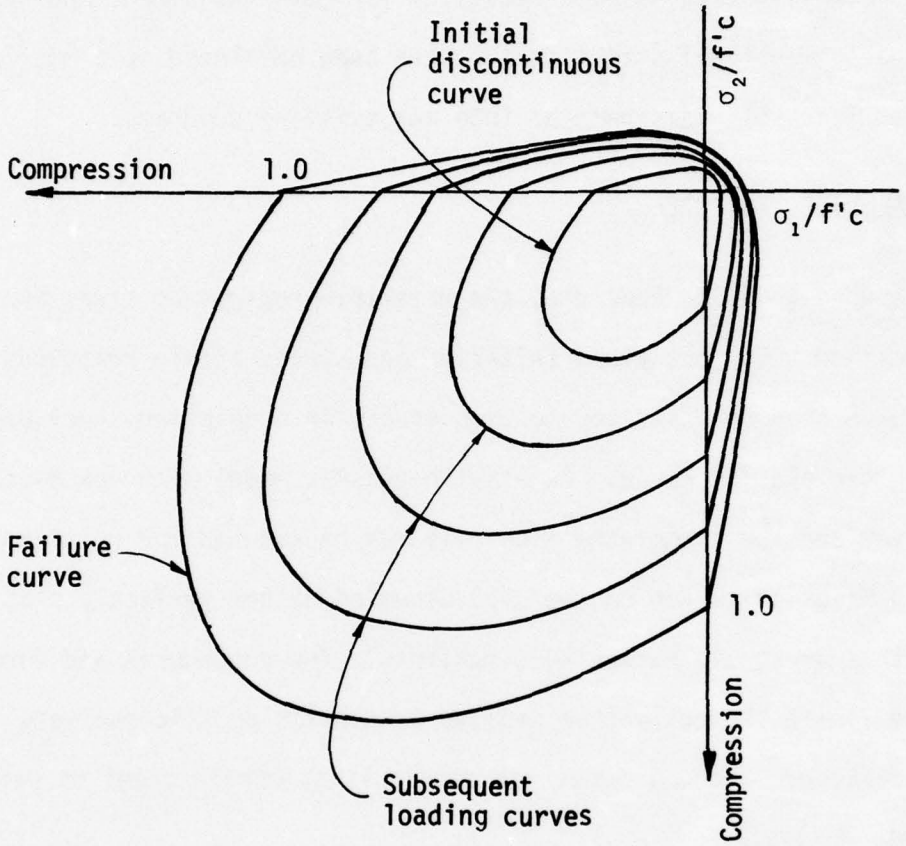

Figure 42. Chen and Chen's Model

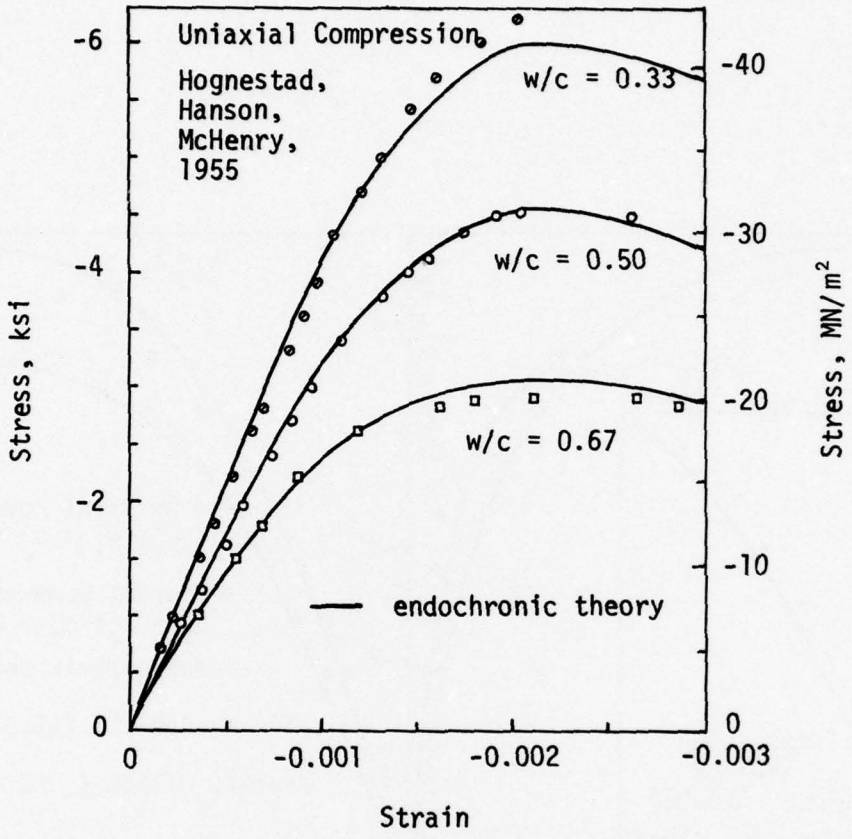

Figure 43. Uniaxial Compression Test

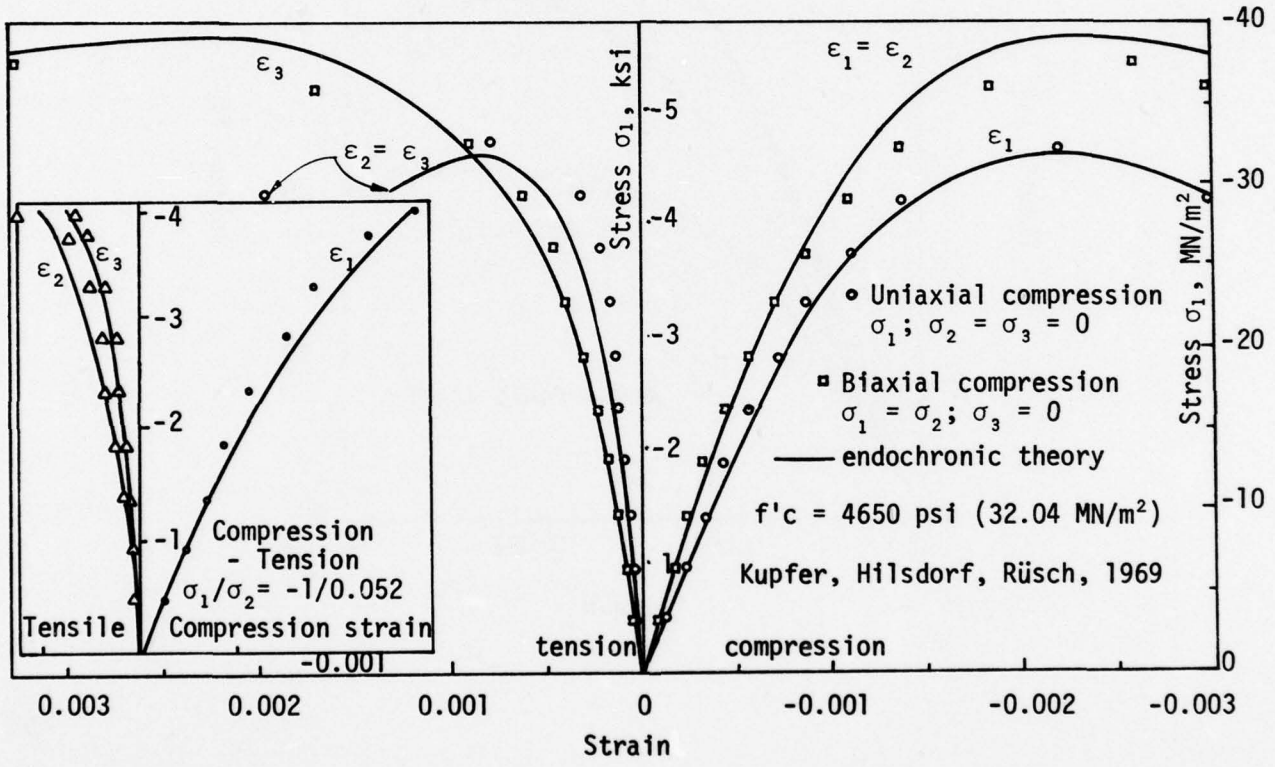

Figure 44 Biaxial Stress-Strain Test

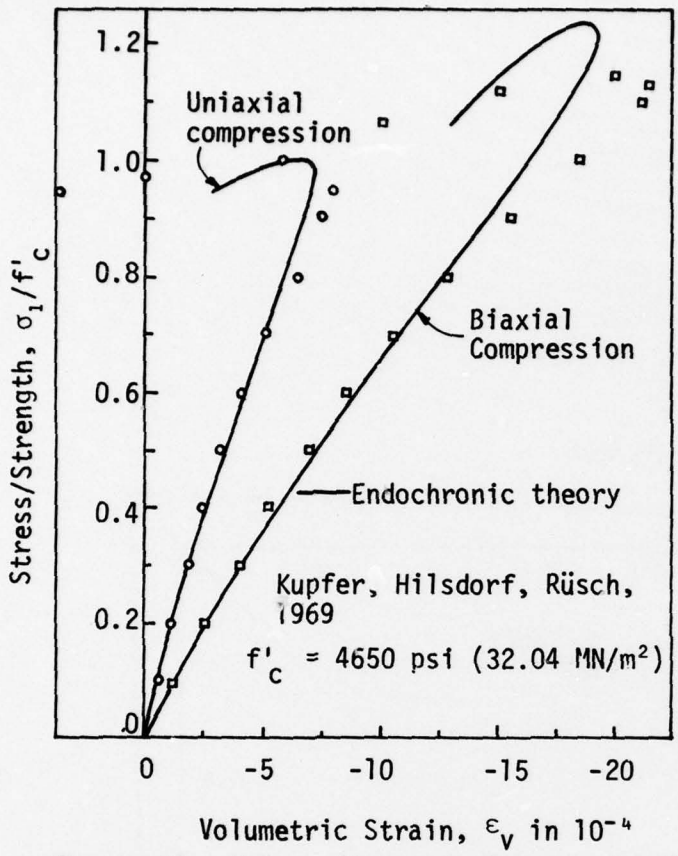

Figure 45. Volume Change in Compression Tests

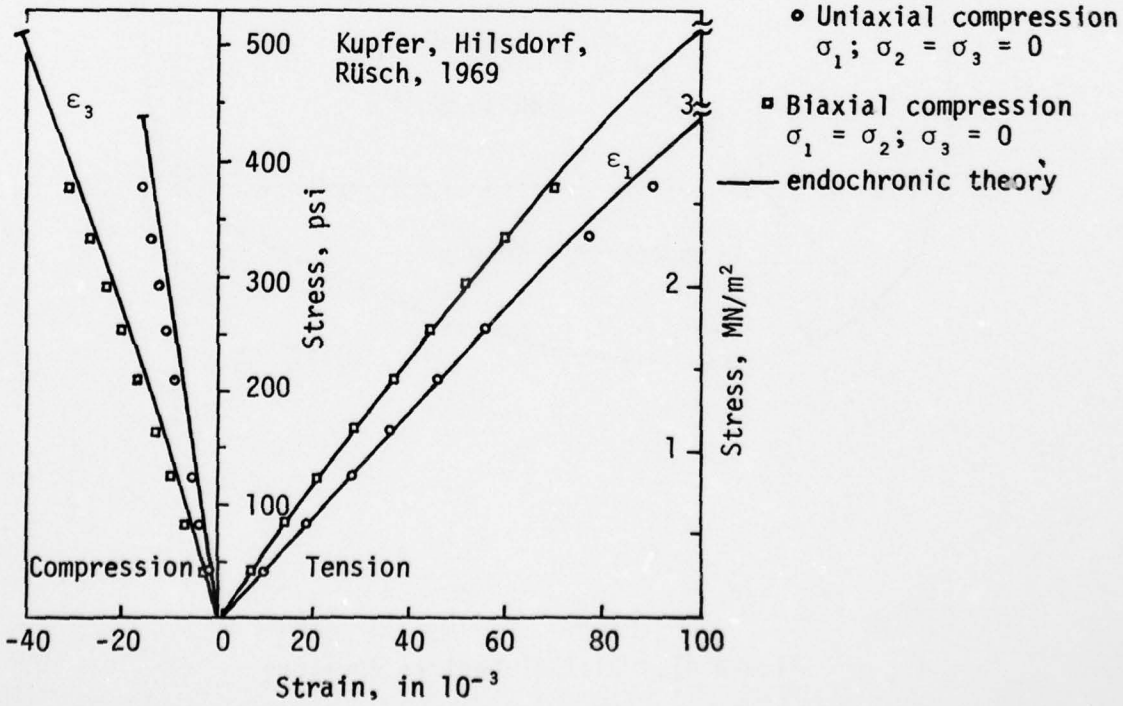

Figure 46. Tension Tests

AD-A070 643 PMB SYSTEMS ENGINEERING INC SAN FRANCISCO CA F/G 11/2
FAILURE CRITERIA FOR REINFORCED CONCRETE STRUCTURES. VOLUME I. --ETC(U)
MAY 79 R W LITTON, J M GIDWANI F29601-76-C-0135

UNCLASSIFIED AFWL-TR-77-239-VOL-1 NL

2 OF 2
AD
A070 643

END
DATE
FILMED
8-79
DDC

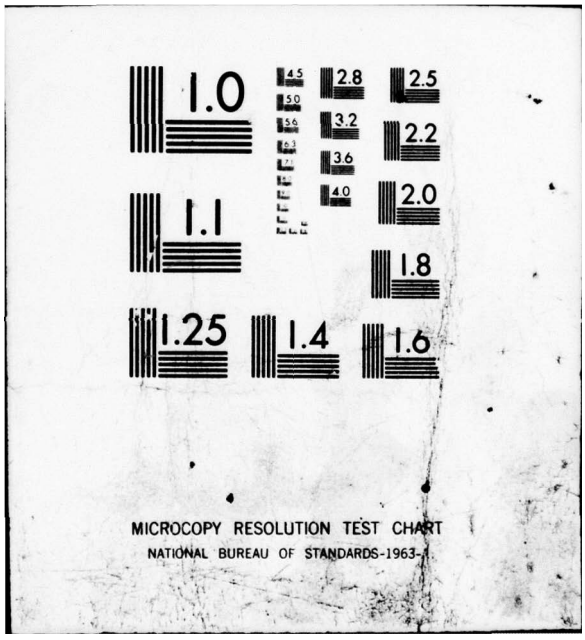
1.0
1.1
1.25
1.4
1.6
1.8
2.0
2.2
2.5
2.8
3.2
3.6
4.0
4.5
5.0
5.6
MICROCOPY RESOLUTION TEST CHART
NATIONAL BUREAU OF STANDARDS-1963-A

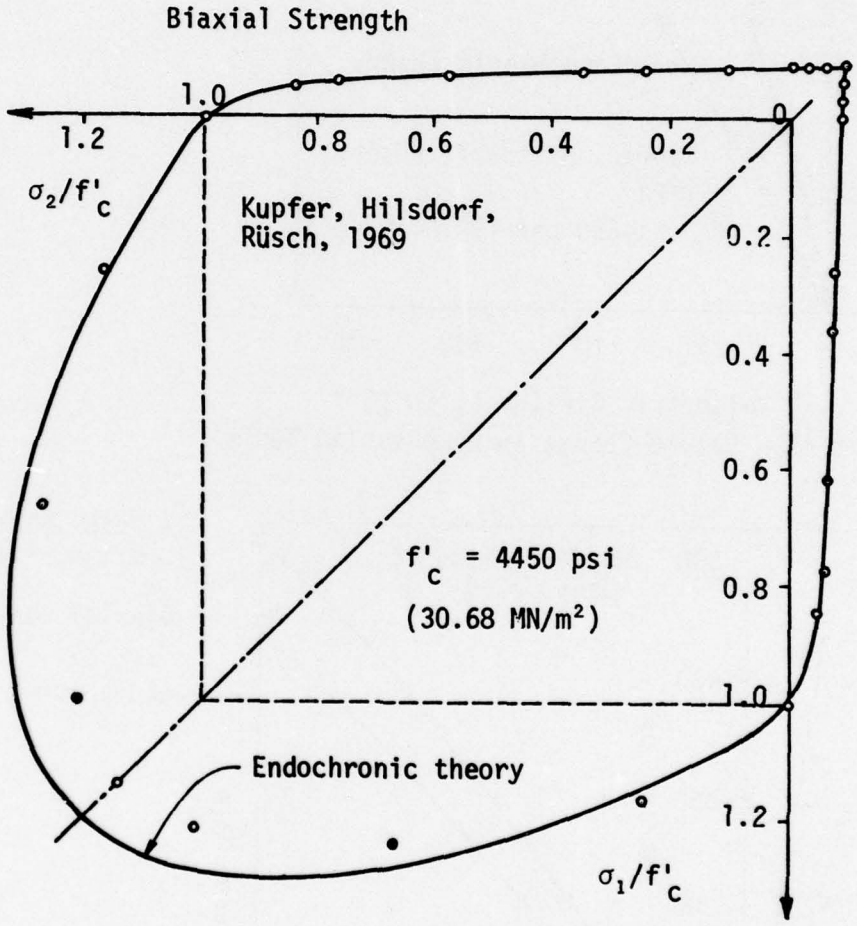

Figure 47. Biaxial Failure Envelope

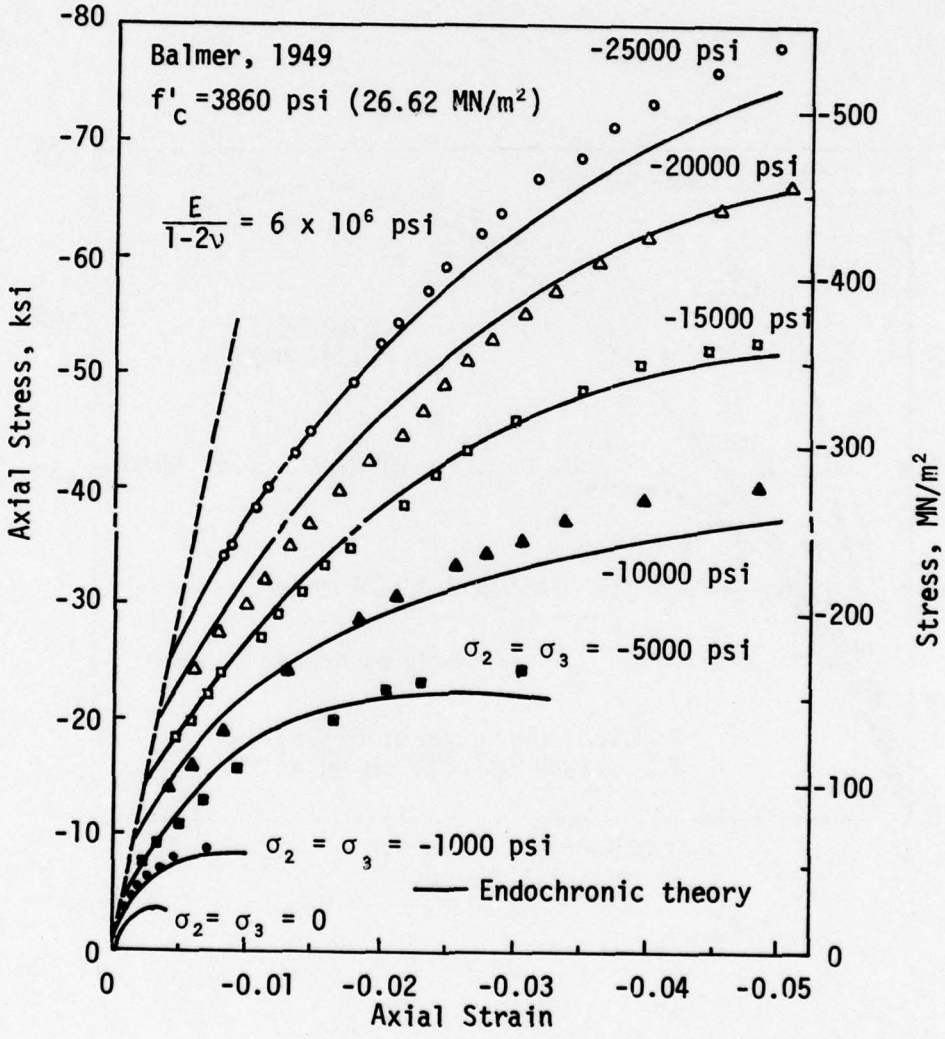

Figure 48. Triaxial Test for Low Strength Concrete

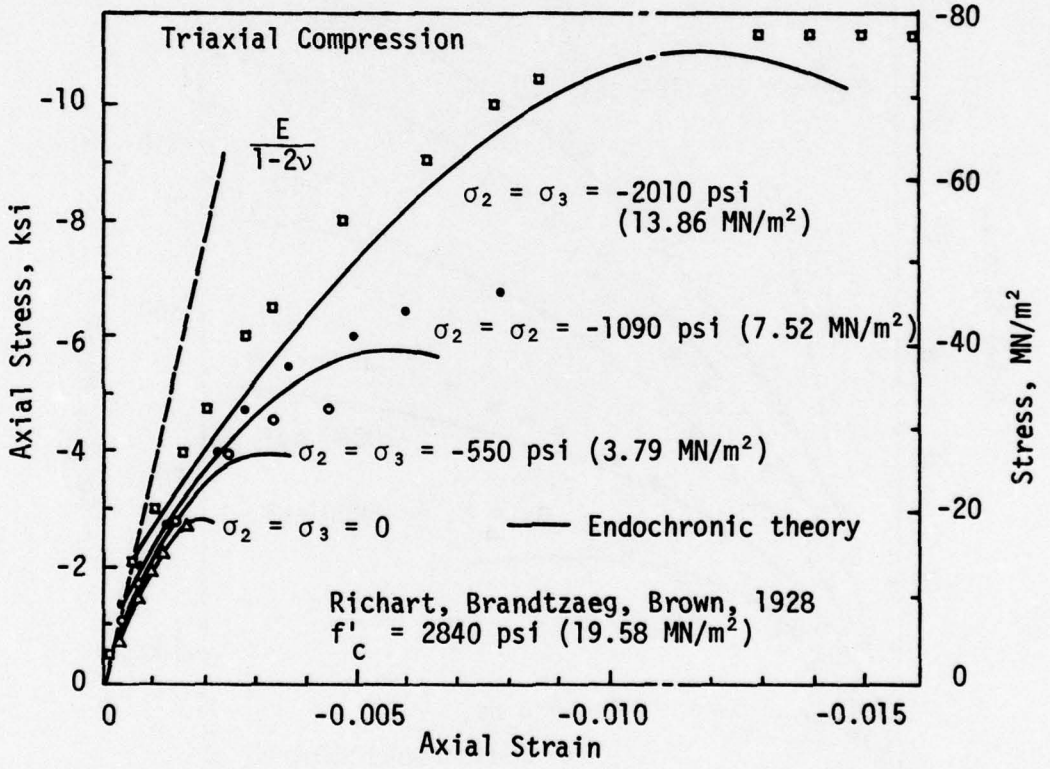

Figure 49. Triaxial Test for Medium Strength Concrete

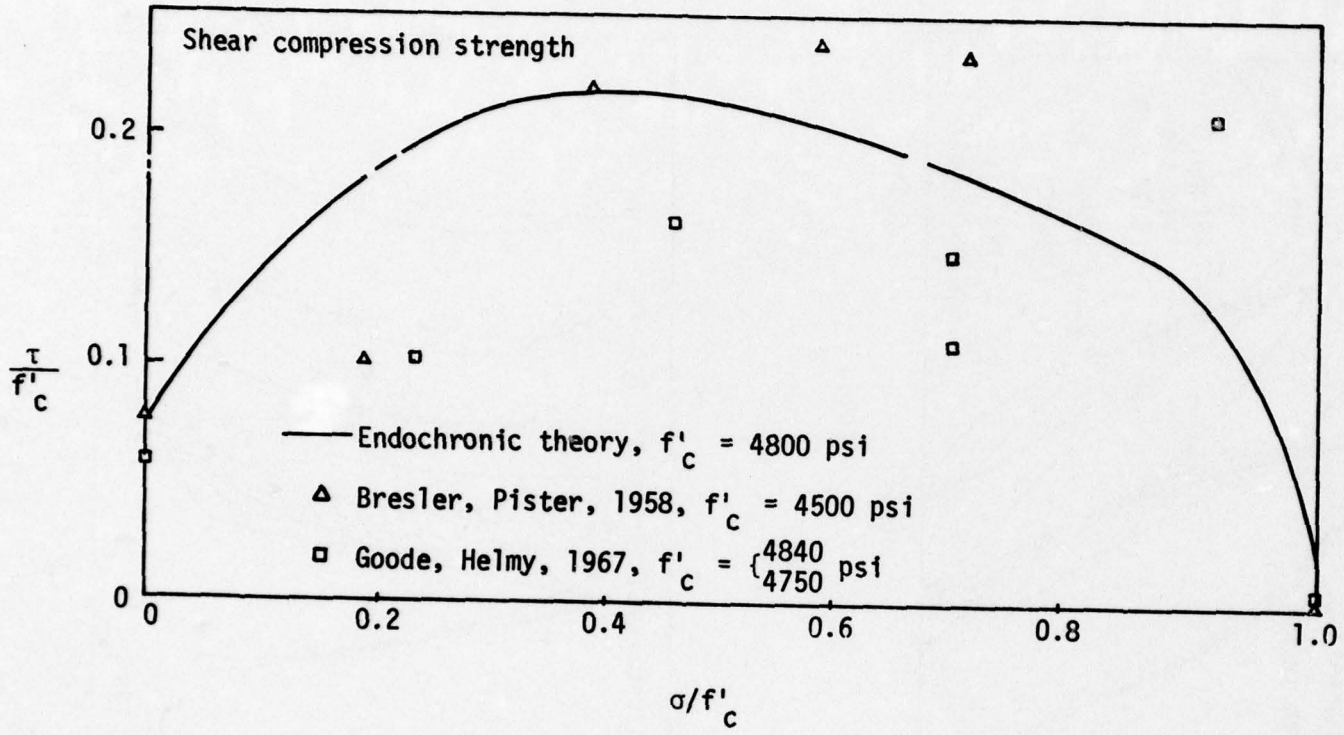

Figure 50. Torsion-Compression Tests

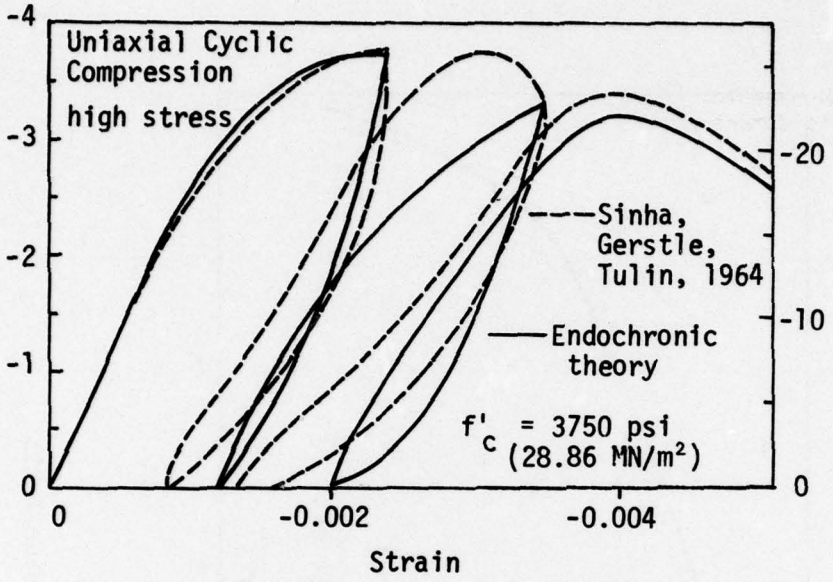

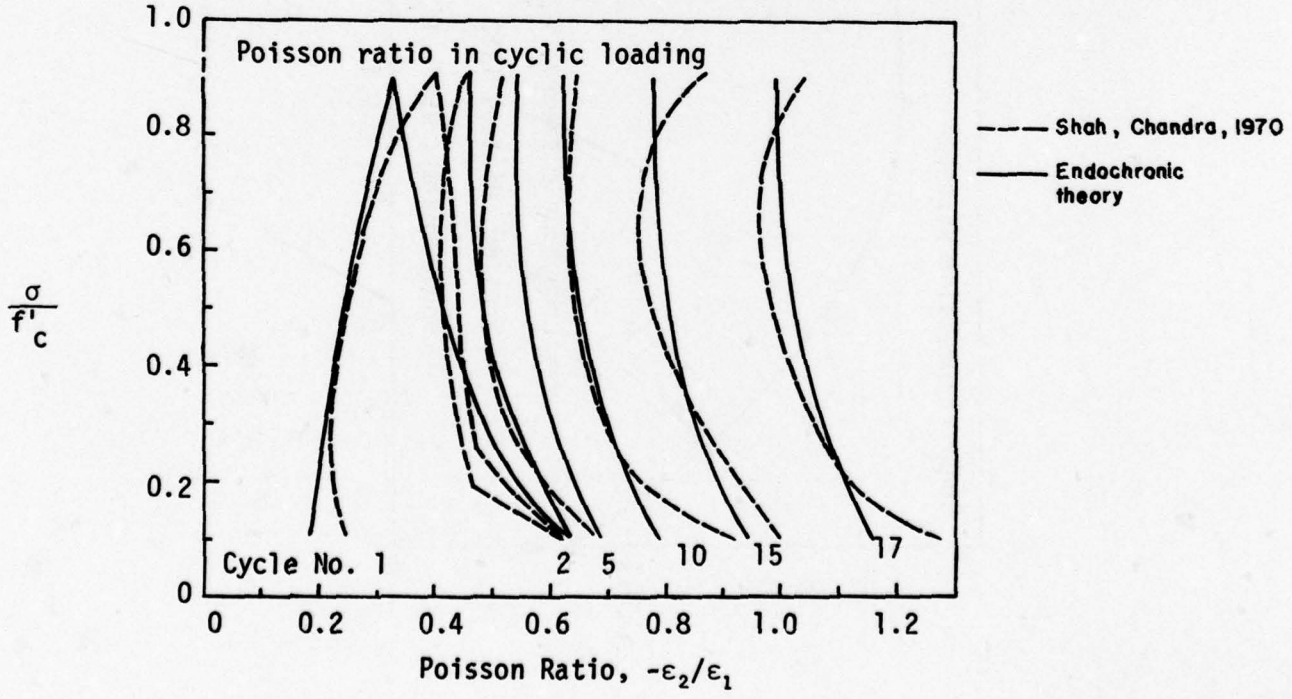

Figure 51. Uniaxial Cyclic Compression Tests

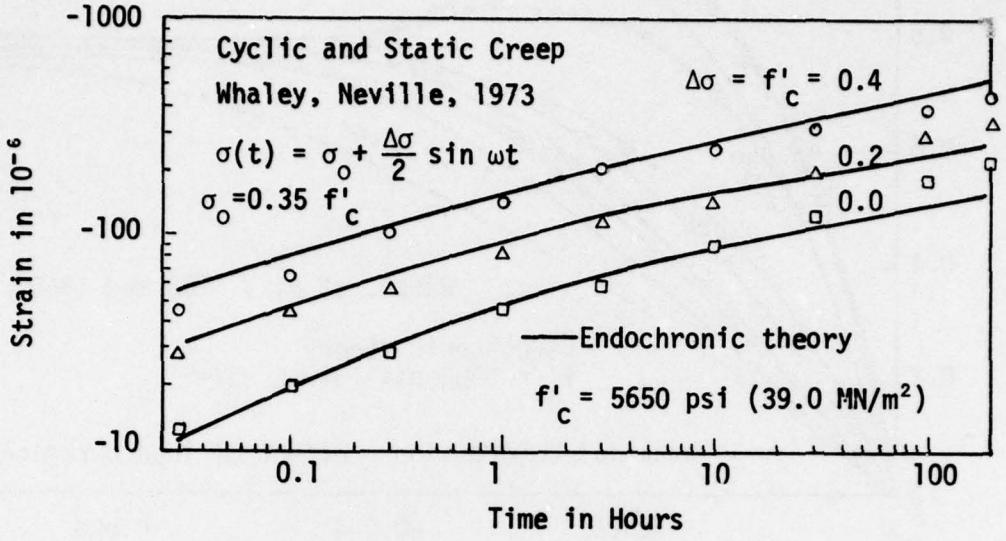

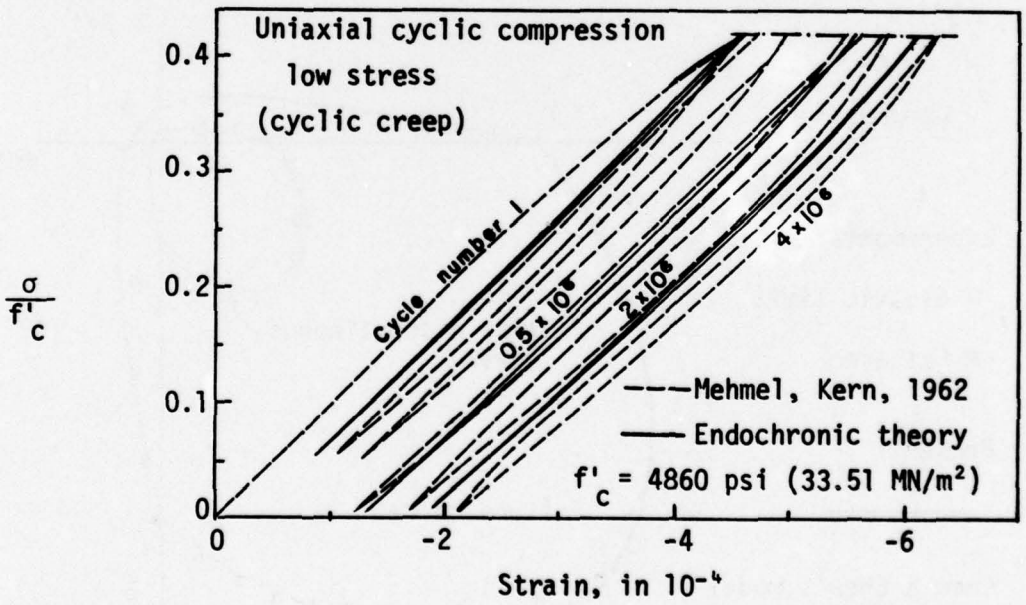

Figure 52. Cyclic Creep Tests

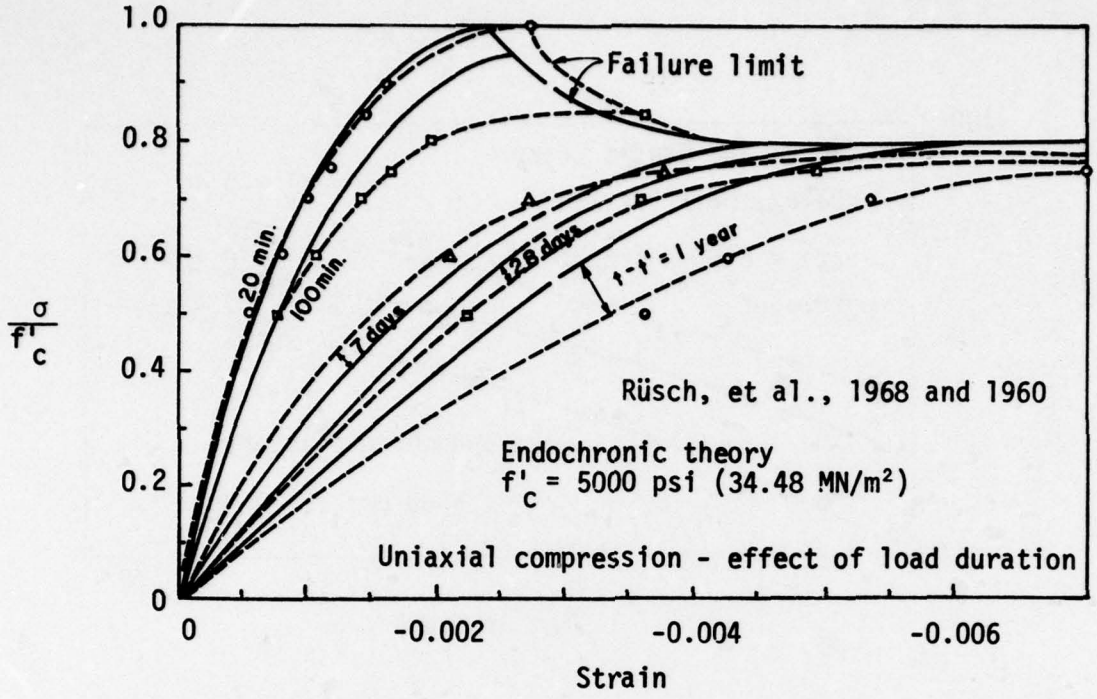

Figure 53. Nonlinear Constant Stress Creep and Long Time Failure

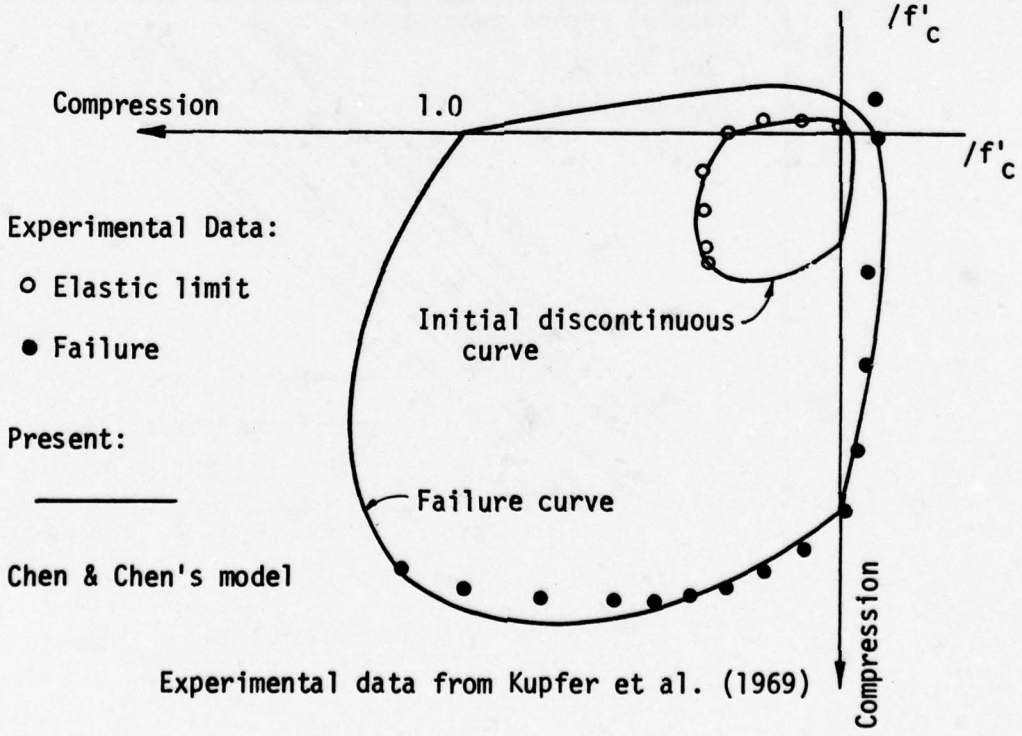

Figure 54. Biaxial Failure Envelope

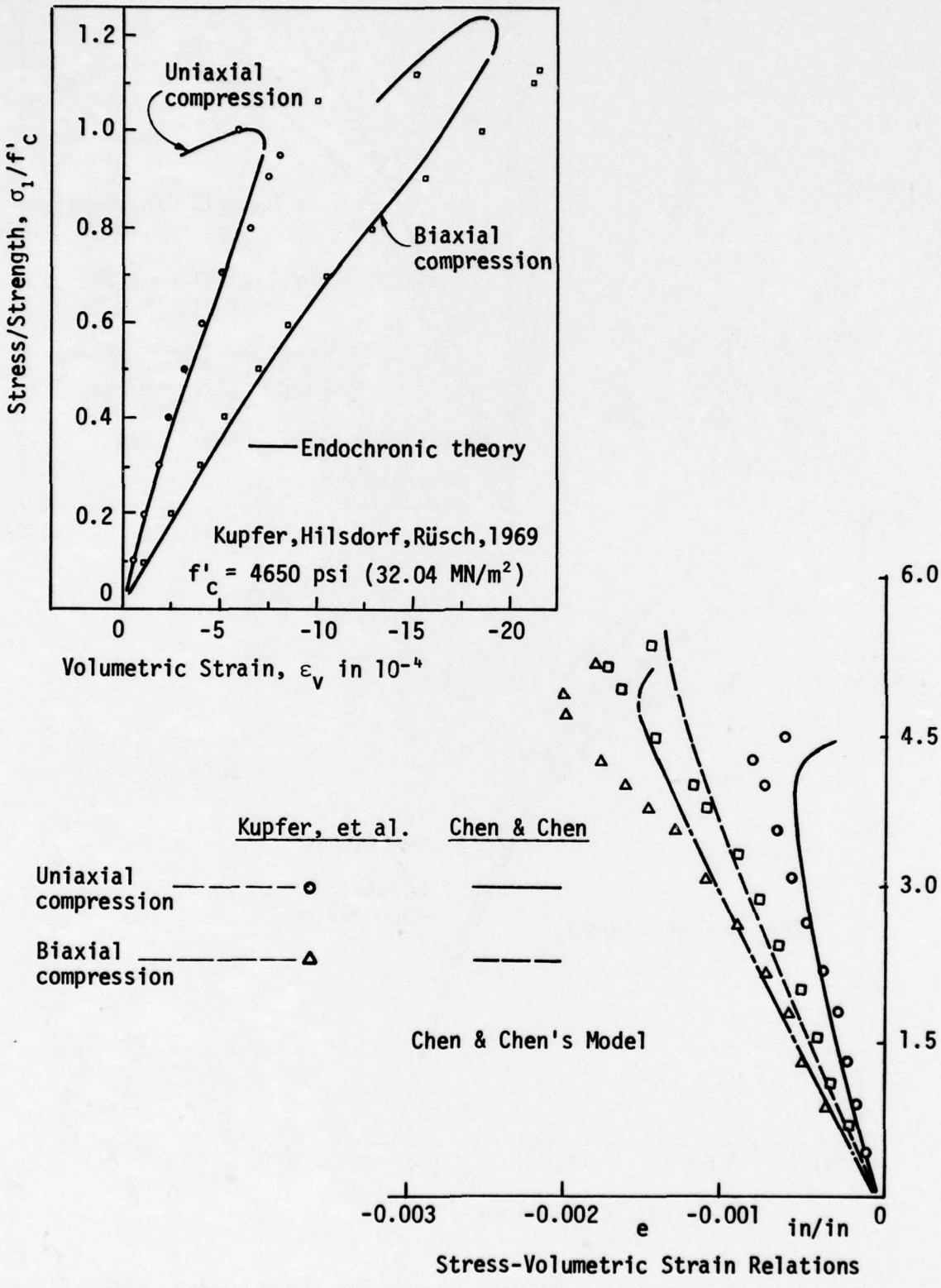

Figure 55. Volume Change in Uniaxial and Biaxial Compression

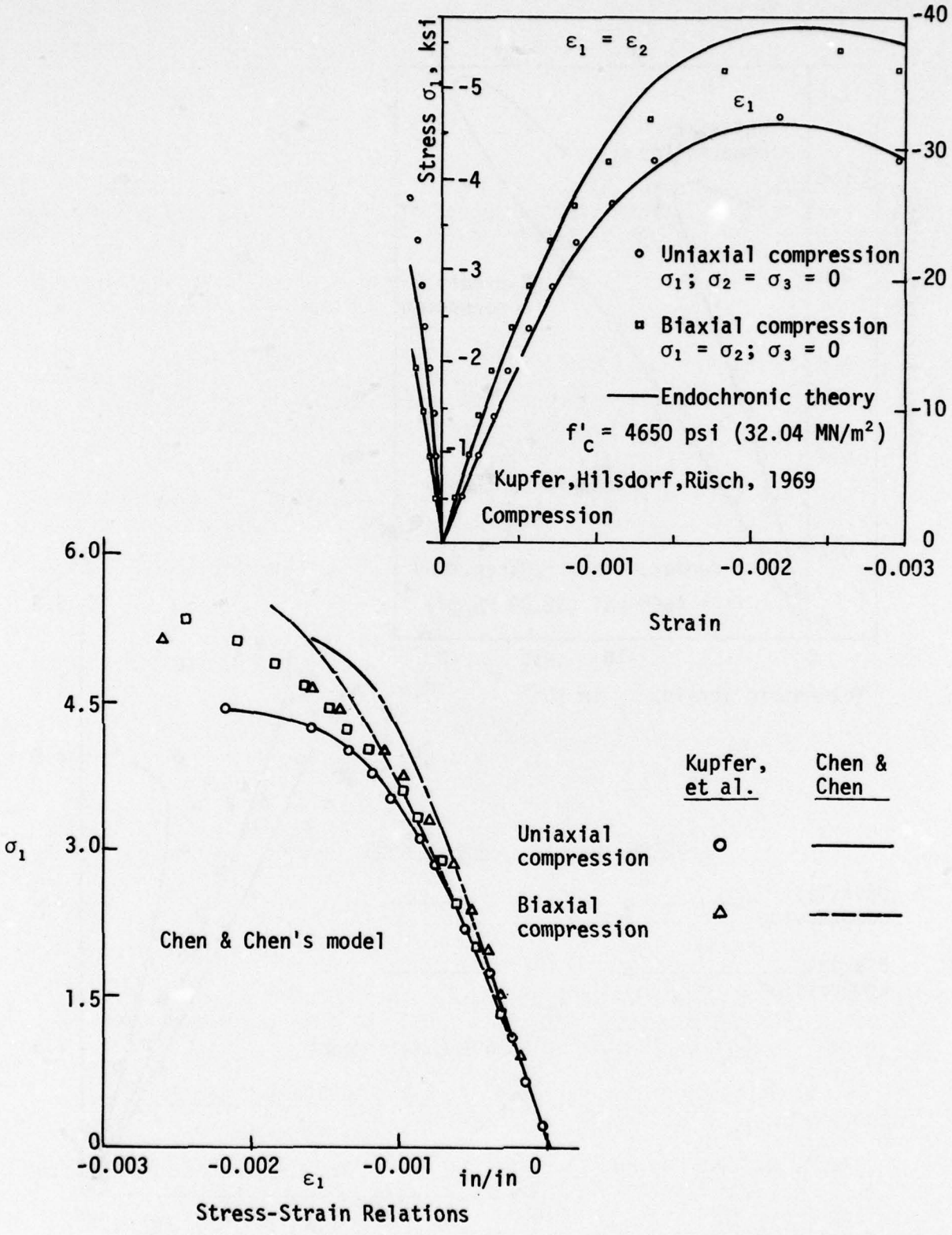

Figure 56. Biaxial Stress-Strain Test with Lateral Strains

REFERENCES

1. VonKarman, Th. V., "Festigkeitversuche Unter Alleseitigem Druck," Nr. 42, Zeitschrift des Vereins Deutscher Ingenieure, 1911.

2. Baker, R., Die Mechanik der Bleinbenden Formanderungen in Kristallinisch Aufgebauten Korpern, VDI-Heft 175/176, Mitteilungen Uber Forschungsarbeiten, 1915.

3. Pichart, F. E., Brandtzaeg, A., and Brown, R. L., "A Study of the Failure of Concrete under Combined Compressive Stresses," Bulletin No. 185, University of Illinois Engineering Experiment Station, Urbana, Illinois, November, 1928.

4. Bresler, B., and Pister, K. S., "Failure of Plain Concrete under Combined Stresses," Vol. 81, No. 674, ASCE Proceedings, April, 1955.

5. Bresler, B., and Pister, K. S., "Failure of Plain Concrete under Combined Stresses,"Vol. 122, pp. 1049, ASCE Transactions, 1957.

6. Bresler, B., and Pister, K. S., "Strength of Concrete under Combined Stresses," Vol. 55, pp. 321-345, Journal of American Concrete Institute, September, 1958.

7. Freudenthal, A., "The Inelastic Behavior and Failure of Concrete, Proceedings, First U.S. National Congress of Applied Mechanics, pp.641-646, Chicago, Illinois, 1951.

8. McHenry, D., and Karni, J., "Strength of Concrete under Combined Tensile and Compressive Stress," Vol. 54, pp. 829-839, Journal, American Concrete Institute, April, 1958.

9. Bellamy, C. J., "Strength of Concrete under Combined Stress," Vol. 58, No. 4, pp. 367-382, Journal, American Concrete Institute, October, 1961.

10. Goode, C. D.,and Helmy, M. A.,"The Strength of Concrete under Combined Shear and Direct Stress," Vol. 19, No. 59, pp. 105-112, Magazine of Concrete Research, London, June, 1967.

11. Foppl, A., Mitteilung aus dem Mech. Techi. Laboratorium der Konig L. Tech. Hocschule, Heft 27 und 28, Munchen, 1900.

12. Wastlund, G., Nya Ron Angaende Betonges Grundlaggende Halfasthetsegenskaper. Vol. 3, Betong (Stockholm), 1937.

13. Glomb, J. "Die Ausnutzbarkeit Zweiachsiger Festigkeit des Betons in Flachentragwerken,"Session I, Nr. 1, Third Spannbetonkongress, Berlin, 1958.

14. Weigler, H., and Becker, G.,"Untersuchungen uber das Bruch and Verformungsverhalten von Beton bei Zweiachsiger Beanspruchung," Hept 157, des Deutschen Ausschusses for Stahlbeton, Berlin, 1963.

15. Vile, G. W. D., "Strength of Concrete under Short-Time Static Biaxial Stress," Paper F2, International Conference on the Structure of Concrete, September, 1965.

16. Robinson, G. S.,"Behavior of Concrete in Biaxial Compression," Vol. 93, No. ST 1, pp. 71-86, Journal of Structural Division, ASCE, February, 1967.

17. Kupfer, H., Hilsdorf, H. K., and Rush, H., "Behavior of Concrete under Biaxial Stresses," Vol. 66, No. 8, pp. 656-666, Proceedings, Journal of American Concrete Institute, August, 1969.

18. Kupfer, H., and Geistle, K., "Behavior of Concrete under Biaxial Stresses," pp. 853-865, Journal of Engineering Mechanics Division, ASCE, August, 1973.

19. Buyukozturk, O., Stress-Strain Response and Fracture of Model of Concrete in Biaxial Loading, No. 337, Department of Structural Engineering, Cornell University, February, 1971.

20. Liu, T. C., Stress-Strain Response and Fracture of Concrete in Biaxial Compression, No. 339, Department of Structural Engineering, Cornell University, February, 1971.

21. Carvno, N. J., "The Behavior of a Model of Plain Concrete Subjected to Compression-Tension and Tension-Tension Biaxial Stresses," No. 357, Department of Structural Engineering, Cornell University, July 1974.

22. Nelissen, L. J. M., "Biaxial Testing of Normal Concrete," Vol. 18, No. 1, HERON, 1972.

23. Hannant, D. J., Frederick, C. O., "Failure Criteria for Concrete in Compression," Vol. 20, No. 64, Magazine of Concrete Research, September, 1968.

24. Endebrock, E. G., Traina, L. A., Static Concrete Constitutive Relations Based on Cubical Specimens," Technical Report No. AFWL-TR-72-59, Vol. I, Air Force Weapons Laboratory, New Mexico, December, 1972.

25. Brink, C., Zimmerman, R., Edington, F., Dynamic Properties of Preloaded Plain Concrete Cylinders, Report No. 42, New Mexico State University, March, 1968.

26. Sparks, P., and Menzies, J., "The Effect of Rate of Loading upon the Static and Fatigue Strengths of Plain Concrete in Compression,"

27. Litton, R. W., A Contribution to the Analysis of Concrete Structures under Cyclic Loadings, Ph.D. Thesis, University of California, Berkeley, June, 1975.

28. Moritz, S., and Kaku, T., Local Bond Stress-Slip Relationship under Repeated Loading, Department of Architectural Engineering, Kyoto University, Japan.

29. Zienkiewicz, O. C., The Finite Element Method in Engineering Science, McGraw Hill, London, 1971.

30. Ngo, D. and Scordelis, A.,"Finite Element Analysis of Reinforced Concrete Beams," Vol. 64, Journal, American Concrete Institute, No. 3, March, 1967.

31. Ngo, D., Scordelis, A., and Franklin, H. A., "Finite Element Study of Reinforced Concrete Beams with Diagonal Tension Cracks," University of California SESM Report No. 70-19, University of California, Berkeley, December, 1970.

32. Nilson, A. H., "Nonlinear Analysis of Reinforced Concrete by the Finite Element Method," Vol. 65, No. 9, Journal, American Concrete Institute, September, 1968.

33. Taylor, M. A., Ronstad, K. M., Hermann, L. R. and Ramey, M. R., A Finite Element Computer Program for the Prediction of the Behavior of Reinforced and Prestressed Concrete Structures Subjected to Cracking, CR72.019, Naval Civil Engineering Laboratory, June, 1972.

34. Romstad, K. M., Taylor, M. A., and Herrmann, L. R., "Numerical Biaxial Characterization for Concrete," Vol. 100, No. EM7, Journal of Engineering Mechanics Division, American Concrete Institute, October, 1974.

35. Kupfer, H., Hilsdorf, H., and Rusch, H., "Behavior of Concrete under Biaxial Stresses," Vol. 66, No. 8, Journal, American Concrete Institute, August, 1969.

36. Salem, M. H., and Mohraz, B., Nonlinear Analysis of Planar Reinforced Concrete Structures, Report No. UILU-Eng-74-2022, University of Illinois, July, 1974.

37. Argyris, J. H., Faust, G., Szimmat, J., Warnke, E. P., and William, K. J., Recent Developments in the Finite Element Analysis of Prestressed Concrete Reactor Vessels, ISF - Report No. 151, Stuttgart, 1973.

38. Argyris, J. H., Faust, G., Szimmat, J., Warnke, E. P., and William, K. J., Finite Element Ultimate Load Analysis of Three-Dimensional Concrete Structures, Stuttgart, August, 1974.

39. Argyris, J. H., Faust, G., William, K. J., Limit Load Analysis of Thick-Walled Concrete Structures, ISD - Report No. 166, Stuttgart, 1975.

40. Sarne, Y., Material Nonlinear Time Dependent Three-Dimensional Finite Element Analysis for Reinforced and Prestressed Concrete Structures, Ph.D. Thesis, Massachusetts Institute of Technology, December, 1974.

41. Adham, S., Bhaumik, A., and Isenberg, J., Reinforced Concrete Constitutive Relations, AFWL-TR-74-72, Air Force Weapons Laboratory, February, 1975.

42. Mikkola, M. J. and Schnobrich, W. C., Material Behavior Characteristic for Reinforced Concrete Shells Stressed beyond the Elastic Range, SRS 367, University of Illinois, August, 1970.

43. Scanlon, A., and Murray, D. W.,"Time Dependent Reinforced Concrete Slab Deflections," Vol. 100, No. ST9, Journal, Structural Division, American Concrete Institute, September, 1974.

44. Yuzugullu, O. and Schnobrich, W. C.,"A Numerical Procedure for the Determination of the Behavior of a Shear Wall Frame," Vol. 70, No. 7, Journal, American Concrete Institute, July, 1973.

45. Yuzugullu, O., and Schnobrich, W. C., Finite Element Approach for the Prediction of Inelastic Behavior of Shear-Wall Frame Systems, 4160-ENG-72-2007, University of Illinois, May, 1972.

46. Cervenka, V., Inelastic Finite Element Analysis of Reinforced Concrete Panels under Inplane Loads, Ph.D. Thesis, University of Colorado, 1970.

47. Cervenka, V., and Gerstle, K. H.,"Inelastic Analysis of Reinforced Concrete Panels, Part I: Theory," Vol. 31-II, IAB5E Publication, 1971.

48. Cervenka, V., and Gerstle, K. H., "Inelastic Analysis of Reinforced Concrete Panels, Part II: Experimental Verification and Application," Vol. 32-II, IAB5E Publication, 1972.

49. Hand, R. R., Pecknold, D. A., and Schnobrich, W. C., A Layer Finite Element Nonlinear Analysis of Reinforced Concrete Plates and Shells, SRS 389, University of Illinois, August, 1972.

50. Hand, R. R., Pecknold, D. A., and Schnobrich, W. C., "Nonlinear Layered Analsysi of RC Plates and Shells," Vol. , ST 7, Journal, Structural Division, American Society of Civil Engineers, July, 1973.

51. Lin, C. S., Nonlinear Analysis of Reinforced Concrete Slabs and Shells, Ph.D. Thesis, University of California, Berkeley, 1973.

52. Lin, C. S., and Scordelis, A. C., "Nonlinear Analysis of RC Shells of General Form," Vol. 101, ST3, Journal of Structural Division, March, 1973.

53. Lin, C. S., and Scordelis, A. C., "Finite Element Study of Reinforced Concrete Cylindrical Shell through Elastic Cracking and Ultimate Ranges," Vol. 72, No. 11, Journal, American Concrete Institute, 1975.

54. Wanchoo, M. K. and May, G. W., "Cracking Analysis of Reinforced Concrete Plates," Vol. 101, No. ST1, Journal of Structural Division, American Society of Civil Engineers, January, 1975.

55. Rajagopal, R. M., Nonlinear Analysis of Reinforced Concrete Beams, Beam-Columns and Slabs by Finite Elements, Ph.D. Thesis, Iowa State University, 1976.

56. Aldstedt, E., Nonlinear Analysis of Reinforced Concrete Frames, Report No. 75-1, Institute of Statikk, NTH Trondheim, Norway, March, 1975.

57. Jofriet, J. C. and McNiece, G. M., "Finite Element Analysis of Reinforced Concrete Slabs," Vol. 97, No. ST3, Journal of Structural Division, American Society of Civil Engineers, March, 1971.

58. Bell, J. C., A Complete Analysis for Reinforced Concrete Slabs and Shells, Ph.D. Thesis, University of Canterbury, New Zealand, 1970.

59. Jofriet, J. C., "Flexural Cracking of Concrete Flat Plates," Journal American Concrete Institute, December, 1973.

60. Ngo, D., A Network - Topological Approach to the Finite Element Analysis of Progressive Crack Growth in Concrete Members, Report No. UCSESM 75-6, University of California, Berkeley, June, 1975.

61. Rashid, Y. R., "Ultimate Strength Analysis of Prestressed Concrete Pressure Vessels," Vol. 7, Nuclear Engineering and Design, 1968.

62. Liu, T. C. Y., Nilson, A. H., and Slate, F. O., "Stress-Strain Response and Fracture of Concrete in Uniaxial and Biaxial Compression," Vol. 69, No. 5, Journal, American Concrete Institute, May, 1972.

63. Kupfer, H. B. and Gerstle, K. H., "Behavior of Concrete under Biaxial Stresses, Vol. 99, No. EM4, Journal of Engineering Mechanics, American Society of Structural Engineers, August, 1973.

64. Coon, M. D., and Evans, R. J.,"Incremental Constitutive Laws and Their Application to Plain Concrete," International Journal of Solids and Structures, September, 1972.

65. Gormack, P. J., Nonlinear Finite Element Analysis of Shear Walls and Two-Dimensional Reinforced Concrete Structures, University of Canterbury, New Zealand, 1974.

66. Darwin, D. and Pecknold, D. A. W., Inelastic Model for Cyclic Biaxial Loading of Reinforced Concrete, SRS No. 409, University of Illinois, July, 1974.

67. Saenz, L. P., "Discussion of Equation for the Stress-Strain Curve of Concrete by Desayi and Krishnan," Vol. 61, No. 9, Journal, American Concrete Institute, September, 1964.

68. Popvics, S., "A Review of Stress-Strain Relationships for Concrete," Journal, American Concrete Institute, March, 1970.

69. Khan, M. H. and Sangy, B. Evaluation of the Influence of Some Concrete Characteristics on Nonlinear Behavior of a Prestressed Concrete Reactor Vessel, SP-34, American Concrete Institute Publication, 1972.

70. Chen, A. C. T. and Chen, W. F., "Constitutive Relations for Concrete," Vol. 101, No. EM4, Journal of Engineering Mechanics, August, 1975.

71 Chen, A. C. T., and Chen, W. F., "Constitutive Equations and Punch Indentation of Concrete," Vol. 101, No. EM6, Journal of Engineering Mechanics, December, 1975.

72. Ville, G. W. D., The Strength of Concrete under Short-Term Static Biaxial Stress, The Structure of Concrete, Cement and Concrete Association, London, England, 1968.

73. Willam, K. J., and Warnke, E. P., Constitutive Model for the Triaxial Behavior of Concrete, Stuttgart, 1974.

74. Green, S. J. and Swanson, S. R., Static Constitutive Relations for Concrete, Report No. AFWL-TR-72-244, Air Force Weapons Laboratory, April, 1973.

75. Bazant, Z. P., and Bhat, P. D., "Endochronic Theory of Inelasticity and Failure of Concrete," Journal of Engineering Mechanics, American Society of Civil Engineers.

76. Valanis, K. C.,"A Theory of Viscoplasticity with a Yield Surface," Vol. 23, Archiwum Mechaniki Stossowanej, 1971.

DISTRIBUTION

No. of Copies

Department of Defense

Director, Defense Advanced Rsch Proj Agency
Architect Bldg, 1400 Wilson Blvd., Arlington, VA 22209
1 ATTN: Technical Library

Defense Documentation Center
Cameron Station, Alexandria, VA 22314
12 ATTN: TC

Director, Defense Intelligence Agency
Washington, DC 20301
1 ATTN: Technical Library

Director, DNA
Washington, DC 20305
2 ATTN: SPSS
3 ATTN: TITL Tech Library
1 ATTN: TISI Archives

Director, Defense Rsch & Engineering
DOD, Washington, DC 20301
1 ATTN: S&SS (OS)

Commander, Field Command
DNA, Kirtland AFB, NM 87115
1 ATTN: FCPR
1 ATTN: FCTMOF

Director, Interservice Nuclear Weapons School
Kirtland AFB, NM 87115
1 ATTN: Tech Lib

Director, Joint Strat Tgt Planning Staff JCS
Offutt AFB, Omaha, NB 68113
1 ATTN: STINFO Library

Chief, Livermore Div, Fld Command DNA
Lawrence Livermore Laboratory, P.O. Box 808, Livermore CA 94550
1 ATTN: FCPRL

1 AUL/LDE/Maxwell AFB, AL 36112

Department of Defesne, cont'd.

No. of
copies

Department of the Army

Director, Construction Engineering Research Laboratory
P.O. Box 4005, Champaign IL 61820
1 ATTN: CERL-SL

Dep Chief of Staff or Rsch Dev & Acq
Dept of the Army, Washington DC 20310
1 ATTN: Technical Library

Deputy, Chief of Staff for Ops & Plans
DOA, Washington, DC 20310
1 ATTN: Technical Library

Commander, Harry Diamond Laboratories
2800 Powder Mill Rd., Adelphi, MD 20783
1 ATTN: DRXDO-TI Tech Lib

Commander, Picatinny Arsenal
Dover, NJ 07801
1 ATTN: Technical Library

Commander, Redstone Scientific Information Center
U.S. Army Missile Command
Redstone Arsenal, AL 35809
1 ATTN: Chief, Documents

Commander, U. S. Army Armament Command
Rock Island, IL 61202
1 ATTN: Technical Library

Director, US Army Ballistic Research Labs
Aberdeen Proving Ground, MD 21005
1 ATTN: Tech Lib

Commander, U. S. Army Communications CMD
Fort Huachuca, AZ 85613
1 ATTN: Technical Library

Commander, U. S. Army Engineer Center
Fort Belvoir, VA 22060
1 ATTN: ATSEN-SY-L

Division Engineer, U.S. Army Engineer Div Huntsville
P.O. Box 1600, West Station, Huntsville, AL 35807
1 ATTN: HNDED-SR

Department of the Army, Cont'd.

No. of
Copies

Division Engineer, U.S. Army Engineer Div Ohio River
P.O. Box 1159, Cincinnati, OH 45201
1 ATTN: Technical Library

Director, US Army Engr Waterways Exper Sta
P.O. Bx631, Vicksburg, MS 39180
1 ATTN: Tech Lib
1 ATTN: William Flathau
1 ATTN: James Ballard

Commander, US Army Mat & Mechanics Rsch Ctr
Watertown, MA 02172
1 ATTN: Technical Library

Commander, US Army Material Dev & Readiness Cmd
5001 Eisenhower Ave., Alexandria, VA 22333
1 ATTN: Technical Library

Commander, US Army Mobility Equip R&D Ctr
Fort Belvoir, VA 22060
1 ATTN: Technical Library

Commander, US Army Nuclear Agency
Ft. Bliss, TX 79916
1 ATTN: Tech Lib

Commandant, US Army War College
Carlisle Barracks, PA 17013
1 ATTN: Library

Department of the Navy

Chief, Naval Research, Navy Dept.
Arlington, VA 22217
1 ATTN: Tech Lib

Civil Engineering Laboratory
Naval Construction Battalion Ctr, port Hueneme, CA 93041
1 ATTN: Technical Lib

Commander, Naval Facilities Engineering Command Hqs
Washington DC 20390
1 ATTN: Technical Library

Superintendent (Code 1424), Naval Postgraduate School
Monterey, CA 93940
1 ATTN: Code 2124 Tech Rpts Librarian

Department of the Navy, Cont'd.

No. of
Copies

Commander, Naval Surface Weapons Ctr
White Oak, Silver Spring, MD 20910
1 ATTN: Code WX21 Tech Lib

Commander, Naval Surface Weapons Ctr
Dahlgren Laboratory, Dahlgren, VA 22448
1 ATTN: Tech lib

President, Naval War College
Newport, RI 02840
1 ATTN: Tech Lib

Commander, Naval Weapons Ctr
China Lake, CA 93555
1 ATTN: Code 533 Tech Lib

Commanding Officer, Naval Weapons Evaluation Facility
Kirtland Air Force Base, Albuq, NM 87117
1 ATTN: Tech Lib

Director, Strategic Systems Project Office
Navy Dept, Washington, DC 20376
1 ATTN: NSP-43 Tech Lib

Department of the Air Force

AF Geophysics Laboratory, AFSC
Hanscom AFB, MA 91731
1 ATTN: SUOL AFCRL Rsch Lib

AF Institute of Technology, AU
Wright-Patterson AFB OH 45433
1 ATTN: Library AFIT Bldg 640 Area B

AF Weapons Laboratory, AFSC
Kirtland AFB, NM 87117
1 ATTN: DE, M. A. Plamondon
2 ATTN: SUL
30 ATTN: DES, Mr Rodney G. Galloway
1 ATTN: HO

HQ, Air Force Systems Command
Andrews AFB, Washington DC 20331
1 ATTN: Tech Lib
1 ATTN: DLWM

Department of the Air Force, Cont'd.

No. of Copies

Commander, Armament Dev & Test Center
Eglin AFB, FA 32542
1 ATTN: Tech Lib

Commander, ASD
WPAFB, OH 45433
1 ATTN: Tech Lib

Commander, Foreign Technology Div, AFSC
1 Wright-Patterson AFB, OH 45433
1 ATTN: TD-BTA Lib

Hq USAF/RD
Washington, DC 20330
1 ATTN: RDQRM, Col S.C. Green
1 ATTN: RDPM
1 ATTN: RDPS, LTC A. Chiota
1 ATTN: RDQPN, Maj F. Vajda

Commander, Rome Air Dev Ctr, AFSC
Griffiss AFB, NY 13440
1 ATTN: EMTLD Doc Library

SAMSO/DE
Norton AFB, CA 92409
1 ATTN: DEB

SAMSO/MN
NORTON AFB, CA 92409
1 ATTN: MNNH
1 ATTN: MMH

Commander in Chief, Strategic Air Command
Offutt AFB, NB 68113
1 ATTN: NRI-Stinfo Lib

U. S. Energy Rsch and Dev Admin

Division of Military Application
U.S. Energy Rsch & Dev Admin, Washington, DC 20545
1 ATTN: Doc Control for Test Office

University of California, Lawrence Livermore Laboratory
P.O. Box 808, Livermore, CA 94550
1 ATTN: Tech Info Dept L-3

U.S. Energy Rsch and Dev Admin, Cont'd.

No. of
Copies

Los Alamos Scientific Laboratory
P.O. Box 1663, Los Alamos, NM 87545
1 ATTN: Doc Control for Reports Lib

Sandia Laboratories
Livermore Laboratory, P.O. Box 969, Livermore, CA 94550
1 ATTN: Doc Control for Tech Lib

Sandia Laboratories
P.O. Box 5800, Albuquerque, NM 87115
1 ATTN: Doc Con for 3141 Sandia Rpt Coll

U.S. Energy Rsch & Dev Admin, Div of Hq Services
Library Branch G-043
Washington, DC 20545
1 ATTN: Doc Con for class Tech Lib

U.S. Energy Rsch & Dev Admin
Nevada Operations Office, P.O. Box 5400, Albuq, NM 87115
1 ATTN: Doc for Tech Lib

U.S. Energy Rsch & Dev Admin, Div of Hq Services
Library Branch G-043
Washington, DC 20545
1 ATTN: Doc Con for Class Tech Lib

US Energy Rsch & Dev Admin
Nevada Operations Office
P.O. Box 14100, Las Vegas, NV 89114
1 ATTN: Doc Con for Tech Lib

Dept of the Interior
Bureau of Mines
Bldg 20, Denver Federal Center, Denver, CO 80225
1 ATTN: Tech Lib

Department of Defense Contractors

Aerospace Corporation
P.O. Box 92957, Los Angeles, CA 90009
1 ATTN: Tech Info Services

Agbabian Associates
250 N. Nash St., El Segundo, CA 90245
1 ATTN: M. Agbabian

Analytic Services, Inc.
5613 Leesburg Pike, Falls Church, VA 22041
1 ATTN: George Hesselbacher

Department of Defense Contractors , Cont'd.

No. of Copies	
	Applied Theory, Inc. 1010 Westwood Blvd, Los Angeles, CA 90024
1	ATTN: John G. Trulio
	Artec Associates, Inc. 26046 Eden Landing Road, Hayward CA 94545
1	ATTN: Steven Gill
	Avco Research & Systems Group 201 Lowell Street, Wilmington MA 01887
1	ATTN: Research Lib A830 Rm 7201
	Battelle Memorial Institute 505 King Ave., Columbus OH 43201
1	ATTN: Tech Lib
	BDM Corporation 1920 Aline Ave,. Vienna VA 22180
1	ATTN: Tech Lib
	Ted Belytschko 6304 No. Hiawatha Ave., Vienna VA 22180
1	ATTN: Ted Belytschko
	Boeing Company P.O. Box 3607, Seattle, WA 98124
1	ATTN: Aerospace Lib
	Brown Engineering Co., Inc Cummings Research Park, Huntsville AL 35807
1	ATTN: Manu Patel
	California Institute of Technology 1201 E. California Blvd, Pasadena CA 91109
1	ATTN: Thomas J. Ahrens
	California Research & Technology, Inc. 6269 Variel Ave., Woodland Hills CA 91364
1	ATTN: Tech Lib
	Calspan Corporation P.O. Box 235, Buffalo NY 14221
1	ATTN: Tech Lib

Department of Defense Contractors, Cont'd.

No. of
Copies

Civil/Nuclear Systems Corp.
1200 University Blvd., NE., Albuquerque NM 87102
1 ATTN: Tech Lib

Dayton, University of
Industrial Security Super KL-505
300 College Park Ave., Dayton, OH 45409
1 ATTN: Hallock F. Swift

University of Denver
Colorado Seminary
Denver Research Institute
p.O. Box 10127, Denver, CO 80210
1 ATTN: Sec Officer for Tech Lib

EG&G, Inc.
Albuquerque Division
P.O. Box 10218, Albuquerque, NM 87114
1 ATTN: Tech Lib

Electric Power Research Institute
3412 Hillview Ave., Palo Alto, CA 94303
1 ATTN: George Sliter

Engrg Decision Analysis Co., Inc.
2400 Michelson Dr., Irvine, CA 92715
1 ATTN: R. P. Kennedy

Franklin Institute
20th Street and Parkway, Philadelphia, PA 19103
1 ATTN: Zenons Zudans

General Electric Co., TEMPO-Center for Advanced Studies
816 State St., (P.O. Drawer QQ), Santa Barbara, CA 93102
1 ATTN: DASIAC

General Research Corporation
P.O. Box 3587, Santa Barbara, CA 93105
1 ATTN: Benjamin Alexander

H-Tech Laboratories, Ind.
P.O. Box 1686, Santa Monica, CA 90406
1 ATTN: B. Hartenbaum

Department of Defense Contractors, Cont'd.

No. of Copies	
	IIT Research Institute 10 West 35th St., Chicago, IL 60616
1	ATTN: Tech Lib
	Institute for Defense Analyses 400 Army-Navy Dr., Arlington, VA 22202
1	ATTN: IDA Librarian Ruth S. Smith
	J. H. Wiggins, co., Inc. 1650 S. Pacific Coast Highway, Redondo Beach, CA 90277
1	ATTN: John Collins
	Kaman Avidyne, Division of Kaman Sciences Corp. 83 Second Ave., Northwest Industrial park, Burlington, MA 01803
1	ATTN: Tech Lib
	Kaman Sciences Corporation P.O. Box 7463, Colorado Springs, CO 80933
1	ATTN: Library
	Karagozian and Case 6330 N. Figueroa St., Los Angeles, CA 90042
1	ATTN: John Karagozian
	Lockheed Missiles & Space Co., Inc. P.O. Box 504, Sunnyvale, CA 94088
1	ATTN: Tech Lib
	Martin Marietta Aerospace, Orlando Div P.O. Box 5836, Orlando, FL 32805
1	ATTN: G. Fotieo
	McDonnell Douglas Corp. 5301 Bolsa Ave., Huntington Beach, CA 92647
1	ATTN: Robert W. Halprin
	Merritt Cases, Inc. P.O. Box 1206, Redlands, CA 92373
1	ATTN: Tech Lib
	Newmark, Nathan M., Consulting Engineering Services 1211 Civil Engineering Bldg., Rm B106A, Univ of Illinois
1	ATTN: Nathan M. Newmark

Department of Defense Contractors, Cont'd.

No. of
Copies

TRW Systems Group
One Space Park, Redondo Beach, CA 90268
1 ATTN: Tech Info Center/S-1930
1 ATTN: Peter K. Dai, R1/2170
1 ATTN: Norm Lipner

TRW Systems Group, San Bernardino Operations
P.O. Box 1310, San Bernardino, CA 92402
1 ATTN: E. Y. Wong, 527/712

TRW Systems Group
Room 712, Bldg 572,Norton AFB, CA 92409
1 ATTN: Gregory D. Hulcher

Universal Analytics, Inc.
7740 W. Manchester Bld., Playa Del Rey, CA 90291
1 ATTN: E. I. Field

URS Research Co.
155 Bovet Rd., San Mateo, CA 94402
1 ATTN: Tech Lib

Eric H. Wang Civil Engineering Rsch Fa, University Station
Box 188, University of NM, Albuquerque, NM 87121
2 ATTN: Jerry Berglund

Weidlinger Assoc. Consulting Engineers
110 East 59th St., New York, NY 10022
1 ATTN: Melvin L. Baron

Weidlinger Associates Consulting Engineers
Suite 245, 3000 Sand Hill Road, Menlo Park, CA 94025
1 ATTN: F. S. Wong
1 ATTN: J. Isenberg

Dept of Civil Engineering
University of California
1 ATTN: Prof Alex. C. Scordelis
729 Davis Hall
Berkeley, CA 94720

Purdue University
School of Civil Engineering
West Lafayette, IN 47907
1 ATTN: Prof W. F. Chen

Department of Defense Contractors, Cont'd.

No. of Copies	
	Pacifica Technology P.O. Box 148, Del Mar, CA 92014
1	ATTN: G. Kent
4	ATTN: Prof. Robert Dunham
	Physics International Co. 2700 Merced St., San Leandro, CA 94577
1	ATTN: Doc Con for Tech Lib
	R & D Associates P.O. Box 9695, Marine Del Rey, CA 90291
1	ATTN: Tech Lib
	Rand Corporation 1700 Main St., Santa Monica, CA 90406
1	ATTN: Tech Lib
	Science Applications, Inc. 2201 San Pedro NE, Albuquerque, NM 87110
1	ATTN: J. L. Bratton
	Science Applications, Inc. P. O. Box 2351, La Jolla, CA 92038
1	ATTN: Tech Lib
	Southwest Research Institute P.O. Box Drawer 28510, San Antonio, TX 78284
1	ATTN: Wilfred E. Baker
	Stanford Research Institute 333 Ravenswood Ave., Menlo Park, CA 94026
1	ATTN: Carl Peterson
	Systems, Science and Software, Inc. p.O. Box 1620, La Jolla, CA 92038
1	ATTN: Tech Lib
1	ATTN: G. Hegemeir, Room 2091
	Terra Tek, Inc. 420 Wakara Way, Salt Lake City, UT 87108
1	ATTN: Tech Lib
	Tetra Tech, Inc 630 North Rosemead Blvd., Pasadena, CA 91107
1	ATTN: Tech Lib

Department of Defense Contractors Cont'd.

No. of
Copies

PMB Systems Eng
500 Sansome Street
San Francisco 94111
15 ATTN: Dr. R. Litton